CH 454

NORTH CAROLINA STATE UNIVERSITY.

Department of Chemistry

Measurements II Laboratory

Advanced Methods

Manual for Students

Chapter 1. Overview of Advanced Measurements

Advanced measurements is a course designed to give the student of Chemistry skills that will be important in any field of chemistry 1.) an understanding of how to connect experiment to theory, 2.) a view of real world applications and 3.) the ability to express your observations and hypothesis in clear and concise language.

One significant goal of the course is give the student experience in how to apply theory to prediction of properties and how to test those predictions. We will review key theory that you have studied. Chemistry is such a vast subject that certain aspects of the theory will be introduced for the first time. For example, much of Raman spectroscopy is not discussed in the undergraduate curriculum in other courses.

The course also provides a chance to learn how to design and troubleshoot experiments. We will put all of your chemical knowledge to work in this course. We will also try to personalize the course so that students can get the kind of training that is of greatest interest to them.

2. Connecting theory and experiment

2.1 Fluorescence Spectroscopy

2.1.1 Emission – the mirror image relationship

Once a photon has been absorbed, the excited state may live for many nanoseconds. During that time vibrational relaxation can occur so that the population of vibrational states in the excited state potential surface is equilibrated. Fluorescence, shown in Figure 3.1, occurs following vibrational relaxation so that the initial state for fluorescence will be mostly 0' with some contribution from thermally populated vibrational states. The overlaps of 0'-0, 0'-1, 0'-2 etc. are the same as 0-0', 0-1', 0-2' etc. Thus, FC factor for emission is the same as that for absorption. The difference is that in absorption we add quanta of energy and in emission we subtract them. This can be seen in Figure 3.1. It is clear that the emission energies will all be lower than 0-0', while the absorption energies will all be higher. The relationship shown in Figure 1 leads to the "mirror image" relationship between absorption and emission lines shown in Figure 3.2.

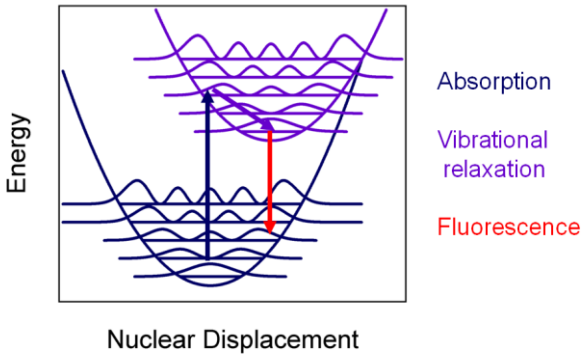

Figure 1. Illustration of the events leading to fluorescence. Absorption is followed by vibrational relaxation. Fluorescence occurs from a relaxed nuclear geometry in the excited state.

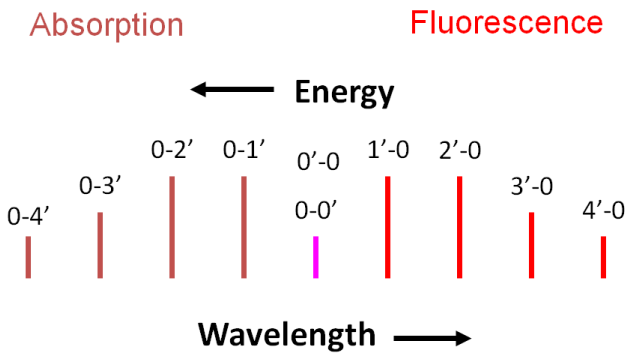

Figure 2. Illustration of the mirror image relationship for absorption and fluorescence spectra.

The commonly used dye Rhodamine shows the mirror image relationship.

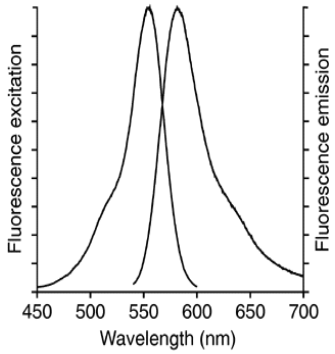

Figure 3. Mirror image relationship of excitation and emission.

Figure 3 shows the excitation spectrum and the emission spectrum. The excitation spectrum is has the same theoretical line shape as the absorption spectrum.

2.1.2 The excited state lifetime

When a molecule is excited, an electron is promoted from the ground state to an excited state. The electron will return to the ground state with lifetime that is determined by both the fluorescence rate constant, k_f and the non-radiative rate constant, k_{nr}. The measured the excited state lifetime, τ_{obs}, depends on both of these processes. First, we note that the rate constant is the inverse of the lifetime,

$$k_{obs} = \frac{1}{\tau_{obs}} \tag{2.1}$$

The observed rate constant is the sum of both intrinsic rate constants,

$$k_{obs} = k_f + k_{nr} \tag{2.2}$$

The measured population of the excited state decreases exponentially according to

$$N(t) = N(0)e^{-k_{obs}t} \tag{2.3}$$

The quantum yield of the fluorescence is given by,

$$\Phi_f = \frac{k_f}{k_f + k_{nr}} \tag{2.4}$$

A single measurement of the kinetics will give only the observed rate constant, k_{obs}. In order to measure the intrinsic rate constant, k_f, we need to measure both the observed lifetime by a kinetics measurement and the fluorescence quantum yield. The lifetime can be measured using time-correlated single photon counting, which is a widely used technique for determining the time course for excited state emission. The fluorescence quantum yield, Φ_f, can be measured in a fluorometer by comparing the emission of an unknown to that of a known standard.

2.1.3 Practical fluorescence spectroscopy

Tryptophan fluorescence

The fluorescence of the amino acid tryptophan is widely used as a probe of protein structural changes. Tryptophan is an aromatic amino acid, whose structure is shown in Figure 4. Tryptophan absorbs light by excitation of $\pi \rightarrow \pi^*$ transitions near 290 nm. We can model the absorption of tryptophan using the particle-on-circle model. Although tryptophan is not truly circular, it is aromatic with 10 electrons in the π-system. Note that we count the nitrogen heteroatom contribution of 2 electrons in addition to the 8 electrons from p-orbitals of the carbon atoms. The model predicts that there will be a strongly absorbing band (allowed) with $\Delta m = \pm 1$, and a weak absorption band with $\Delta m = \pm 5$.

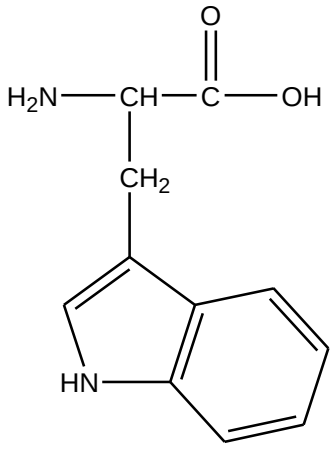

Figure 4 Structure of tryptophan

The observed band at 290 nm is the weak band, which is formally forbidden. As is the case for benzene, porphyrins and other aromatic molecules, the low energy "forbidden band" has structure, which is known as vibronic structure. The structure arises from the fact that vibrational distortions of the molecule lead to coupling of the weak L band to the stronger B band. This is shown in Figure 5, which shows the extinction coefficient of tryptophan.

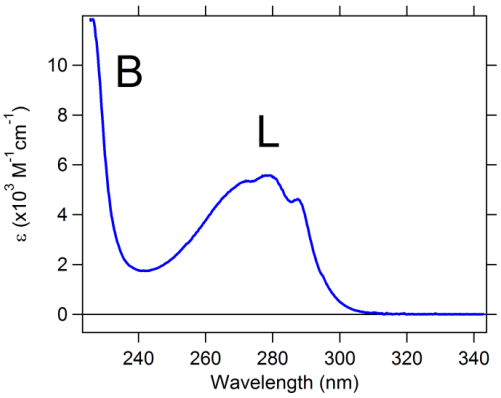

Figure 5 Absorption spectrum of tryptophan.

The emission spectrum of tryptophan is shown along with the absorption spectrum in Figure 6.

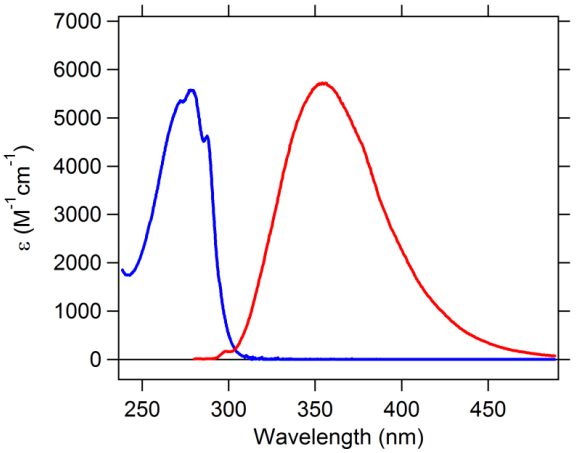

Figure 6 Tryptophan absorption (blue) and fluorescence (red).

At first, it may appear that the mirror image relationship is not obeyed. The red-colored emission spectrum has significantly different shape, i.e. it is much broader than the absorption spectrum. However, this different is an artifact due to the fact that we have plotted both absorption and emission as a function of wavelength, λ, rather than wave number, $\tilde{\nu}$. If we convert to units of cm^{-1}, the appearance of these data is shown in Figure 7.

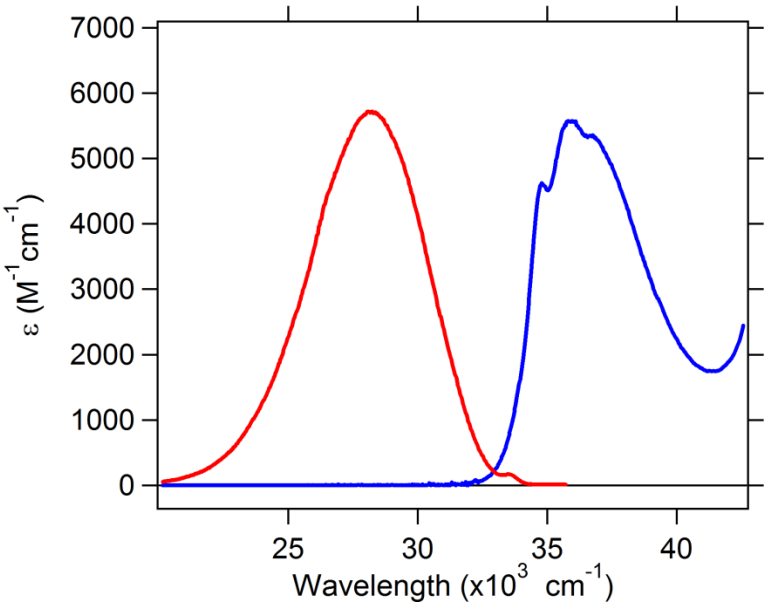

Figure 7. Absorption and emission spectra of tryptophan plotted as a function of wave number.

There is still some difference owing to the apparent broadening of the emission line shape relative to the absorption line shape. This occurs due to rapid dephasing processes in the excited state that give rise to broadened lines in the emission spectrum, relative to the absorption spectrum, which is initiated from the ground state. The absorption and fluorescence data for tryptophan were obtained from the resource known as PhotochemCAD. For more information on this resource students should consult the publication, H. Du, R. A. Fuh, J. Li, A. Corkan, J. S. Lindsey, "PhotochemCAD: A computer-aided design and research tool in photochemistry," *Photochemistry and Photobiology*, 68, 141-142, 199

The wavelength and intensity of tryptophan emission is sensitive to hydrogen bonding and hydrophobicity. If a protein unfolds, for example, there will be a large change in the fluorescence yield and fluorescence wavelength. Figure 8 shows the example of a folding study of the enzyme, caspase 3. Caspases are cysteine proteases that are activated during apoptosis. As with other proteases they have an inactive form, the zymogen form, and an active form. Splicing of caspases to remove a short peptide, called a pro-peptide, is required to initiate their function in controlled cell death. Shown in the figure is the structure of caspase-1. Note that the structure indicates that two subunits have been cleaved and are intermingled. This type of fold following removal of the pro-peptide produces the active form of the enzyme.

One can study the folding of the protein by monitoring its unfolding as the concentration of urea is increased. This is shown in Figure The tryptophan fluorescence wavelength changes as a function of the temperature. Of course, the interpretation of such wavelength changes depends on experience, but the significant point is that the changes in wavelength are sensitive to the environment so that protein unfolding can be successfully followed in an experiment. In this particular case, the data were interpreted to indicate that there are two folding intermediates. One of them consists of monomer caspase and one of them of dimer caspase protein.

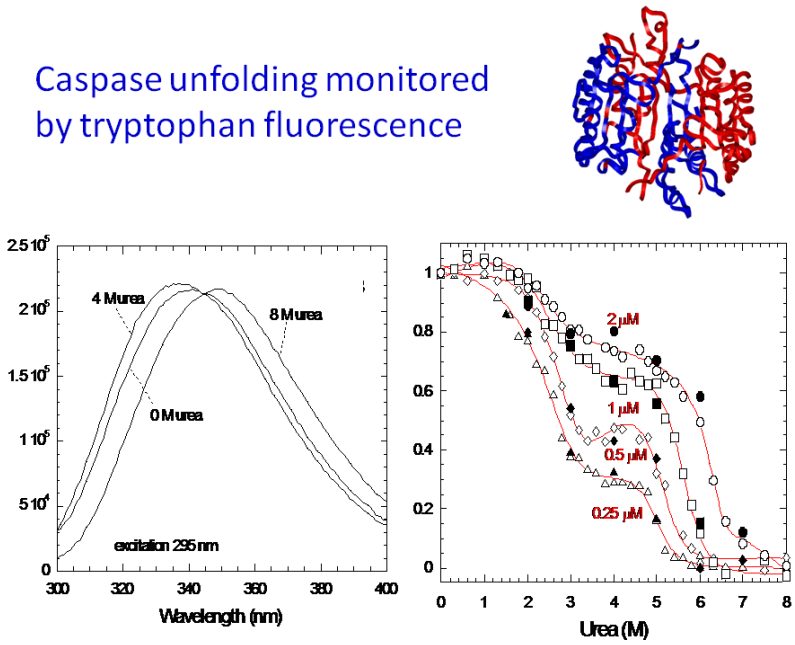

Figure 8 Study of the unfolding of caspase using

tryptophan fluorescence to monitor protein structure.

Data obtained courtesy of the laboratory of Prof. Clay Clark, NCSU, Biochemistry.

Green fluorescent protein

The green fluorescent protein (GFP) is found in a jellyfish that lives in the cold waters of the north Pacific. The jellyfish contains a bioluminescent protein-- aequorin--that emits blue light.

Green fluorescent protein converts this light to green light, which is what we actually see when the jellyfish lights up. Solutions of purified GFP look yellow under typical room lights, but when taken outdoors in sunlight, they glow with a bright green color. The protein absorbs ultraviolet light from the sunlight, and then emits it as lower-energy green light.

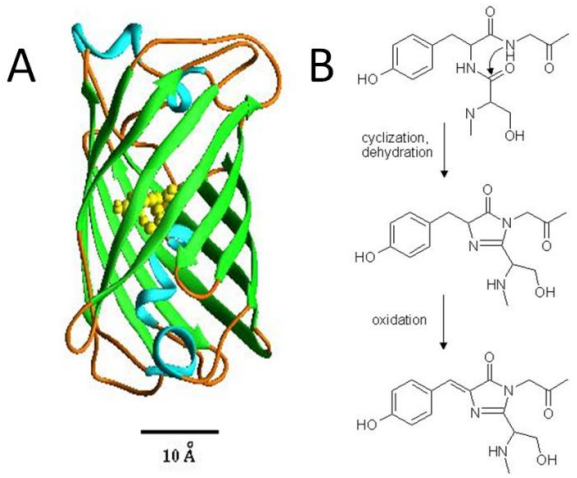

Figure 9. A. Overall structure of green fluorescent protein.

B. Sequence of reactions leading to the formation of the fluorophore.

GFP is useful in scientific research, because it allows us to look directly into the inner workings of cells. It is easy to see where GFP is at any given time: you just have to shine UV light, and any GFP will glow bright green. So the trick is to attach GFP to any object that you are interested in watching. The structure of GFP (Figure 9A) is a β-barrel, with the GFP chromophore in the center of the cylindrical fold. The remarkable property of GFP is that the chromophore forms spontaneously in any cell where GFP is expressed and can fold. Following protein folding, several chemical transformations occur: As shown in Figure 9B, the glycine forms a chemical bond with the serine, forming a new closed ring, which then spontaneously dehydrates. Then, over the course of an hour or so, oxygen from the surrounding environment attacks a bond in the tyrosine, forming a new double bond and creating the fluorescent chromophore. Since GFP makes its own chromophore, it is perfect for genetic engineering. You don't have to worry about manipulating any strange chromophores; you simply engineer the cell with the genetic instructions for building the GFP protein, and GFP folds up by itself and starts to glow.

The reporter gene technology uses GFP as an indicator of gene expression. As shown in Figure 10, the GFP gene is placed next to a gene of interest. Then when the gene of interest is expressed, the cells will also express GFP. An example shown in Figure 10 comes from research into the development of the nematode, *C. elegans*. As genes are expressed during *C. elegans* development in genetically modified organisms, different regions of the nematode show fluorescence from GFP.

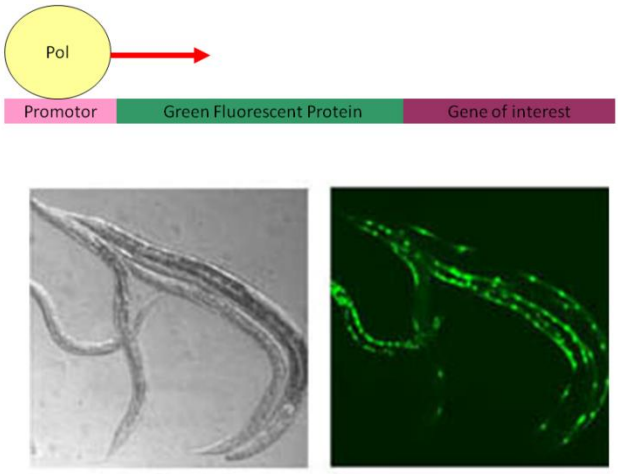

Figure 10 Illustration of the reporter gene concept.

2.1.4 Fluorescence quenching and energy transfer

The quantum yield gives the intrinsic fraction of the molecules that decay by a emitting light. In addition, the fluorescence emission can be further quenched by:

1. Collisional quenching – molecular collisions in solution
2. Intersystem crossing – conversion from singlet to triplet
3. Electron transfer – $^{1}DA \rightarrow D^{+}A^{-}$
4. Energy transfer – emission is transferred to an acceptor

Fluorescence quenching can be both beneficial and a source of error in experiments. Since fluorescence is subject to quenching, one must be careful to account for any possible fluorescence quenching that may occur during an experiment. However, the intentional addition of quenchers can be used to monitor the accessibility of fluorophores, and is thus a useful method for determining the location of fluorophores in a cell. Collisional quenching is a function of concentration, and is found in all solutions. This type of quenching can be minimized by keeping the concentration of fluorophores low. Typically, it is best to work in the micromolar range or lower. Intersystem crossing occurs due to the "heavy atom effect". Halogens like bromine and iodine, metals, and other elements, including heavy noble gases such as Xenon can give rise to spin flips that change the singlet excited state to a triplet excited state. Since fluorescence is emission from the singlet excited state, the singlet→triplet conversion, known as intersystem crossing, causes a decrease the fluorescence quantum yield. Electron transfer occurs when electron acceptors are in solution. The loss of an electron from a molecular excited state leads to a reduction in the fluorescence quantum yield. Energy transfer is similar, but the energy transfer process can lead to fluorescence from another molecule. Energy transfer is very useful in biomolecular studies since it is a strong function of the distance between the donor and acceptor. Thus, energy transfer can be used to determine whether there are changes in the distance of the donor and acceptor on the nanometer length scale. It is a molecular ruler.

Stern-Volmer quenching

The Stern-Volmer equation is:

$$\frac{\Phi_0}{\Phi} = 1 + k_q \tau_{obs}[Q] \tag{4.1}$$

k_q is the quenching rate constant, τ_{obs} is the observed lifetime in the absence of quencher, [Q] is the quencher concentration. An example of quenching is shown in Figure 11. The molecular EDANS (5-((2-aminoethyl)amino)naphthalene-1-sulfonic acid) is a fluorophore. When the energy is transferred to DABCYL (e-(4-dimethylaminophenylazobenzoyl) -L-lysine), there is no emission. DABCYL loses its energy exclusively by a non-radiative decay.

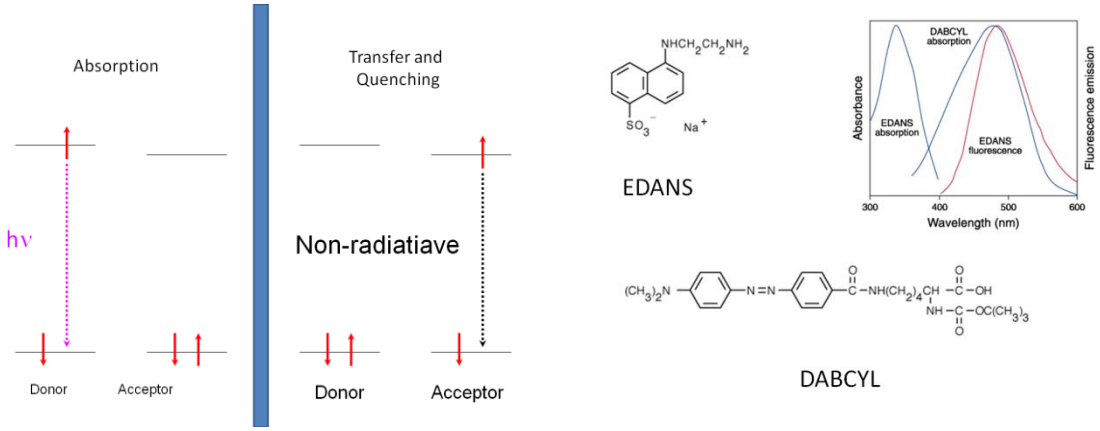

Figure 11. Quenching of radiation by energy transfer to a molecule with no emission.

2.1.5 Fluorescence resonant energy transfer (FRET)

Fluorescence resonance energy transfer (FRET) is a distance-dependent interaction between the electronic excited states of two dye molecules in which excitation is transferred from a donor molecule to an acceptor molecule without emission of a photon. FRET is dependent on the inverse sixth power of the intermolecular separation, making it useful over distances comparable with the dimensions of biological macromolecules. Thus, FRET is an important technique for investigating a variety of biological phenomena that produce changes in molecular proximity.

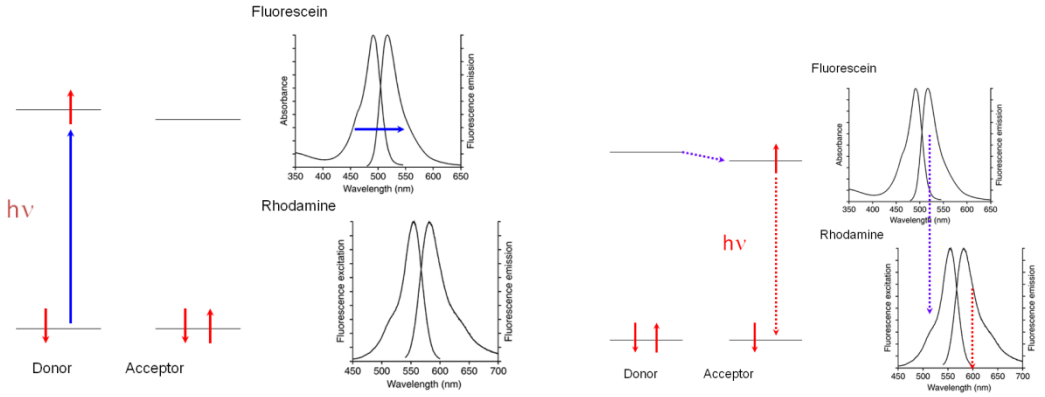

Figure 12 Energy transfer from one fluorophore (fluorescein) to another (rhodamine).

There are several requirements for energy transfer to occur. Because of the steep distance dependence, the donor and acceptor molecules must be in close proximity to one another (typically 10–100 Å). The absorption spectrum of the acceptor must overlap fluorescence emission spectrum of the donor. The donor and acceptor transition dipole orientations must be approximately parallel for maximum effect. The orientation dependence is $\sin^2\theta$, where θ is the angle between the transition dipole moments of the donor and acceptor.

The rate constant for energy transfer can be written in a simple form that emphasizes the distance dependence,

$$k_{DA} = (R_0/R)^6 \tag{4.2}$$

The $1/R^6$ distance dependence arises from the fact that energy transfer is a dipole-dipole interaction. Speaking more precisely, it is the interaction of the transition dipole moment on the donor and the acceptor that gives rise to the distance dependence. In Eqn. 7.2, the constant R_0 represents the distance at which the energy transfer efficiency is 50%:

$$R_0 = \sqrt[1/6]{\frac{8x\ 10^{-28}\kappa^2\Phi_f J(\lambda)}{\tau_{obs} n^4}} \tag{4.3}$$

In Eqn. 7.3 the following quantities are defined as:

κ - orientation factor (2/3 for an isotropic sample)

n - index of refraction

Φ_f - quantum yield of the donor

The spectral overlap integral is,

$$J(\lambda) = \int \varepsilon(\lambda) F_D(\lambda) \lambda^4 d\lambda \tag{4.4}$$

Two examples of so-called FRET pairs are given in Table 1

Table 1 Example of FRET pairs, including the distance of 50% FRET efficiency, R_o.

Donor	Acceptor	R_o (Å)
Fluorescein	Tetramethylrhodamine	55
IAEDANS	Fluorescein	46

2.1.6 Relaxed and resonance fluorescence: the time-dependent Stokes shift

Franck-Condon transitions are vertical transitions that occur from the ground to the excited state (or in emission from the excited state to the ground state). The pattern of vibronic bands is determined by the displacement of the excited state relative to the ground state potential energy surface as shown below. The overlap of the vibrational wavefunctions in the two states gives rise to the progression in terms such as ⟨0|0⟩, ⟨0|1⟩, ⟨0|2⟩ , ⟨0|n⟩ etc. We can represent this within the harmonic approximation

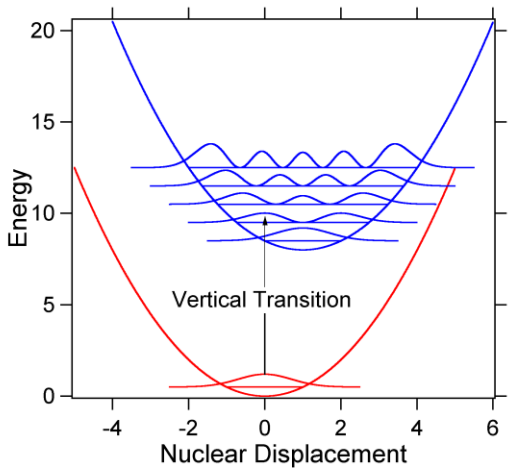

Figure 13. Vertical transition according to Franck-Condon principle that nuclei are frozen during an electron promotion to an excited state.

The shape of the absorption band is determined by the displacement of the potential energy surface in both the harmonic and realistic picture. In addition, we can identify two types of emission that can occur. The emission that occurs instantaneously following photoexcitation is called resonance fluorescence. It is shown below.

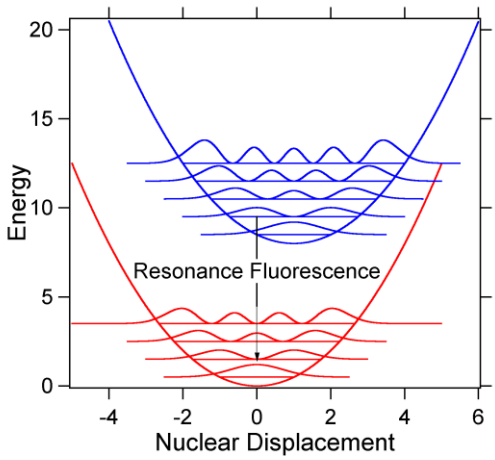

Figure 14. Resonance fluorescence or unrelaxed fluorescence that occurs prior to vibrational relaxation.

However, typical excited states live long enough that the vibrational energy of the excited state can be dissipated to the surroundings. This energy dissipation is known as vibrational relaxation. Following vibrational relaxation the populated vibrational modes in the excited state are in thermal equilibrium. If emission occurs from these modes the Franck-Condon vertical transition occurs from the equilibrium nuclear position of the excited state. This is called relaxed fluorescence and is shown below.

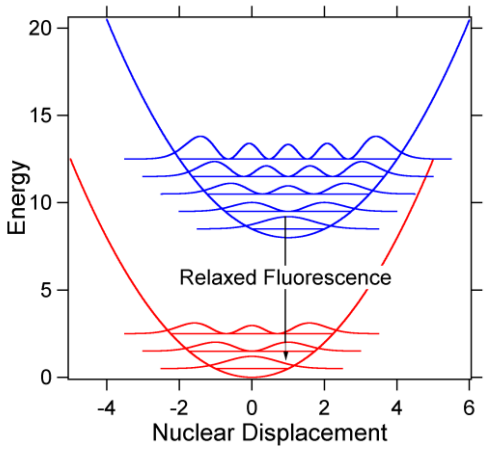

Figure 15. Relaxed fluorescence, which is normal fluorescence that occurs after vibrational relaxation.

Thus, resonance fluorescence occurs at the λ_{max} of the absorption spectrum but the λ_{max} of relaxed fluorescence is shifted. The shift between resonance and relaxed fluorescence is known as the Stokes shift. We usually quote the values of these shifts in cm^{-1} (wavenumbers) where wavenumbers = $10^7/\lambda(nm)$. The energy difference between resonance and relaxed fluorescence is called the reorganization energy. If we consider the coordinates of the molecule the reorganization energy is $\Delta^2/2$ for each Franck-Condon active mode. This is illustrated for a single vibrational mode below:

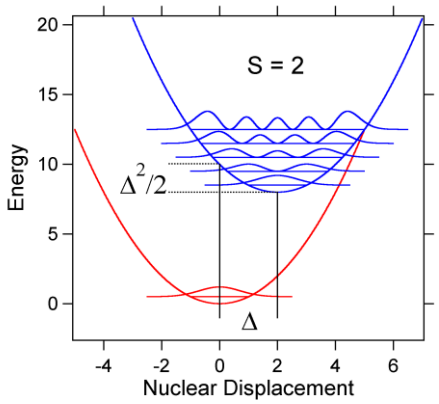

Figure 16 Depiction of an excited state displacement of S = 2.

For N coupled Franck-Condon active modes we have

$$E_{reorganization} = \sum_{i=1}^{N} \frac{\Delta_i^2}{2} \hbar\omega_i$$

for a classical model. The reorganization energy is the energy required to distort the molecule to the equilibrium nuclear position of the ground state along the excited state potential energy surface. This is equivalent to the energy required to distort the molecule to the equilibrium position of excited state along the ground state potential energy surface. Note that quantum-mechanically for each mode the energy required is S (the electron-phonon coupling constant) time the mode energy. Thus, for a quantum-mechanical model we have:

$$E_{reorganization} = \sum_{i=1}^{N} S_i \hbar\omega_i$$

The discussion thus far assumes that there is no excited state photochemistry. We treat photodissociation and predissociation phenomena below.

The Franck-Condon active modes will be totally symmetric modes of the molecule. This is because the excited state must have the same symmetry as the ground state in a Franck-Condon transition. Recall that since the transition is vertical the nuclei do not have a chance to change

their positions during the time of the electronic transition. This alone requires that the symmetry remain the same. Thus, the relevant vibrational modes depicted in the Figures above must be totally symmetric modes (belonging the symmetries A, A_1, A_{1g} etc. if the molecule has high enough symmetry to belong to one of the point groups in the character tables).

2.1.7 Summary of important aspects of fluorescence

The mirror image relationship in fluorescence spectra

The Franck-Condon factors are identical for absorption and emission. This means that the line shapes are related. However, for emission the energies are lower than the 0 → 0' transition, while those for absorption are greater than 0 →0' transition resulting a mirror image relationship for fluorescence spectra.

Measurement of the intrinsic fluorescence rate constant

The fluorescence emission rate constant, k_f, is a fundamental quantity that can be determined by measurement of two experimental quantities; the observed lifetime, k_{obs}, and the fluorescence quantum yield, Φ_f. A single measurement will not suffice because neither has enough information to uniquely determine k_f.

$$\Phi_f = \frac{k_f}{k_f + k_{nr}} \; ; \; k_{obs} = k_f + k_{nr}$$

Applications of fluorescence

Fluorescence is probably the most used kind of spectroscopy. Since fluorophores can be used to stain cells and as indicators in complex materials, one can measure local effects that include the dielectric function and the proximity of the fluorophores to quenchers. Quenchers include dyes that can undergo energy transfer. Fluorescence energy transfer can be applied as a molecular ruler to determine the distance between two fluorescence molecules in a sample. This has applications in polymer science, cell biology, DNA hybridization, protein folding, and single molecule detection.

2.2 Raman Spectroscopy

2.2.1 General Considerations

Raman spectroscopy is a light scattering experiment. The Raman effect depends on a change in polarizability of the molecule as radiation interacts with the molecule. The result is an inelastic light scattering process. This means that there is an exchange of energy between the light and the vibrations of the molecule. The frequency of the incident light is shifted and the molecule is left in an altered vibrational state. This is shown in the Figure below. The incident photon in this experiment is the v = 0 state and the scattering process leaves the molecule in the v = 1 state. The process shown in Figure 17 is a resonant Raman process since the incident light is in resonance with an absorptive transition. In this case the absorptive transition is Franck-Condon active. However, this FC activity is not required for a Raman process to be observed.

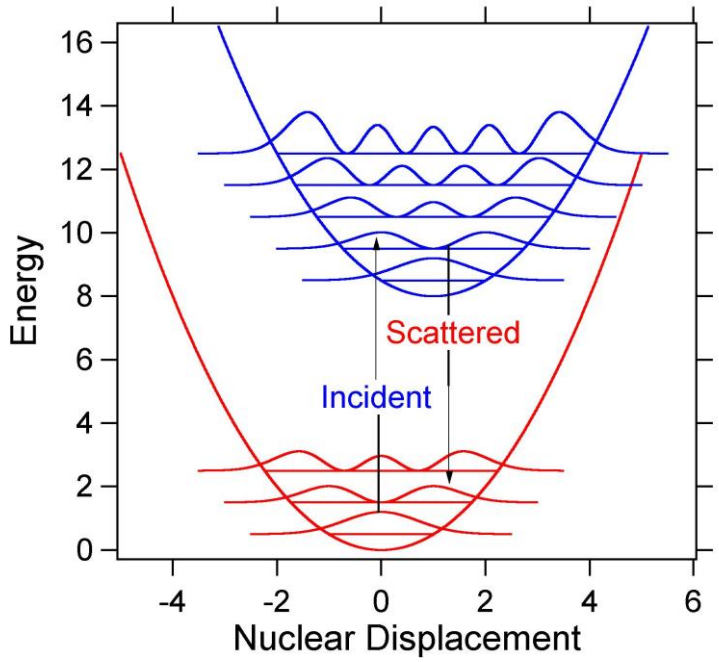

Figure 17. Illustration of the Raman effect.

In a typical Raman experiment polarized light impinges on the sample. The scattered light is detected using a spectrograph and an array detector to obtain a spectral region that will have peaks due to scattered intensity. The wavenumber shift of the peaks relative to the incident laser corresponds to the wavenumber of Raman active vibrational modes of the molecule. Figure 17 shows this effect for a specific resonant excited state excitation. If the laser wavenumber is not in resonance with an absorptive transition we can refer to the process as non-resonant Raman scattering. The further from resonance one tunes the laser, the lower is the Raman scattered intensity. Some books refer to "pre-resonant" Raman scattering when the laser frequency is near resonance. As will be shown below, one can always refer to non-resonant scattering as off-resonant (i.e. detuned from resonance).

2.2.2 Experimental configuration

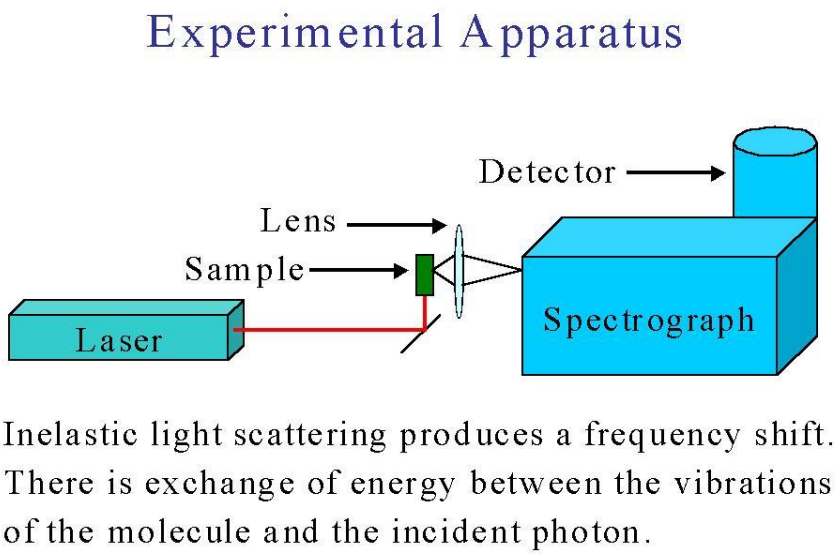

Figure 18. Raman scattering apparatus.

The scattered light can have two polarization components, parallel or perpendicular to the incident polarization. These polarizations are detected using an analyzing polarizer in front of the entrance slit of the spectrograph. The depolarization ratio is an important experimental observable and can give information that leads to vibrational mode assignment. In resonance Raman the intensity of the Raman scattered signal depends on the displacement of the potential energy surface of the excited state and on the excited state dynamics. This dependence is more complicated than the Franck-Condon factors in absorption spectroscopy.

The definition of polarization

For Z-polarized incident radiation we can detect scattered light using a 90 degree geometry shown below. The incident light propagates along the X-direction and the scattered light along the Y-direction. The uppercase letters here refer to the laboratory coordinate system.

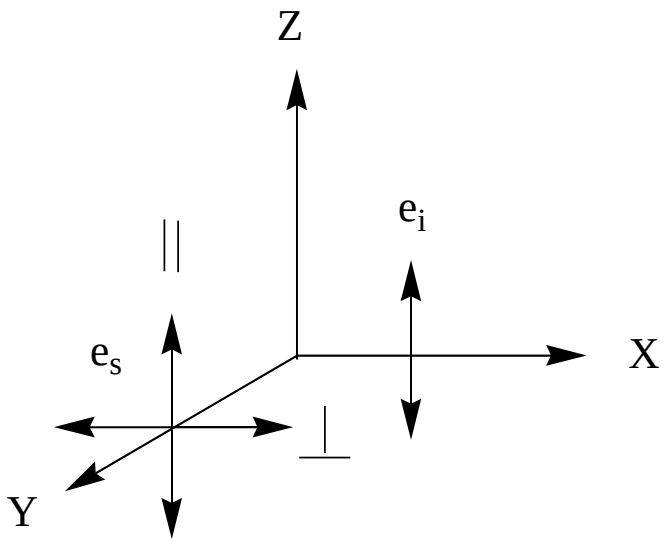

Figure 19. Definition of Raman polarization.

A polarization analyzer between the sample and the detector can be used to distinguish the polarization of scattered light. If the polarization in the scattered light is the same as the incident we refer to this as $I_{\parallel}$, I_{ZZ} or I_{pol}. If the polarization in the scattered light is perpendicular to the incident we refer to this as $I_{\perp}$, I_{XZ} or I_{dep}. The depolarization ratio ρ is $\rho = I_{dep}/I_{pol}$.

Collection of the light

Although we discuss the light scattered along Y it must be understood that light is in fact scattered into all directions. The solid angle of a sphere is 4π stearadians and the solid angle collected is $d\Omega$ where $d\Omega < 4\pi$. The f-number of a lens is the ratio of the diameter, D of the lens divided by its focal length, F. The two parameters needed to calculate the f-number are shown in Figure 20.

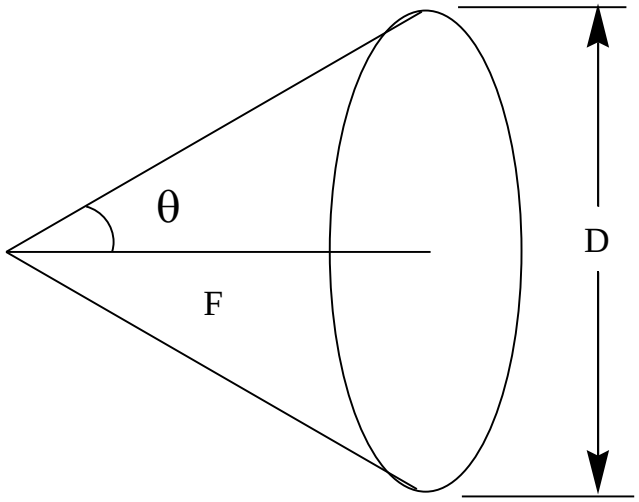

Figure 20. Illustration of collection optics for Raman scattered light.

The solid angle for collection can be calculated by integration to angle θ, which is determined by the ratio of the inverse tangent of the radius of the lens to the focal length.

$$\theta = arctan\left(\frac{Radius}{Focal\ length}\right) \tag{2.1}$$

Once this angle shown in Figure 20 has been calculated, the fraction of the light collected (relative to 4π stearadians) is given by,

$$\frac{1}{4\pi}\int_0^{2\pi} d\phi \int_0^{\theta} sin\theta' d\theta' \tag{2.2}$$

For example, if the f-number of a collection lens is 1, as shown in Figure 20, D = F and we have θ = arctan(1/2) = 26.56^o = 0.147π radians. The solid angle here can be calculated by integrating the differential volume element dΩ = dθ sinθ dϕ over the limits 0 to 2π and 0 to 0.147π.

$$\frac{1}{4\pi}\int_0^{2\pi} d\phi \int_0^{0.147\pi} sin\theta d\theta = (2\pi)[-cos\theta]_0^{0.147\pi} \approx 0.1$$

(2.3)

When we evaluate the integral over the limits shown we find that the second term is approximately 0.1. So the solid angle defined by f/1 collection optics is 0.4π stearadians. This arrangement leads to collection of about 10% of the total light scattered from the sample.

2.2.3 Definition of the differential cross section

The part of the cross-section $d\sigma$ that contributes to the detected scattered intensity is the ratio of the power at the detector dP to the incident intensity I_0. From $dP = I_0\, d\sigma$ we obtain

$$d\sigma = \frac{dP}{I_0}$$

(3.1)

The differential power dP is proportional to the solid angle d□ subtended by the detector. The scattered irradiance is the power per stearadian at the detector such that $dP = I_s d\square$. Note the difference between irradiance and intensity. Incident light $dP = I_0 d\square$ where I_0 is in units of W/cm^2. Scattered light $dP = I_s d\square$ where I_s is in units of W/sr. Thus, the differential cross section is

$$\frac{d\sigma}{d\Omega} = \frac{I_S}{I_0}$$

(3.2)

which has units of cm^2/sr. The Raman cross section is related to square of the projection of the polarizability tensor onto the incident e_i and scattered e_s directions in the laboratory frame.

$$\left(\frac{d\sigma}{d\Omega}\right) = \frac{16\pi^4 \nu_s^3 \nu_i}{c^4} (\hat{e}_s \cdot \alpha_{si} \cdot \hat{e}_i)^2$$

(3.3)

Or in terms of the angular frequency

$$\left(\frac{d\sigma}{d\Omega}\right) = \frac{\omega_s^3 \omega_i}{c^4} (\hat{e}_s \cdot \alpha_{si} \cdot \hat{e}_i)^2$$

(3.4)

Based on this definition we can determine the total Raman scattering cross section σ_R by

$$\sigma_R = \int \left(\frac{d\sigma}{d\Omega}\right) d\Omega = \int_0^{2\pi} d\phi \int_0^{\pi} \left(\frac{d\sigma}{d\Omega}\right) sin\theta d\theta \tag{3.5}$$

2.2.4 Symmetry and Raman activity

The transition polarizability is a tensor. The transition polarizability tensor can be written as,

$$\alpha = \begin{pmatrix} \alpha_{xx} & \alpha_{yx} & \alpha_{zx} \\ \alpha_{xy} & \alpha_{yy} & \alpha_{zy} \\ \alpha_{xz} & \alpha_{yz} & \alpha_{zz} \end{pmatrix} \tag{4.1}$$

In form this has the appearance of the ground state polarizability tensor. As is evident in 3.34, the only difference between transition polarizability and ground state polarizability is the final state |f>, which is the same as the initial state in the ground state polarizability and is different by one or more vibrational quanta in the transition polarizability. Thus, the elements of the transition polarizability tensor can be symmetry, α_{xx}, α_{yy}, or α_{zz} or non-totally symmetric, α_{xy}, α_{xz}, or α_{yz}.

Normal modes of vibration can be analyzed in terms of symmetry in order to assign Raman spectra. Franck-Condon active modes are totally symmetric. These modes can be Raman active since vibration along the normal mode coordinates gives rise to a transition polarizability as required by the Kramers-Heisenberg-Dirac model described in Chapter 12. In molecules of high symmetry, the totally symmetric modes can be identified in the character table as those modes that contain x^2, y^2 and z^2. Depending on the symmetry of the molecule, the total symmetric mode may contain, $x^2 + y^2 + z^2$ (O_h and T_d), $x^2 + y^2$ and z^2 (D_{4h}) or x^2, y^2 and z^2 (lower symmetry point groups). The relationship between x^2, y^2 and z^2 ultimately determines the depolarization discussed in Section 2.1 (see also 4). Examination of the character tables shows that infrared and Raman active modes are mutually exclusive in molecules with a center of symmetry (i.e. molecules that contain an inversion center, *i*). In molecules of lower symmetry, that do not contain the symmetry operation, *i*, vibrational modes can be both infrared and Raman active.

Non-totally symmetric vibrational modes can be Raman active provided that they contribute to changes in the polarizability tensor. In the character tables, these are the modes that transform as xz, xy and yz.

2.2.5 The depolarization ratio

The depolarization ratio is defined experimentally as the ratio of the perpendicular to parallel scattered radiation. Thus,

$$\rho = \frac{I_{\perp}}{I_{\parallel}} \tag{5.1}$$

in terms of intensity or

$$\rho = \frac{\left(\frac{\partial\sigma}{\partial\Omega}\right)_{\perp}}{\left(\frac{\partial\sigma}{\partial\Omega}\right)_{\parallel}} \tag{5.2}$$

in terms of the differential scattering cross sections. The depolarization ratio can be used to correct the Raman scattering cross section for orientation. It can be shown that

$$\left(\frac{d\sigma}{d\Omega}\right)_{\theta,\phi} = \left\{1 - \left(\frac{1-\rho}{1+\rho}\right) cos^2\theta\right\}\left(\frac{d\sigma}{d\Omega}\right)_{90^o} \tag{5.3}$$

and the Raman scattering cross section is

$$\sigma_R = \frac{8\pi}{3}\left(\frac{1+2\rho}{1+\rho}\right)\left(\frac{d\sigma}{d\Omega}\right)_{90^o} \tag{5.4}$$

Orientation averaging of the depolarization ratio

Thus far we have considered the elements of the transition polarizability tensor in the molecular frame x, y, and z. In a Raman experiment we measure the scattering in the lab frame X, Y, and Z. The scattering signal is the average of all molecular orientations in the lab frame. Traditional methods of carrying out the orientation averaging involve the use of direction cosines.

For a rank 2 tensor (e.g. transition polarizability) we can write down three rotational invariants, Σ^J, that are linear combinations of the α_M^J that are independent of reference frame. These are

$$\Sigma^J = \sum_{M=-J}^{J} \left(\alpha_M^J\right)^2$$

(5.3)

where J = 0, 1, 2… and M = 0 , $\pm$ 1 ,…, $\pm$ J. Each Σ^J is called an invariant because it is independent of orientation. The length of a vector is independent of its orientation. That is the same thing as saying that for the vector $\boldsymbol{\mu}$, the combination $\mu_x^2 + \mu_y^2 + \mu_z^2$ is a rotational invariant. A second rank tensor has three invariants,

$$\Sigma^0 = \frac{1}{3}\left(\alpha_{xx} + \alpha_{yy} + \alpha_{zz}\right)^2$$

$$\Sigma^1 = \frac{1}{2}\left(\left(\alpha_{xy} - \alpha_{yx}\right)^2 + (\alpha_{xz} - \alpha_{zx})^2 + \left(\alpha_{zy} - \alpha_{yz}\right)^2\right)$$

$$\Sigma^2 = \frac{1}{2}\left(\left(\alpha_{xy} + \alpha_{yx}\right)^2 + (\alpha_{xz} + \alpha_{zx})^2 + \left(\alpha_{zy} + \alpha_{yz}\right)^2\right)$$
$$+ \frac{1}{3}\left(\left(\alpha_{xx} - \alpha_{yy}\right)^2 + \left(\alpha_{yy} - \alpha_{zz}\right)^2 + (\alpha_{zz} - \alpha_{xx})^2\right)$$

(5.4)

The invariants are

Σ^0 isotropic part

Σ^1 anti-symmetric anisotropy

Σ^2 symmetric anisotropy

The isotropic part of the polarizability is proportional to the square of the trace of the polarizability tensor $\Sigma^0 = (\mathrm{Tr}\alpha)^2/3$. The trace of tensor α (written as Trα) is the sum of diagonal elements of the tensor. Therefore, Σ^2 represents the deviation of the polarizability from spherical symmetry. The lab frame components $|a_{ZZ}|^2$ and $|a_{XZ}|^2$ can be written as linear combinations of the invariants.

$$(\alpha_{ZZ})^2 = \frac{1}{3}\Sigma^0 + \frac{2}{15}\Sigma^2$$

$$(\alpha_{XZ})^2 = \frac{1}{6}\Sigma^1 + \frac{1}{10}\Sigma^2$$

(5.5)

The depolarization ratio is

$$\rho = \frac{(\alpha_{XZ})^2}{(\alpha_{ZZ})^2}$$

(5.6)

assuming the scattering geometry shown above. Using the invariants the depolarization ratio is

$$\rho = \frac{5\Sigma^1 + 3\Sigma^2}{10\Sigma^0 + 4\Sigma^2}$$

(5.7)

2.2.6 The depolarization ratio in non-resonant Raman scattering

The form of α in the molecular frame depends on the symmetry of the vibration. For non-resonant Raman the polarizability tensor is symmetric and therefore the anti-symmetric anisotropy Σ^1 is zero. Inspection of the anti-symmetric anisotropy shows that it is zero when $\alpha_{\rho\sigma} = \alpha_{\sigma\rho}$. Σ^2 depends on non-zero off diagonal terms and on differences in the diagonal terms. It is not necessarily zero in non-resonant Raman scattering.

Totally symmetric modes

The polarzability tensor for a totally symmetric vibrational mode preserves this symmetry. These are the modes that we think of a Franck-Condon active modes in absorption spectroscopy. The Cartesian Raman tensor for any totally symmetric mode is of the form:

$$\alpha = \begin{pmatrix} a & 0 & 0 \\ 0 & b & 0 \\ 0 & 0 & c \end{pmatrix}$$

(6.1)

For molecules with spherical symmetry a = b = c.

Symmetric top molecules have two equal components, so a = b ≠ c.

Asymmetric top molecules have a ≠ b ≠ c.

We can show this in the following simplified model, which we will assume that the small tensor elements are equal to zero. We can represent the three possible Raman tensors in this approximation as follows.

$$\begin{pmatrix} \alpha & 0 & 0 \\ 0 & \alpha & 0 \\ 0 & 0 & \alpha \end{pmatrix} \qquad \begin{pmatrix} \alpha & 0 & 0 \\ 0 & \alpha & 0 \\ 0 & 0 & 0 \end{pmatrix} \qquad \begin{pmatrix} \alpha & 0 & 0 \\ 0 & 0 & 0 \\ 0 & 0 & 0 \end{pmatrix}$$

Spherically symmetric | Symmetric top | Asymmetric top

For example, the Raman polarizability tensor for any totally symmetric mode of a totally symmetric molecule (CCl_4 or SF_6) has three equivalent diagonal components and so

$$\alpha = \begin{pmatrix} a & 0 & 0 \\ 0 & a & 0 \\ 0 & 0 & a \end{pmatrix} \tag{6.2}$$

Thus, $\Sigma^1 = \Sigma^2 = 0$ and $\rho = 0$. It is often convenient to write out the totally and non-totally symmetric part of the polarizability,

$$\alpha = \bar{\alpha} \begin{pmatrix} 1 & 0 & 0 \\ 0 & 1 & 0 \\ 0 & 0 & 1 \end{pmatrix} + \beta \tag{6.3}$$

where we define the average polarizability:

$$\bar{\alpha} = \frac{Tr\alpha}{3} = \frac{\left(\alpha_{xx} + \alpha_{yy} + \alpha_{zz}\right)}{3} \tag{6.4}$$

and the tensor β is the anisotropy of the polarizability:

$$\beta = \begin{pmatrix} (\alpha_{xx} - \bar{\alpha}) & \alpha_{yx} & \alpha_{zx} \\ \alpha_{xy} & (\alpha_{yy} - \bar{\alpha}) & \alpha_{zy} \\ \alpha_{xz} & \alpha_{yz} & (\alpha_{zz} - \bar{\alpha}) \end{pmatrix}$$

(6.5)

This equation assumes that the Raman tensor is symmetric (and is only valid for non-resonant Raman scattering). Non-symmetric molecules β can be non-zero even for totally symmetric modes.

On the other hand if a = b ≠ c, which corresponds to planar molecules such as benzene and metalloporphyrins, which usually means $\alpha_{xx} + \alpha_{yy} = \alpha$ and $\alpha_{zz} = 0$. We have

$$\Sigma^0 = \frac{1}{3}\left(\alpha_{xx} + \alpha_{yy}\right)^2 = \frac{4\alpha^2}{3}$$

$$\Sigma^1 = 0$$

$$\Sigma^2 = \frac{1}{3}\left(\left(\alpha_{yy}\right)^2 + (\alpha_{xx})^2\right) = \frac{2\alpha^2}{3}$$

The result is

$$\rho = \frac{3\Sigma^2}{10\Sigma^0 + 4\Sigma^2} = \frac{3\left(\frac{2\alpha^2}{3}\right)}{10\left(\frac{4\alpha^2}{3}\right) + 4\left(\frac{2\alpha^2}{3}\right)} = \frac{1}{8}$$

(6.6)

Finally, for asymmetric top molecules we have a ≠ b ≠ c, which be approximated in the simplest case as means $\alpha_{xx} = \alpha$ and $\alpha_{zz} = \alpha_{yy} = 0$. We have

$$\Sigma^0 = \frac{1}{3}(\alpha_{xx})^2 = \frac{\alpha^2}{3}$$

$$\Sigma^1 = 0$$

$$\Sigma^2 = \frac{1}{3}((\alpha_{xx})^2 + (\alpha_{xx})^2) = \frac{2\alpha^2}{3}$$

The result is

$$\rho = \frac{3\Sigma^2}{10\Sigma^0 + 4\Sigma^2} = \frac{3\left(\frac{2\alpha^2}{3}\right)}{10\left(\frac{\alpha^2}{3}\right) + 4\left(\frac{2\alpha^2}{3}\right)} = \frac{1}{3} \tag{6.7}$$

Thus, we see that the depolarization ratio for totally symmetric modes varies from 0 to 1/3 depending on the relative magnitude of the diagonal tensor elements, α_{xx}, α_{yy}, and α_{zz},.

Non-totally symmetric modes

Non-totally symmetric modes are the modes that responsible for vibronic coupling or Herzberg-Teller coupling in absorption spectroscopy. For these modes Tr α vanishes and only β contributes to the non-resonant Raman scattering cross section. Since Tr α vanishes for non-totally symmetric modes we also have $\Sigma^0 = 0$. For non-resonant Raman, we assume that $\alpha_{\sigma\rho} = \alpha_{\rho\sigma}$, so that we can write,

$$\Sigma^0 = 0$$

$$\Sigma^1 = 0$$

$$\Sigma^2 = 2\left(\left(\alpha_{xy}\right)^2 + (\alpha_{xz})^2 + \left(\alpha_{yz}\right)^2\right)$$

From which we see that only Σ^2 is non-zero. The depolarization ratio then becomes,

$$\rho = \frac{5\Sigma^1 + 3\Sigma^2}{10\Sigma^0 + 4\Sigma^2} = \frac{3\Sigma^2}{4\Sigma^2} = \frac{3}{4} \tag{6.8}$$

Thus, we see that the depolarization ratio is equal to ¾ regardless of the precise symmetry of the non-totally symmetric modes. In non-resonant Raman scattering ρ is never larger than 3/4.

2.2.7 Raman scattering results from a transition polarizability

In the molecular frame of reference the transition polarizability can be expressed using the Kramers-Heisenberg-Dirac (KHD) expression

$$\left(\alpha_{\rho\sigma}\right)_{if} = \frac{1}{\hbar}\left\{\sum_{n}\left(\frac{\langle i|\mu_\rho|n\rangle\langle n|\mu_\sigma|f\rangle}{\omega + \omega_{nf} + i\Gamma_{\mathrm{n}}} - \frac{\langle i|\mu_\sigma|n\rangle\langle n|\mu_\rho|f\rangle}{\omega - \omega_{ni} - i\Gamma_{\mathrm{n}}}\right)\right\} \equiv \langle i|\alpha_{\rho\sigma}|f\rangle \tag{7.1}$$

The transition polarizability $\alpha_{\rho\sigma}$ is expressed as a function of the incident radiation frequency ω_0. The transition polarizability is a Cartesian tensor where ρ and σ are direction x,y,z in the molecular frame. The first term is an anti-resonant term and the second term is a resonant term. Both terms are important for off-resonance or non-resonant Raman scattering. Only the second term is important for resonant Raman scattering. In the resonant term the energy denominator would approach infinity were it not for the damping term $i\Gamma_n$. Γ_n arises due to the finite lifetime of the intermediate state. The shorter the lifetime in the intermediate state, the smaller the Raman cross section. This is particularly important for resonant Raman scattering. The states involved can be defined in terms of all 3N - 6 vibrational modes by writing:

$$|i> = |\phi_g(q;Q)> |\chi_{gv}(Q_1)\chi_{gv}(Q_2)\ldots.\chi_{gv}(Q_{3N-6})>$$

$$|n> = |\phi_e(q;Q)> |\chi_{ev_1'}(Q_1)\chi_{ev_2'}(Q_2)\ldots.\chi_{ev_{3N-6}'}(Q_{3N-6})>$$

$$|f> = |\phi_g(q;Q)> |\chi_{gv''}(Q_1)\chi_{gv''}(Q_2)\ldots.\chi_{gv''}(Q_{3N-6})> \tag{7.2}$$

Notice that only one of the modes actually changes its quantum number in the Raman process (the first one labeled by Q_1). The remaining modes end up in the same state that they started in. The potential energy surface is a 3N - 6 dimensional surface and the Raman process is occuring along only one dimension. This can be represented as follows:

$v \rightarrow v''$

$\{v_1,v_2,\ldots v_{3N-6}\} \rightarrow \{v''_1,v_2,\ldots v_{3N-6}\}$

The quantum numbers v and v" represent the two states shown.

As shown in Eqn. 7.1, polarizability arises due to state mixing. The KHD expression shows mixing of the ground state with one or more higher electronic states. In other words the states |i⟩ and |f⟩ refer to two different vibrational states in the ground electronic state. The states |n⟩ refer to a set of vibrational states in one or more electronic state. When we consider resonant Raman scattering we will consider resonance with a single electronic state. For non-resonant Raman scattering the intermediate must be a superposition. In practice, we cannot calculate the magnitude of the non-resonant Raman cross section due to the complex nature of a superposition state. We can, however, determine the polarization, symmetry properties, and selection rules for non-resonant Raman scattering.

2.2.8 Introduction of the vibronic coupling operator: approach to resonance

If the frequency of exciting radiation is far removed from the resonant frequency, i.e. $\omega_0 \ll \omega_{eg}$ then vibrational energy terms in the energy denominator can be ignored compared to $\omega_0 - \omega_{eg}$ and $\omega_0 + \omega_{eg}$. The transition polarizability becomes

$$\left(\alpha_{\rho\sigma}\right)_{0v''} = \frac{1}{\hbar}\left\{\sum_{ev}\left(\mu_{ge}^{0}\right)_{\rho}\left(\mu_{ge}^{0}\right)_{\sigma}\left(\frac{\langle 0|v'\rangle\langle v'|v''\rangle}{\omega_0 + \omega_{eg}} - \frac{\langle 0|v'\rangle\langle v'|v''\rangle}{\omega_0 - \omega_{eg}}\right)\right\} \tag{8.1}$$

The quantities ⟨0|v⟩ and ⟨v|v"⟩ are vibrational overlaps. The square of a vibrational overlap is a Franck-Condon factor so the Raman excitation profile bears a defined relationship to the absorption spectrum. Here the v quantum numbers refer to the intermediate state vibrational energy levels. Since excitation is off-resonance there are in pricnciple many vibrational and electronic states that can contribute. The above approach is a sum-over-states approach. We can use the closure relation $\Sigma_v|v\rangle\langle v| = 1$ to simplify the expressions.

$$\left(\alpha_{\rho\sigma}\right)_{0v''} = \frac{2}{\hbar}\left\{\sum_{ev}\left(\mu_{ge}^{0}\right)_{\rho}\left(\mu_{ge}^{0}\right)_{\sigma}\left(\frac{\delta_{0v''}}{\omega_{eg} - \omega_0}\right)\right\}$$

$$\left(\alpha_{\rho\sigma}\right)_{00} = \frac{2}{\hbar}\left\{\sum_{ev}\left(\mu_{ge}^{0}\right)_{\rho}\left(\mu_{ge}^{0}\right)_{\sigma}\left(\frac{1}{\omega_{eg} - \omega_0}\right)\right\} \tag{8.2}$$

The bottom equation describes Rayleigh scattering. The initial and final vibrational states are the same in Rayleigh scattering. There are no selection rules. All molecules are active Rayleigh scatterers. The Kroenecker delta in the top equation is $\delta_{0v''} = \langle 0|v''\rangle$ where $\delta_{0v''} = 0$ if $0 \neq v''$. Thus the first term and the second term are the same here. This means that non-resonant Raman scattering will not occur within the Condon approximation. This observation, first made by Albrecht, represents a paradox for Raman scattering. In reality the restriction that Raman scattering can only be observed for a breakdown of the Condon approximation is a result of the simplicity of the model. We can call this breakdown, Albrecht's paradox. Obviously, totally symmetric modes are observed in non-resonant Raman spectra of molecules.

In order to explain non-resonant Raman scattering within the formalism of Eqn. 8.2, we must consider the coordinate dependence to the transition dipole moment, e.g. expand the transition dipole moment in a power series

$$\mu_{ge}(Q) = \mu_{ge}^{0} + \sum_{i=1}^{3N-6} \left(\frac{\partial \mu_{ge}}{\partial Q}\right)_0 Q_i \tag{8.3}$$

and keep only the first term we find that the coordinate dependence of the transition moment can play a role. The reason for this is that even though $\langle 0|v''\rangle = 0$ for $0 \neq v''$, in general $\langle 0|Q|v''\rangle$ does not need to be zero. Thus, for Raman scattering to be allowed we use the linear term above and make the substitution

$$\mu_{ge}^{0}\langle 0|v''\rangle \rightarrow \left(\frac{\partial \mu_{ge}}{\partial Q}\right)_0 \langle 0|Q|v''\rangle \tag{8.4}$$

The transition polarizability is

$$\left(\alpha_{\rho\sigma}\right)_{0v''} = \frac{1}{\hbar}\left\{\sum_{e}\left(\frac{\left(\mu_{ge}^{0}\right)_{\rho}\left(\frac{\partial \mu_{ge}}{\partial Q}\right)_{\sigma}\langle 0|Q|v''\rangle}{\omega_0 + \omega_{eg}} - \frac{\left(\mu_{ge}^{0}\right)_{\sigma}\left(\frac{\partial \mu_{ge}}{\partial Q}\right)_{\rho}\langle 0|Q|v''\rangle}{\omega_0 - \omega_{eg}}\right)\right\} \tag{8.5}$$

The selection rules arise from the requirement that $\langle 0|Q|v''\rangle$ does not vanish. We can define a polarizability derivative such that the transition polarizability is

$$\left(\alpha_{\rho\sigma}\right)_{vv''} = \left(\frac{\partial \alpha_{\rho\sigma}}{\partial Q_i}\right)\langle v|Q_i|v''\rangle$$

(8.6)

where $\alpha_{\rho\sigma}$ is the polarizability derivative also called the derived polarizability. The terms $\alpha_{\rho\sigma}$ and $(\partial\alpha_{\rho\sigma}/\partial Q_i)$ are equivalent. For a harmonic oscillator $\langle v|Q|v''\rangle$vanishes except when v" = v± 1. Thus, the selection rule of $\Delta v = \pm 1$ applies to non-resonant Raman scattering as well as infrared spectroscopy (within the harmonic approximation).

2.2.9 Albrecht theory of resonant Raman Scattering

If the incident frequency ω_0 is in resonance with an electronic transition of the molecule the anti-resonant term (with $\omega_0 + \omega_{eg}$ in the denominator) can be neglected and only the resonant term contributes to Raman scattering. If we keep terms up to linear in Q, we may express the transition polarizability as a sum of two terms

$$\left(\alpha_{\rho\sigma}\right)_{vv''} = A_{v'v''} + B_{v'v''}$$

(9.1)

These terms are called the Albrecht A and B terms. The first of these terms arises from the Condon approximation. The Condon approximation states that there is no nuclear coordinate dependence to the wave function so that all terms in the expansion vanish except the μ_{ge}^0 term that does not depend on Q_i.

$$A_{v',v''} = \frac{1}{\hbar}\left\{\sum_{ev}\left(\mu_{ge}^0\right)_\rho\left(\mu_{ge}^0\right)_\sigma\left(\frac{\langle 0|v'\rangle\langle v'|v''\rangle}{\omega_{ev',gv} - \omega_0 - i\Gamma_{\mathrm{ev}}}\right)\right\}$$

(9.2)

In this expression the energy of an incident photon is equal to that of the energy difference between a ground state vibrational energy level gv' and an excited state level ev. The term $i\Gamma_{\mathrm{ev}}$ is a phenomenological damping term. This term arises from dephasing and lifetime broadening in the excited state levels. One can envision the contribution of Γ as an energy width to each of the excited state energy levels.

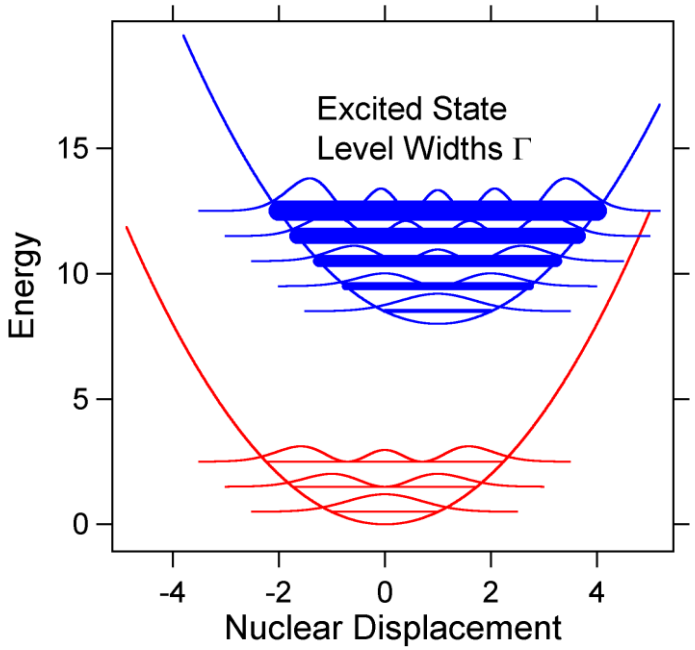

Figure 21 Depiction of the dependence of dephasing rate on the excited state quantum number.

The thickness of the blue excited state levels is dependent upon excited state lifetimes and dephasing processes. The various levels have different energy widths to illustrate the fact that the dephasing rate can depend on vibrational state. Without the dephasing rate Γ_{ev} the resonance term would approach when $\omega_{ev,gv'} = \omega_0$. The larger the dephasing terms $i\Gamma_{ev}$ the smaller the overall resonant Raman cross section. The terms $\langle v'|v\rangle$ and $\langle v|v''\rangle$ are Franck-Condon factors. In fact, these are the same Franck-Condon factors found in absorption spectroscopy. Just as in absorption spectroscopy there must be displacement along a normal mode coordinate upon electronic excitation in order for it to be Franck-Condon active.

The Albrecht B-term describes resonance Raman scattering of a vibronically active vibrational mode. In electronic absorption a vibronic mode is one which causes a transition to be allowed by distortion of the molecule to lower the symmetry. In resonant Raman scattering a vibronic mode has a resonance enhancement pattern that is different from a Franck-Condon active mode for the same reason. The Franck-Condon active modes are the totally symmetric modes of the molecule and the vibronic modes are the non-totally symmetry modes of the molecule. The B term is more complicated than the A term. In the A term the transition moment for the ground to excited state electronic transition μ_{ge} is contributes and in B-term scattering it is the terms in $(\partial\mu_{ge}/\partial Q_i)_0 Q_i$ that contribute. In Albrecht theory the B-term is given by,

$$B_{v',v''} = \frac{1}{\hbar}\left\{\sum_{e}\left(\frac{\left(\mu_{ge}^{0}\right)_{\sigma}\left(\frac{\partial \mu_{ge}}{\partial Q}\right)_{\rho}\langle 0|Q|v''\rangle}{\omega_{ev',gv} - \omega_{0} - i\Gamma_{\mathrm{ev}}}\right)\right\} \tag{9.4}$$

2.2.10 Polarization in resonant Raman scattering

Totally symmetric modes

The polarizability depends on the symmetry of the electronic transition. For example, in a z-polarized transition a totally symmetric A-term mode has only one non-zero tensor component, α_{zz}. From this consideration we can readily calculate that $\rho = 1/3$, as shown above for asymmetric top molecules. A doubly degenerate resonant electronic state (i.e. a state that x,y polarized such as in porphyrins) results in two equal diagonal tensor components, e.g. $\alpha_{xx} = \alpha_{yy}$, which leads to $\rho = 1/8$. If the electronic transition is triply degenerate (i.e. if the molecule is spherically symmetric such as SF_6) then $\alpha_{xx} = \alpha_{yy} = \alpha_{zz}$. In this case $\rho = 1/\infty = 0$. These examples show that the limiting cases for the depolarization ratio of totally symmetric modes are $0 \leq \rho \leq 1/3$.

Vibronic coupling and anomalous polarization in non-totally symmetric modes

Vibronic coupling of two states can lead to Raman tensors in which $\alpha_{\sigma\rho} \neq 0$, but $\alpha_{\sigma\sigma} = 0$. Such vibrational modes are non-totally symmetric. The origin of coupling via non-totally symmetric modes can be found in the Herzberg-Teller coupling between two states. As a molecule vibrates along a non-totally symmetric mode coupling is induced with other electronic states. This coupling results in enhancement at molecule geometries that are distorted from the equilibrium geometry. This is precisely what is described in the B-term of Albrecht theory. B term enhancement can also lead to anomalous polarization in which $\rho > 3/4$. Vibronic coupling of two states can lead to Raman tensors in which $\alpha_{\sigma\rho} \neq \alpha_{\rho\sigma}$. A nonzero value of Σ^1 can lead to a depolarization ratio of greater than 3/4.

Anomalous polarization can be explained as follows using the Herzberg-Teller approach. Suppose that the electronic transition g → e is x polarized and the transition g → r is y polarized leading to a Raman activity of the fundamental transition of a non-totally symmetric vibration of symmetry $\Gamma_v = \Gamma_x\Gamma_y$. The transition is resonant with $|e0\rangle$ and $|e1\rangle$ intermediate states. Herzberg-Teller coupling requires that vibronic coupling to state mix $|e0\rangle$ with $|r1\rangle$ and $|e1\rangle$ with $|r0\rangle$. The vibronic intermediate states are:

$$|e0>' = |e0> + \frac{\langle r1 \left| \left(\frac{\partial H}{\partial Q}\right) Q \right| e0\rangle}{\hbar\omega_{r1} - \hbar\omega_{e0}} |r1>$$

$$|e1>' = |e1> + \frac{\langle r0 \left| \left(\frac{\partial H}{\partial Q}\right) Q \right| e1\rangle}{\hbar\omega_{r0} - \hbar\omega_{e1}} |r0>$$

(10.1)

Using the above states to write the Albrecht B-term leads to the following xy and yx Raman tensor components:

$$\left(\alpha_{xy}\right)_{01} = \frac{1}{\hbar^2}\left\{\frac{\langle r0 \left| \left(\frac{\partial \mu_{ge}}{\partial Q}\right) \right| e1\rangle}{\omega_{r0} - \omega_{e1}} \frac{\left(\mu^0_{ge}\right)_x \left(\mu^0_{gr}\right)_y \langle 0|Q|1\rangle}{\omega_{e1,g0} - \omega_0 - i\Gamma_e}\right\}$$

$$\left(\alpha_{yx}\right)_{01} = \frac{1}{\hbar^2}\left\{\frac{\langle r1 \left| \left(\frac{\partial \mu_{ge}}{\partial Q}\right) \right| e0\rangle}{\omega_{r1} - \omega_{e0}} \frac{\left(\mu^0_{ge}\right)_x \left(\mu^0_{gr}\right)_y \langle 1|Q|0\rangle}{\omega_{e0,g0} - \omega_0 - i\Gamma_e}\right\}$$

(10.2)

The α_{xy} component dominates when the incident frequency is resonant with the g0 → e1 transition, while the α_{yx} component is resonant with the g0 → e0 transition. If the energy levels of the states e and r are well separated then the energy denominators are nearly equal:

$$\omega_{r0} - \omega_{e1} \approx \omega_{r1} - \omega_{e0}$$

(10.3)

If ω_0 is far from resonance then $\alpha_{xy} \approx \alpha_{yx}$. This is a non-resonant condition where the Raman tensor is symmetric, $\Sigma^1 = 0$, and $\rho = 3/4$. On the other hand, close to resonance with the 0-1 transition, we have $\alpha_{xy} >> \alpha_{yx}$ and for ω_0 close to the frequency of the 0-0 transition, $\alpha_{yx} >> \alpha_{xy}$. When the exciting radiation is midway between the 0-0 and 0-1 resonances, the relationship $\alpha_{xy} \approx -\alpha_{yx}$ results. This leads to $\Sigma^1 \neq 0$, while $\Sigma^0 = \Sigma^2 = 0$. At this frequency the depolarization ratio approaches infinity. Anomalous polarization was first observed in the vibronic bands of hemes.

Appendix. The integration of the rotational invariants in the molecular frame

Here we give an intuitive argument to explain the contributions of the various invariants to depolarization ratio. The crucial property of an invariant is that the excitation is independent of the orientation. Therefore, to determine the contribution to the polarization we only need to consider the interaction of the molecular polarizability with the X and Z polarized light waves in the laboratory frame. The totally symmetric invariant involves excitation and scattering from the same direction. for α_{ZZ}. Since the direction cosine from z in the molecular frame to Z in the lab frame is cosθ. The square of this value is

$$(\alpha_{ZZ})^2_{zz} = |e_z \cdot \alpha_{zz} \cdot e_z|^2 = \frac{(\alpha_{zz})^2}{4\pi} \int_0^{2\pi} d\phi \int_0^{\pi} \cos^2\theta \sin\theta d\theta = \frac{(\alpha_{zz})^2}{3}$$

We can show that similar relationships will hold for α_{xx} and α_{yy}, gives the rotational invariant, which in this case is the average excitation of all three

$$(\alpha_{ZZ})^2_{sym} = \frac{1}{3}\Sigma^0$$

Since each of the terms in this sum has the same properties with respect to the orientation average the total invariant is multiplied by the factor of 1/3 calculated above.

The off-diagonal terms are:

$$(\alpha_{ZZ})^2_{xz} = |e_z \cdot \alpha_{xz} \cdot e_z|^2 = \frac{(\alpha_{xz})^2}{4\pi} \int_0^{2\pi} \cos^2\phi d\phi \int_0^{\pi} \cos^2\theta \sin^2\theta \sin\theta d\theta = \frac{(\alpha_{xz})^2}{15}$$

Since the matrix is symmetric (by assumption)

$$(\alpha_{ZZ})^2_{zx} = |e_z \cdot \alpha_{zx} \cdot e_z|^2 = \frac{(\alpha_{zx})^2}{4\pi} \int_0^{2\pi} \cos^2\phi d\phi \int_0^{\pi} \cos^2\theta \sin^2\theta \sin\theta d\theta = \frac{(\alpha_{zx})^2}{15}$$

The second contribution to the symmetric anisotropy gives a similar value. Thus,

$$(\alpha_{ZZ})^2_{sym-aniso} = \frac{2}{15}\Sigma^2$$

For the totally symmetric contribution to the perpendicular component we find.

$$(\alpha_{XZ})^2_{xz} = |e_z \cdot \alpha_{xz} \cdot e_x|^2 = \frac{(\alpha_{xz})^2}{4\pi} \int_0^{2\pi} \cos^4\phi d\phi \int_0^{\pi} \sin^4\theta \sin\theta d\theta = \frac{(\alpha_{xz})^2}{20}$$

As above since there are two identical tensor elements $\alpha_{xz} = \alpha_{zx}$ that have this relationship, so the factor is 1/10.

$$(\alpha_{xz})^2_{sym-aniso} = \frac{1}{10}\Sigma^2$$

3. Reaction Kinetics

3.1 Michaelis-Menten kinetics

The rate of an enzyme catalyzed reaction in which substrate S is converted into products P depends on the concentration of the enzyme E even though the enzyme does not undergo any net change.

$$E + S \underset{k_{off}}{\overset{k_{on}}{\leftrightarrow}} ES \overset{k_{cat}}{\rightarrow} P + E \tag{1}$$

$$\frac{d[S]}{dt} = -k_{on}[E][S] + k_{off}[ES] \tag{2}$$

$$\frac{d[ES]}{dt} = k_{on}[E][S] - \left(k_{off} + k_{cat}\right)[ES] \tag{3}$$

$$\frac{d[P]}{dt} = k_{cat}[ES] \tag{4}$$

These rate equations comprise three processes:

Process 1. Bimolecular formation of the enzyme E and and substrate S: E + S → ES with rate of formation of $d[ES]/dt = k_{on}[E][S]$

Process 2. Unimolecular decomposition of the complex:

ES →E + S rate of decomposition of ES = $-k_{off}[ES]$

Process Formation of products and release from the enzyme: ES → P + E with rate of formation of $P = k_{cat}[ES]$

The rate law of interest is the formation of the product in terms of E and S.The enzyme substrate complex is formed transiently and can be approximated using the steady state approximation.

$$k_{on}[E][S] - \left(k_{off} + k_{cat}\right)[ES] \approx 0$$

(5)

The result of this approximation is

$$[ES] = \frac{k_{on}[E][S]}{k_{off} + k_{cat}}$$

(6)

In an experiment we know the total enzyme concentration $[E]_0$ and not the unbound enzyme [E].

The total concentration of enzyme $[E]_0 = [E] + [ES]$.

$$[ES] = \frac{k_{on}([E]_0 - [ES])[S]}{k_{off} + k_{cat}}$$

(7)

which rearranges to

$$[ES] = \frac{k_{on}[E]_0[S]}{k_{off} + k_{cat} + k_{on}[S]}$$

(8)

The rate of formation of product can be written where K_M is the Michaelis constant and k_{cat} is the maximum turnover number.

$$\frac{d[P]}{dt} = k_{eff}[E]_0$$

(8)

Where

$$k_{eff} = \frac{k_{cat}[S]}{K_M + [S]}$$

(9)

The Michaelis constant is:

$$K_M = \frac{k_{off} + k_{cat}}{k_{on}}$$

(10)

Often the Michaelis-Menten equation is plotted as the rate, V, which is equal to d[P]/dt. In this form we have,

$$V = \frac{V_{max}[S]}{K_M + [S]}$$

(11)

There are several special regimes that can be useful to understand the Michaelis-Menten equation:

Maximal rate: If there is excess substrate present the rate is limited by the rate at which the ES complex falls apart. The rate of formation of products is a maximum and $V_{max} = k_{cat}[E]_0$is called the maximum velocity.

Half-maximal rate: If $V = V_{max}/2$, then $[S] = K_M$.

Second order regime: If $[S] << K_M$ then the rate of formation of products is $d[P]/dt = k_{cat}/K_M [E]_0[S]$. The rate depends on [S] as well as $[E]_0$.

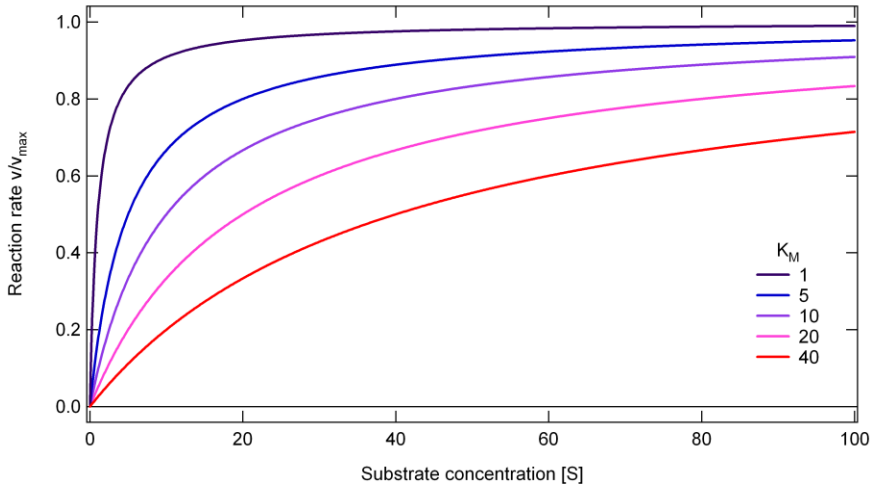

Figure 22. Michaelis-Menten curves showing the saturation of the kinetics at high [S]

A plot of 1/k yields k_{cat} and K_M but not the rate constants k_{on} and k_{off}. The latter rate constants can be obtained from stopped-flow experiments.

3.1.1 Lineweaver-Burke plots

The Michaelis-Menton expression is non-linear. The Lineweaver-Burke plot is linearized plot of data obtained by inverting both side of the Michaelis-Menten equation.

$$\frac{1}{V} = \frac{K_M + [S]}{V_{max}[S]} = \frac{1}{V_{max}} + \left(\frac{K_M}{V_{max}}\right)\frac{1}{[S]} \tag{12}$$

This expression has the form of an equation for a line:

y = intercept + slope x

Such plots are not necessary today with common non-linear fitting programs. However, they have historically played an important role in the application of the Michaelis-Menten equation.

3.1.2 Transition state stabilization

The original idea of the enzyme having maximum complementarity to the transition state (TS) was put forward by Linus Pauling in 1946. It wasn't until the early 70's that the idea was put on a more solid foundation. As put forward by Lienhard and Wolfenden the idea is as follows: the substrate binds to the enzyme more tightly in the transition state than in the equilibrium geometry. This concept is shown in Scheme 1.

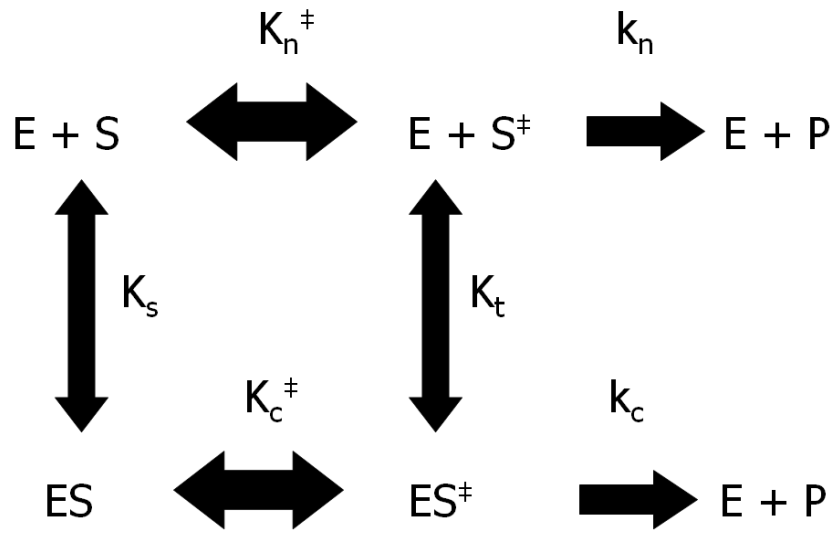

Scheme 1. Transition state stabilization. The top pathway involves activation of the substrate not bound to the enzyme. The non-catalyzed transition state equilibrium is $K_n{}^{\ddagger}$. The bottom pathway is the catalyzed pathway with equilibrium constant $K_c{}^{\ddagger}$ for the transition state. The transition complex is $ES^{\ddagger}$ in this case. The transition state hypothesis suggests that the substrate is much more tightly bound in the transition state geometry $ES^{\ddagger}$ than the original geometry, ES.

Defining the equilibrium constants as association constants:

$$K_n{}^{\ddagger} = \frac{[S^{\ddagger}]}{[S]} \ , K_t = \frac{[ES^{\ddagger}]}{[E][ES^{\ddagger}]} \tag{13}$$

from transition state theory:

$$\Delta G^{\ddagger} = -RTln\, K^{\ddagger}$$

and

$$k_{obs} = \frac{k_B T}{h} e^{-\Delta G^{\ddagger}/RT}$$

Thus,

$$k_n = \frac{k_B T}{h} K_n{}^{\ddagger} \ , \qquad k_c = \frac{k_B T}{h} K_c{}^{\ddagger} \tag{14}$$

where c means catalyzed and n means uncatalyzed.

From the scheme you can see that

$$K_s\, K_c{}^{\ddagger} = K_n{}^{\ddagger}\, K_t$$

hence

$$\frac{K_t}{K_s} = \frac{K_c{}^{\ddagger}}{K_n{}^{\ddagger}}$$

However,

$$\frac{k_c}{k_n} = \frac{K_c{}^{\ddagger}}{K_n{}^{\ddagger}}$$

The observed rate enhancement is:

$$\frac{k_c}{k_n} = \frac{K_t}{K_s} \gg 1 \tag{15}$$

Therefore, we can conclude that the transition state geometry $S^{\ddagger}$ must bind more tightly than the substrate S in its equilibrium geometry! The transition state stabilization hypothesis was tested by designing so-called transition state analogs, molecules which mimic the real TS as closely as possible. One of the first enzymes examined was proline racemase, which catalyzes the isomerization shown in Scheme 2.

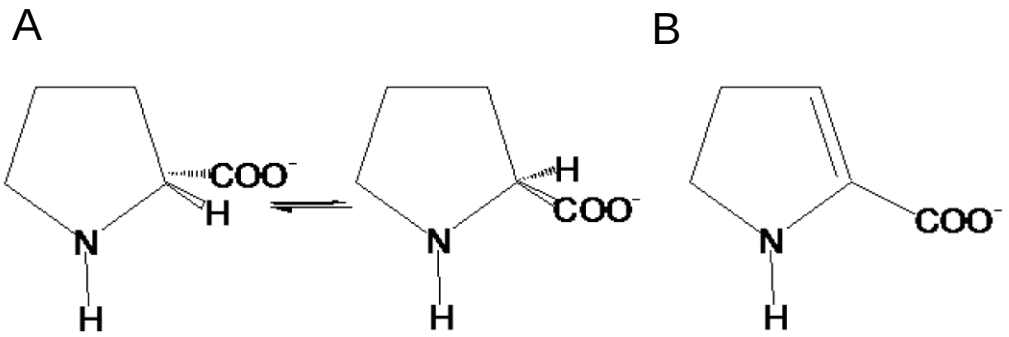

Scheme 2. A. Racemization of proline. B. The transition state analog is a planar molecule.

The compound on the right is a planar TS state analog. This molecule was found to be a good inhibitor, with K_i some two orders of magnitude smaller than K_m.

3.1.3 The role of entropy

In a seminal paper Page and Jencks showed that the loss in entropy in going from a bimolecular to a unimolecular reaction, i.e. E + S ←→ ES, could account for as much as 10^8 of the observed rate enhancement. In other words, this much free energy would come from the intrinsic binding energy. The entropy loss arises from the loss of translational and rotational degrees of freedom when the substrate is bound. The configurational entropy is:

$$S = k_B \ln W$$

where W is the number of degrees of freedom available to a molecule.

3.1.4 Inhibition

An inhibitor is any compound that causes a decrease in the catalytic rate. We will consider non-covalent ligands that can bind to the enzyme. The general scheme is shown below:

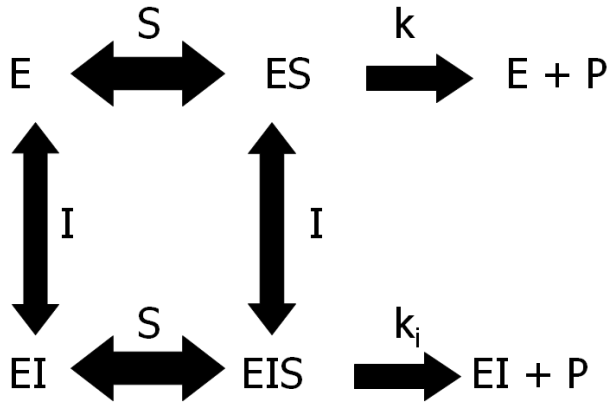

Competitive inhibition kinetic scheme

Although the scheme does not reveal the binding site of the inhibitor, there are a number of different possibilities. If the inhibitor binds in exactly the same site as the substrate, then it competes for that site, leading to competitive inhibition. On the hand, if the inhibitor binds to a remote site, but reduces the affinity of substrate binding, then binding is called uncompetitive. We contrast the solution of the equations for these two cases.

Competitive inhibition

Competitive inhibition results from the direct competition between the I and S for the substrate binding site. There is an additional equilibrium constant:

$$E + I \leftrightarrow EI \tag{16}$$

With dissociation constant

$$K_I = \frac{[E][I]}{[EI]}$$

(17)

The velocity under these conditions turns out to be:

$$V = \frac{V_{max}[S]}{\alpha K_M + [S]} \tag{18}$$

where

$$\alpha = 1 + \frac{[I]}{K_I} \tag{19}$$

Uncompetitive inhibition

Uncompetitive inhibition arises when the inhibitor, I, can bind at site that is not the same as the substrate binding site. The equation for the binding of the inhibitor is identical to that for competitive inhibition, Eqns. 16, 17 and However, for uncompetitive inhibition, the complex EI indicates that the inhibitor does not bind in the same site as the substrate. The velocity under these conditions is:

$$V = \frac{V_{max}[S]}{K_M + \alpha[S]} \tag{20}$$

4. Experimental methods

4.1 Excited State Processes and Application to Lasers

The technology of the laser (Light Amplified by Stimulated Emission of Radiation) was developed in the early 1960s. The technology is based on an understanding of excited state processes. We have thus far considered absorption and emission, without detailed consideration of the evolution of the excited state. The Einstein coefficients tell us that there are two fundamental emission processes in the excited state, spontaneous and stimulated emission. However, there is vibrational relaxation and there are other competing processes that can cause non-radiative decay from the excited state. In this chapter we consider excited state dynamics and how it relates to the use of stimulated emission as a technology.

The fate of excited states can be divided into the processes that take place within the initially prepared excited state and transitions from that state. Within the initial excited state, a molecule can relax to a new equilibrium position of the nuclei. That position is different from the nuclear equilibrium position both in terms of the bonds and the salvation shell around the

molecule. Vibrational relaxation (shown in Figure 23) leads to a new equilibrium distribution of the vibrational energy in the excited state. Likewise, following fluorescence or other processes that take the system back to the ground state, there will be vibrational relaxation in the ground state manifold. We refer to a manifold as collection of vibrational levels in a potential energy surface.

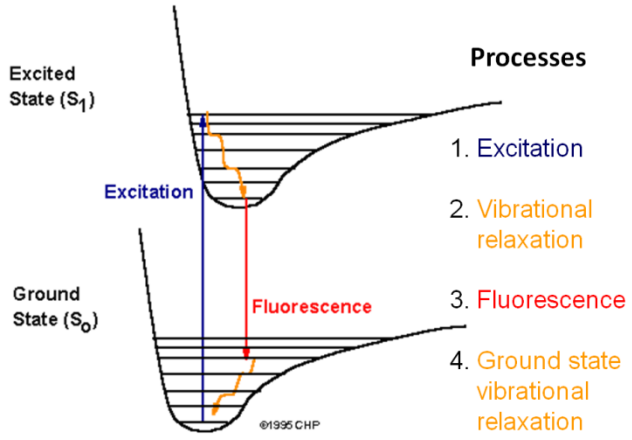

Figure 23. Relaxation processes within an excited state or the ground state.

Relaxation between states is usually represented using a Jablonski diagram, such as that shown in Figure 24. The ground state S_0 refers to a singlet. Not all ground states are singlets, but this is a common situation. The first singlet excited state is S_1. The triplet state is T_1. The non-radiative processes shown include internal conversion (IC) and intersystem crossing (ISC), which represent conversion of the S_1 state to the singlet ground state and triplet states, respectively. Both of these processes compete with fluorescence and reduce the fluorescence quantum yield. Internal conversation involves coupling of the excited state to the ground state by means of the Born-Oppenheimer breakdown operator,

$$H = \frac{\partial}{\partial Q}$$

This operator represents a part of the Hamiltonian neglected when the Born-Oppenheimer approximation is made Section 6.6. This term can couple states perturbatively. Coupling of the S_1 state to T_1 involves the spin-orbit coupling coupling operator. The relaxation of the triplet state to the ground state can be non-radiative, i.e. yet another ISC process, or radiative. A radiative $T_1 \rightarrow S_0$ process is called phosphorescence. Since triplet-singlet processes are formally forbidden the lifetime of the triplet state is typically quite long compared to the singlet state.

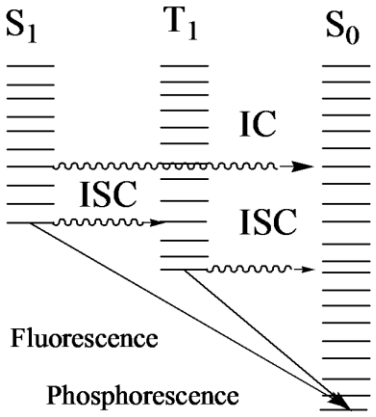

Figure 24. Example Jablonski diagram shown the processes of internal conversion (IC), intersystem crossing (ISC), $S_1 \rightarrow S_0$ fluorescence and $T_1 \rightarrow S_0$ phosphorescence.

Stimulated emission is only practical from a singlet state. The ideal laser material has a large absorption, and therefore stimulated emission, coefficient. However, spontaneous emission can compete with the stimulated emission. In practice organic laser dyes are fluorophores as well.

4.1.1 Basic features of a laser

The laser phenomenon involves a stimulated emission of light that results in gain. One input photon can stimulate emission of a second photon, which initiates a chain reaction. However, in order for such a chain reaction to take place the system must be poised so that there is a great deal of excess energy in the excited state. It must be pumped in some way and it must be able to store the energy. We have already shown in the section on the Einstein coefficients that the maximum excited state population is ½ in a two-level system. We shown this again in a slightly different way below and compare a two-level system with a three level system and qualitatively with a four-level system to show progressively greater efficiency in generating the population inversion. Aside from this gain medium, the lasing process must take place in a cavity that can store the energy. The condition for this is that the round trip distance in the laser cavity (2L) must be equal to an integral number of wavelengths (N□). If this condition is not satisfied the laser light interferes with itself. The laser must have a partially reflective mirror (output coupler) to permit a small fraction of the energy to escape and be used. Thus, the essential features of a laser are that it must have:

1. a gain medium

2. a laser cavity (reflecting mirrors)

3. an output coupler (semi-reflective mirror)

4. standing waves, which can be obtained for (N□/2=L)

5. birefringent filters, etalons, or gratings to modulate the frequency bandwidth

4.1.2 The gain medium

Although laser light is perhaps the purest form of light, it is not of a single, pure frequency. All lasers produce light over some natural bandwidth or range of frequencies. A laser's bandwidth of operation is determined primarily by the gain medium that the laser is constructed from, and the range of frequencies that a laser may operate over is known as the *gain bandwidth*. For example, a HeNe gas laser has a gain bandwidth of1.5 GHz. Ti:sapphire has a bandwidth of about 128 THz We will consider some of the most widely used gain media below, once we have understood the combined basic phenomena needed. The gain bandwidth will permit certain standing waves to be amplified as shown in Figure 25.

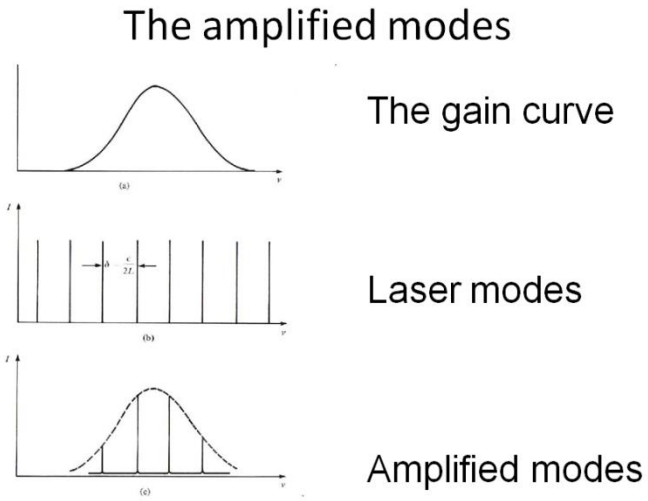

Figure 25. The gain curve is the frequency dependence of the gain medium. The laser modes are those modes that are permitted in laser cavity of length L (=N□/2). The amplified modes is the combination of the gain curve and the allowed laser modes.

Depending on the width of the gain curve hundreds or thousands of laser modes will be allowed in a given laser medium and cavity combination.

4.1.3 The laser cavity

The gain of a lasing medium can be enhanced by placing it between a pair mirrors to increase the effective length and restrict the allowed spatial and spectral modes of operation, greatly improving coherence and reducing pumping power requirements. This optical configuration is similar to the Fabry-Perot cavity, and is the most common laser interferometer. The basic laser cavity is shown in Figure 26. The gain medium is externally excited by light or voltage to generate excited states that can be stimulated. As light passes back and forth through the gain medium it builds up to an intense beam.

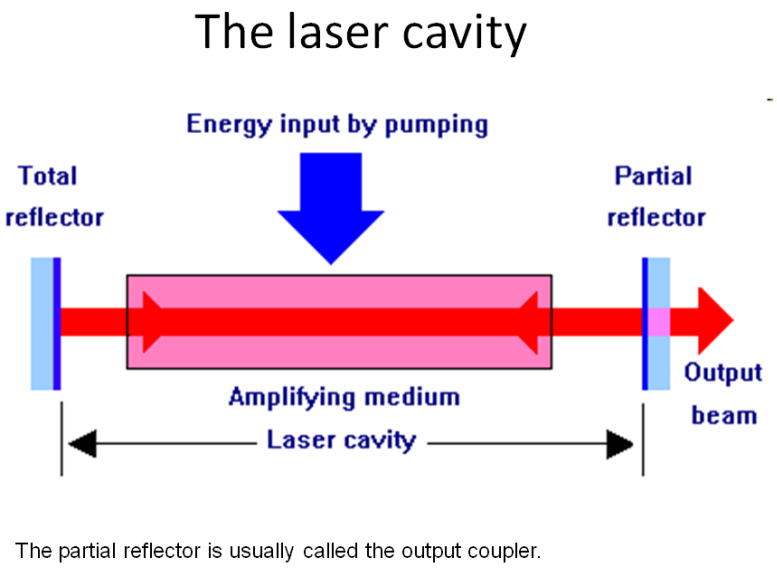

Figure 26. The laser cavity is shown with an amplifying medium (gain medium) and two mirrors. The total reflector is 100% reflecting and the partial reflector permits a small amount of the laser light to escape from the cavity.

4.1.4 Longitudinal modes

These standing waves form a discrete set of frequencies, known as the longitudinal modes of the cavity. These modes are the only frequencies of light, which are self-regenerating and allowed to oscillate by the resonant cavity; all other frequencies of light are suppressed by destructive interference. For a simple plane-mirror cavity, the allowed modes are those for which the separation distance of the mirrors L is an exact multiple of half the wavelength of the light λ, such that $L = N\lambda/2$, when N is an integer known as the mode order.

In practice, the separation distance of the mirrors L is usually much greater than the wavelength of light λ, so the relevant values of N are large (around 10^5 to 10^6). Of more interest is the frequency separation between any two adjacent modes N and $N+1$; this is given (for an empty linear resonator of length L) by $\Delta\nu$:

$$\Delta\nu = \frac{c}{2L} \tag{4.1}$$

where c is the speed of light ($\approx 3\times10^8$ m·s^{-1}).

4.1.5 Output modes

Figure 25 shows the combination of the gain bandwidth and longitudinal modes. This leads to a discrete set of wavelengths that are output from the laser within the bandwidth.

4.1.6 The population inversion

Gain represents the increase in photons emitted from the sample compared to a Boltzmann distribution. The Boltzmann distribution will never allow for more population in an excited state than in the ground state. Therefore, gain represents a non-Boltzmann distribution induced by optical or electrical pumping. Figure 27 shows why a population inversion is needed. It you want to get more photons out than you put in you need many molecules in the excited state to start a cascade of output photons. In Figure 27A the idea of a single photon excited more than one output photon requires that there be more population on the upper level (Level 2). As shown below, it is not possible to generate the required population inversion in a two level system. Figure 27B shows a three-level system, which is one method to generate a population inversion. First the transition of 0 → 2generates population in 2, which rapidly relaxes to state 1. The population in state 1 builds up and surpass the population in state 0. The amount of stimulated emission is still limited in a three level system because the population of state 0 can never be zero. Since it would be advantageous to have the largest population difference possible, the four-level system shown in Figure 27C is a common type of system used in laser design.

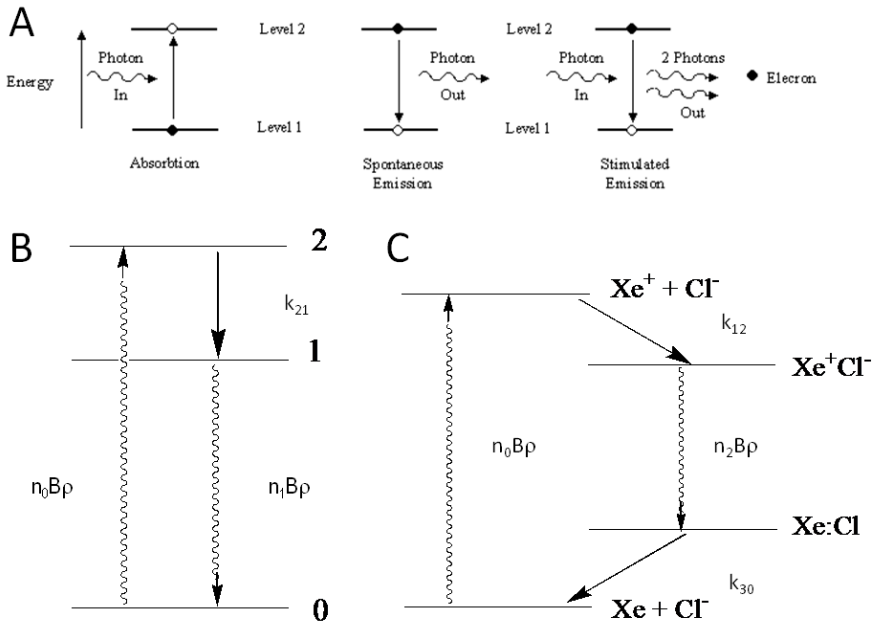

Figure 27. A. Illustration of the stimulated emission effect to create an amplification. B. Depiction of the three-level system used to generate a population inversion in state 1. C. Depiction of a four-level system, which leads to a population inversion an upper state that emits to a vacant state.

Two level systems

For states 0 and 1 the Einstein B coefficients are equal. High fluence limit results in a ratio of populations determined by microscopic reversibility. At equilibrium

$$W_{absorption} = W_{emission}$$

which leads intuitively to the conclusion that the excited state population cannot exceed the ground state population. This can be seen from the rate equations for a two level system with transition rate constant B (Einstein coefficient $B_{21} = B_{12}$) and energy density ρ.

$$\frac{\partial n_0}{\partial t} = -n_0 B\rho + n_1 B\rho = (n_1 - n_0)B\rho$$

$$\frac{\partial n_1}{\partial t} = -n_1 B\rho + n_0 B\rho = (n_0 - n_1)B\rho$$

(4.2)

The trial solution is

$$n_0 = Ae^{-\lambda t}$$

(4.3)

This system of equations can be solved using the secular determinant

$$det\begin{vmatrix} -B\rho - \lambda & B\rho \\ B\rho & -B\rho - \lambda \end{vmatrix} = 0$$

$$\lambda = 2B\rho$$

$$n_1 = n_0(1 - e^{-2B\rho t})$$

(4.4)

This significance of this equation is that n_1 is zero at t = 0. If a light source with energy density ρ is used to illuminate the sample the population of the excited state, n_1, will increase. However, even if the intensity is infinite (i.e. $e^{-2B\rho t} = 0$) the population n_1 can at most be equal to n_0, but never greater. A population inversion is impossible.

Three level systems

Optical or electrical pumping can be used in a three level system. The pumping process populates an intermediate state that decays into long-lived emissive state (i.e. the lasing state).

However, the ground state population must still be sufficiently depleted to make a population inversion in the emissive state. This can be done at high pumping rates, but it is difficult. The ruby laser is an example of the three level system. Cr:Al_20_3 is the gain medium in which Cr d-d transitions give a population inversion in a state that emits at 694 nm.

$$\frac{\partial n_0}{\partial t} = -n_0 B\rho + n_1 B\rho$$

$$\frac{\partial n_1}{\partial t} = -n_1 B\rho + k_{21} n_2$$

$$\frac{\partial n_2}{\partial t} = -n_0 B\rho - k_{21} n_2 \tag{4.5}$$

This scheme is simplified since it assumes that the Einstein coefficient for states 1 and 2 are the same with respect to 0. We can simplify the rate equations by assuming that if $k_{21}n_2 >> n_1 B\rho$ then a population build-up in n_1 can lead to a population inversion $n_1 >> n_0$. Still has disadvantage that population in n_0 is dominating at equilibrium.

Four level systems

The most robust lasers have been constructed using a four level system. Here, the trick is to find a way to populate an excited state that can relax to a level that has no population when the system is at rest. This sounds unlikely, but consider the d-orbital energy levels of a metal ion. There can be numerous energy levels, some of which have no population (particularly for metal ions with low electron counts). If one can populate an excited state efficiently then it is possible that the stimulated emission of that state could occur to an empty d-orbital. Then the ion relaxes to the ground state on a slower time scale, but this does not matter as long as the lower level is basically not populated at steady state. Lasing occurs between an excited state with population and a ground state that has no population. This is what occurs in the Ti ion of Ti:sapphire. Lanthanides can also be the basis of a good laser, based on the same principle in the f-orbital manifold. There are even more possibilities among the f-orbitals. Neodymium, Nd, is an example of a four level system.

4.1.7 Laser technology implementation

Lasers can be divided into continuous wave and pulsed lasers. Atomic lasers include the ion lasers (Ar+ and Kr+), HeNe and HeCd lasers and metal vapor lasers (Cu and Au). Molecular lasers include CO_2, N_2 and Excimer. All of these laser types are pumped to an excited state electrically. The dye lasers consist of fluorescent dyes that can be pumped into a liquid jet excited by another laser to produce new laser wavelengths. Solid state lasers include

neodymium lasers, Nd:YAG and Nd:YLF, transition metal lasers, ruby and alexandrite, and the workhorse of modern laser technology, Ti:sapphire (titanium sapphire).

Argon ion and Krypton ion lasers

The principle of operation of the noble gas ions laser involves creation of high energy ions in an electric discharge. The ions have specific electronic transitions that give rise to lasing at specified wavelengths. The gain bandwidth is typically very narrow in these lasers. This is positive aspect of these lasers since it means that reasonably narrow pulses in the frequency domain can be obtained without the need for optical elements to filter the laser pulse (e.g. birefringent filters used in Ti:sapphire and other broad band gain media). Ar^+ ion lines are observed at 275, 363, 457, 476, 488, 501 and 514.5 nm. Kr^+ ion lines are observed at 406, 413 and 752 nm. Gas phase lasers of this type are continuous wave (cw) and are non-tunable. They provide a useful narrow bandwidth source for pumping cw dye lasers.

4.2 Detectors

In this section we consider the most common detectors using in spectroscopic experiments. We will consider the device characteristics and the advantages of each type of detector. One common consideration for all detection is the signal-to-noise ratio of the measurement. One aspect of the work is to maximize the magnitude of the signal. However, we are often limited by experimental constraints. Increasing the sensitivity of a detector is not necessarily a solution to this problem since the noise may increase proportionally to the signal if the detector design is poor. One of the major improvements in detectors over the years has been in the minimization of noise. In the case of the modern charge coupled device (CCD) the chip design is important, but also the fact that the detector is cooled to temperatures below -100 ^oC. The cooling is essential for these detectors. In fact, we can think of a CCD as being like the chip in the digital camera in every cell phone. But, its sensitivity is much higher and the noise is controlled by the design, minimization of stray light and cooling.

Noise can be divided into two categories: externally induced noise, and internally generated noise. External noise includes those disturbances that appear in the system as a result of an action outside the system. Two examples of external noise are hum picked up from 60-hertz power lines and static caused by electrical storms. Internal noise, on the other hand, includes all noise that's generated within the system itself. We now know that every resistor produces a discernible noise voltage and every electronic device (such as vacuum tubes and semiconductor elements) has internal sources of noise. You can think of internal noise as an ever-present limit to the smallest signal that the system can handle.

We most often will measure voltage. The voltage is most often converted from a current flow, which in turn is induced by the absorption of photons on a photoactive surface. We will discuss how current is converted into voltage below in specific cases, But, if the signal is measured in voltage then we can define the fluctuations, i.e. noise, in terms of the voltage as

well. If the average voltage of a particular signal is $\langle V \rangle$, then we can define the mean square voltage as:

$$\langle V - \langle V \rangle \rangle^2 = \frac{1}{T} \int_0^T (V - \langle V \rangle)^2 dt$$

(4.6)

This is a convenient way of defining the fluctuation in a real system. The square root of this voltage is one measure of noise. We define the root-mean-square voltage as:

$$V_{rms} = \sqrt{\langle V - \langle V \rangle \rangle^2}$$

(4.7)

The term "shot noise" is normally associated with vacuum tubes in which the stream of electrons creates a noise due to the random fluctuations in the rate of arrival of electrons at the anode. This noise may be likened to the noise of a hail of shot striking a target. Hence the name shot noise. Shot noise is present in all photon detectors due to the random arrival rate of photons from the source of radiant energy under measurement and background radiation. This shot noise is often called "photon noise." Photon noise is the true ultimate limitation to detector performance. Even if all internal noise sources were eliminated, photon noise would set the ultimate limit for detector performance. Shot noise is proportional to the square root of the total number of counts on the detector. It is proportional to the square of the number of counts.

$$N_{shot} \propto \sqrt{N}$$

(4.8)

Shot noise is always present even when all other sources of noise have been reduced or eliminated. Moreover, the existence of shot noise gives a rule about signal averaging. Since shot noise is always present even when have eliminated all other kinds of noise and since the shot noise increases as the square root of the total number of photons we can predict that the “shot-noise-limited” signal-to-noise (S/N) ratio (i.e. the ideal or best such ratio) will improve as the square root of the number of averages of the data. This rule of thumb gives us an idea how many averages are sensible to acquire in a given experiment. We can always improve the S/N ratio, but the question is this: is it worth the wait? How long will it take to get a certain improvement? The square root rule gives us a good way to reason through situations. For example, if the S/N ratio is 5 for a given measurement that took one hour (which is really not very good) and we desire a S/N = 50 then we know that we must average at least 100 times as long it took to get the S/N ratio of 5. It will take us 100 hours of averaging to get 50 with the experimental setup that we currently have. Whether it makes sense to proceed depends on many factors (cost, stability, etc.). We may decide that a different measurement or different sample may be better because it will

simply take too long or there may be a possibility of failure during the 100 hours for some reason (sample degradation, instrumental instabilities, operator falls asleep etc.).

The issues associated with noise and signal averaging are common to all detectors. However, there are many important differences in sensitivity, spectral range, stability and so on that we must consider for the individual types of detectors.

4.2.1 Silicon photodiodes

Silicon photodiodes are among the oldest and most robust devices for detection of optical signals. The optical response of a typical Si photodiode is shown in Figure 28B in terms of the spectral responsivity in amps per watt of incident light. Silicon photodiodes are well suited to transient absorption measurements where the change in light level can be measured quantitatively, but Si photodiodes are not sufficiently sensitive to be used in most fluorescence applications where low light levels are common. As shown in Figure 28B the useful wavelength range for photodiodes is between 400-1000 nm with an optical response between 700-900 nm in the near IR. One of the disadvantages of standard diodes is the significant fall off in their responsivity in the blue part of the visible spectrum. Si photodiodes are the simplest device for converting light into a current and therefore a detectable electronic signal. Other technologies that are widely used such as Si avalanche photodiodes, photomultiplier tubes and charge coupled devices (CCDs) can all be understood easily once one understands the use of the Si photodiode. In considering the advantages and limitations of the Si photodiode we will introduce the crucial aspects of gain, noise and time response, which affect any detector. We will use this section to introduce the rudimentary electronics needed to understand detector response.

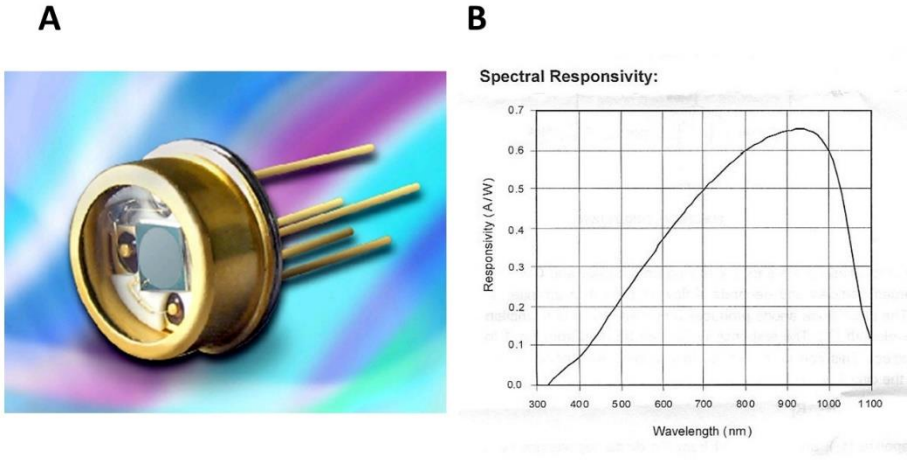

Figure 28. A. Picture of a typical Si photodiode in its case with electronic leads. B. Spectral responsivity of a typical Si photodiode in terms of the amps of current generated per watt of incident light.

Silicon photodiodes usually operate in current mode as evident from the spectral responsivity in Figure 28B. Light strikes the diode and generates a current so one measures the diode response in terms of the amps generated per watt of incident light. The first requirement for quantitative measurement of changes in light level is to convert the current into a voltage, i.e. to include a resistor in the circuit that will result in a measurable voltage change since V = IR. Typical currents are very small (i.e. in the microamp range), which means that the voltages are also very small. Normally, measurement of a voltage using an analog-to-digital converter requires voltages of the order of 1 Volt rather than the 1 milliVolt that one would obtain using a simple circuit with a resistor as the current-to-voltage converter.

In order to then the Si photodiode into a useful device we need to introduce gain into the system. Gain can achieved using a operational amplifier (op-amp). The circuit for the inverting op-amp configuration is shown. This circuit has the output 180 degrees out of phase with the input. The positive input is grounded. The input to the op-amp itself draws no current and this means that the current flowing in the resistors R_1 and R_2 is the same. Using Ohm's law we can relate the output voltage, which is that across R_2 to the input voltage caused by the current flowing through R_1 into the inverting operational amplifier.

$$\frac{V_{out}}{R_2} = -\frac{V_{in}}{R_1} \tag{4.9}$$

Hence the voltage gain of the circuit is:

$$Gain = \left|\frac{V_{out}}{V_{in}}\right| = \frac{R_2}{R_1} \tag{4.10}$$

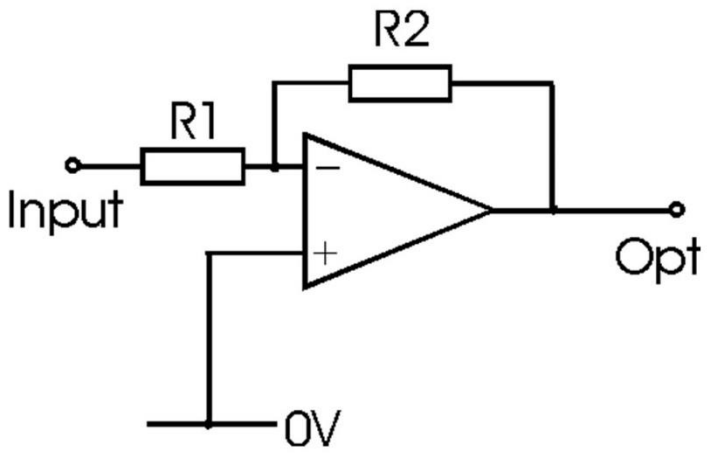

Figure 29. Standard operational amplifier circuit. An op amp is used to amplify signals and has wide use in Si photodiode technology.

Any circuit that contains an op amp has an intrinsically limited time response that is determined by the magnitude of the resistance (in Ohms) and the capacitance (in Farads). Although there is no capacitor in the circuit shown in Figure 29 above, capacitance is always present just because of the different voltages in the wires themselves. This is sometimes known as stray capacitance. The rate of charging of typical circuit with resistance, R, and capacitance, C, is given by Eqn. 4.11.

$$I = C\frac{dV_{out}}{dt} = \frac{V_{in} - V_{out}}{R} \tag{4.11}$$

The solution has an exponential form with a time constant of RC.

$$V = \Delta V\left(1 - e^{-t/RC}\right) \tag{4.12}$$

In an op-amp circuit there is a significant resistance in the kiloOhm range since the difference in resistors is the essence of gain and the initial resistor also cannot be arbitrarily small if one wishes to convert the current into a voltage that can be measured. While the capacitance is usually kept to a minimum, it cannot be zero. So-called stray capacitance is at least a few picoFarads and that is enough to put severe limitations on the time response of an amplifier circuit. The RC time constant of a typical circuit, such as that shown in Figure 30, is measured in units of RC, which is typically kiloOhms times picoFarads, RC = 10^3 Ohm x 10^{-12} Farad = 10^{-9} seconds. Thus, we can see that in a well-designed circuit the best time resolution we can hope for is in the nanosecond range. In practice, fast Si photodiodes have a 5-10 ns time response.

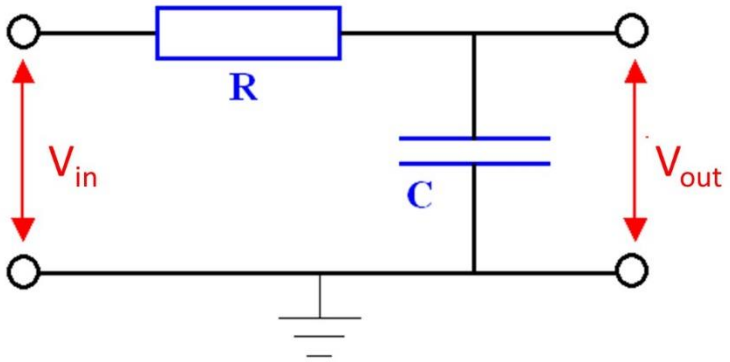

Figure 30. Basic circuit containing both a resistor, R, and capacitor, C. The time it takes for a change in voltage to be registered in the circuit depends exponentially on a time constant known as the RC time constant.

4.2.2 Silicon avalanche photodiodes

An avalanche photodiode (APD) is a highly sensitive semiconductor electronic device that uses the photoelectric effect to convert light to electricity in a manner analogous to a Si photodiode. APDs are photodetectors that provide a built-in first stage of gain through avalanche multiplication. From a functional standpoint, they can be regarded as the semiconductor analog to photomultipliers. By applying a high reverse bias voltage (typically 100-200 V in silicon), APDs show an internal current gain effect (around 100) due to impact ionization (avalanche effect). However, some silicon APDs employ alternative doping techniques compared to traditional APDs that allow greater voltage to be applied (> 1500 V) before breakdown is reached and hence a greater operating gain (> 1000). In general, the higher the reverse voltage the higher the gain. Thus, one significant different with respect to an ordinary Si photodiode is the application of a bias voltage, which leads to more sensitive response to incident light.

4.2.3 Photomultiplier tubes

We have seen that current is proportional to light intensity in a typical Si photodiode. The main limitation in a Si photodiode is its relative lack of sensitivity. This can solved by a Si avalanche photodiode, which is based on the idea of the photomultiplier tube. In a photomultiplier tube a photon strikes the plate (photocathode) and causes an “electron cascade”, which is an amplification through a chain of dynodes. Instead, of a single photon causing a single event that leads to a single electron flowing as current the amplification in the chain of dynodes results in a burst of many electrons as a response to a single photon. Photomultiplier tube plates are sensitive only over a narrow range of the spectrum. The next two slides show the combination of window coatings and photocathode materials that lead to specific spectral response.

When an electron strikes the photocathode it initiates a cascade of electrons which increase in number for each dynode. The amplification occurs in the dynode chain because a large bias voltage. Photodetectors are characterized by a photocurrent response that's linear with incident radiation over a wide range. Any variation in responsivity with incident radiation represents a variation in the linearity of the detector. If we plot the output current of the detector versus the input radiation level, the slope of the line from the lowest level of radiation to the highest level of radiation should not change. Noise in the detector or system will determine the lowest level of incident radiation detectable. The upper limit of this input/output linearity characteristic is established by the maximum current capability that the detector can handle without becoming saturated (no change in output for a change in input).

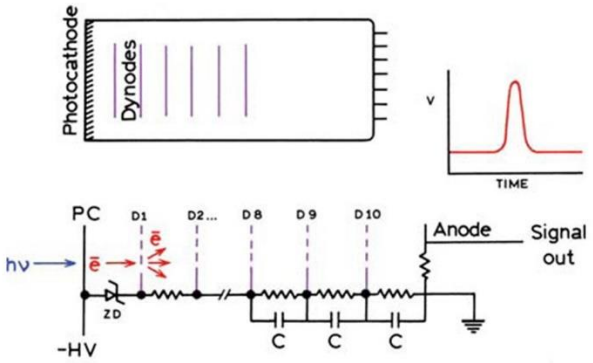

Figure 31. Simplified schematic of a photomultiplier tube circuit. The photocathode is the optically active surface. The single electron that emerges from the photocathode after excitation by light is amplified by a chain of dynodes, each of which emits numerous electrons in response to a single electron trigger. Thus, after the chain a single electron has been converted into a burst of millions of electrons. The amplification leads to a sensitive conversion of watts of incident light into amperes of current. No op amp is needed in this case.

4.2.4 Charge coupled device (CCD) detector

The CCD can be thought of as an array of Si photodiodes. However, it is quite a bit more sophisticated since the read-out requires a separate accounting of the number of photons that strike each individual element of the array. Modern CCD cameras are quite sensitive and can detect wavelengths over a broad range of the visible spectrum and even into the UV by means of sensitizer dyes on the surface of the CCD. Since the CCD can capture a range of dispersed wavelengths in a single read-out, one does not need to scan wavelength in order to obtain a fluorescence or Raman spectrum. The Si photodiode, avalanche photodiode and photomultiplier are all single wavelength detectors. They require a scanning monochromator. The detection is quite time consuming since each scan may take many minutes. Since the light that enters a spectrograph

is dispersed across the CCD the same read-out takes only seconds on CCD detector. The savings in time to accumulate data is enormous.

There is an array version of the photomultiplier tube, called a microchannel plate. These devices are very sensitive and have the advantage of a CCD. However, they are more expensive and also are quite susceptible to damage from overexposure to light. In practice, the CCD has become the dominant detector in most of spectroscopy.

In an imaging CCD for, there is a photoactive region (epitaxial Si), and a transmission region made out of a shift register shown in the series of images in Figure 32B. An image is projected through a lens onto the capacitor array (the photoactive region), causing each capacitor to accumulate an electric charge proportional to the light intensity at that location. Once the array has been exposed to the image, a control circuit causes each capacitor to shift the charge and finally to dump it to an amplifier, which converts it to a voltage for storage.

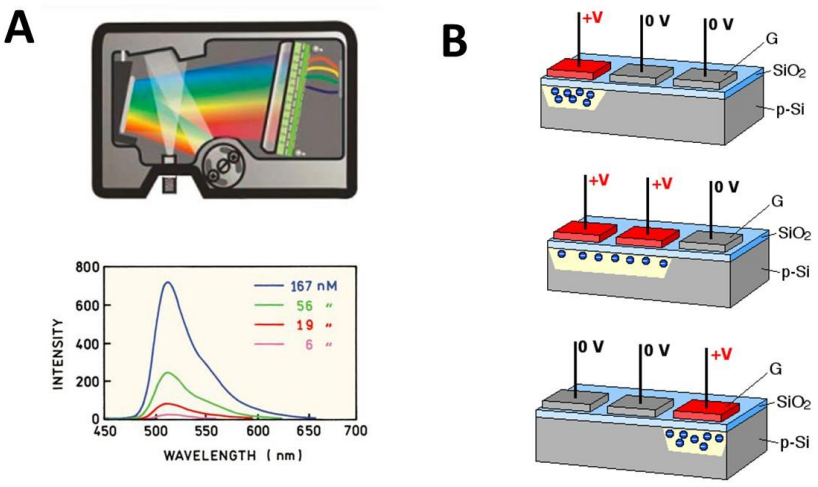

Figure 32. The concept of a CCD is illustrated. A. The concept of dispersing light onto the CCD chip is shown. The dispersion by a single grating takes place in a spectrograph. B. The mechanism for storing a record of a photon striking the photoactive surface is illustrated.

The intensity of emission, scattering or transient absorption is recorded on each pixel as a function of wavelength because the incident light is dispersed and each wavelength falls on a different set of pixels on the CCD chip. At the end of a period of time the device is read, which means that the stored electrons are swept out and converted into a voltage, which gives an electron count that struck each element. Often in spectroscopic applications the CCD chip is binned in the vertical dimension since the light is dispersed horizontally and the wavelength should not change in the vertical dimension.

5. Data analysis tools

In CH452, Measurements Laboratory, students have learned the basics of linear regression and curve fitting using non-linear regression. Non-linear fitting is widely used and has been implemented in numerous commercial programs (Excel, Origin, IgorPro etc.). There are a number of important methods that can be used to determine the minimum in parameter space. The most important of these are the Levenberg-Marquardt algorithm and the Simplex method.

5.1 Levenberg-Marquardt algorithm

Given a set of m data points (xi,yi) where xi is the independent variable and yi is the dependent variable, we wish to find a function $f(x_i, \beta)$ that passes through the points with a minimum value for the residuals. β represents the parameters in the fit function. The model curve will be a best fit when the sum of the squares of the residuals is minimized.

$$\hat{\beta} = \min \sum_{i=1}^{m} (y_i - f(x_i, \beta))^2 \tag{5.1}$$

The algorithm is an iterative procedure for finding the parameters, which minimize the residuals. Following an initial guess, β, the algorithm provides a systematic change in the parameters $\beta + \delta$. We can determine δ using a linearization procedure

$$f(x_i, \beta + \delta) \approx f(x_i, \beta) + J_i \delta \tag{5.2}$$

The approximation is based on a Taylor's series so that the coefficient J_i is

$$J_i = \frac{\partial f(x_i, \beta)}{\partial \beta} \tag{5.3}$$

Therefore, in this case the sum of squares has a minimum when$J_i \approx 0$

$$\mathrm{S}(\beta + \delta) = \sum_{i=1}^{m} (y_i - f(x_i, \beta) - J_i \delta)^2 \tag{5.4}$$

In a manner entirely analogous to linear fitting we can expand $\mathrm{S}(\beta + \delta)$

$$(J^T J)\delta = J^T (y - f(\beta)) \tag{5.5}$$

Which gives a set of linear equations that can be solved for δ. Levenberg came up with the idea of allowing the procedure to take place in smaller steps. This is called the damped version

$$(J^T J + \lambda I)\delta = J^T(y - f(\beta))$$

(5.6)

This is a more detailed view of what was presented in the manual for CH452, where we showed that you can minimize the residuals (actually their sum of squares) using the formula $\mathbf{(J^T J)^{-1} J^T Y}$. **J** contains the derivatives of the fit function f(x; $\boldsymbol{\beta}$) versus each parameter in each chosen data point. This means that we need to have an idea of what $\boldsymbol{\beta}$ is before we can compute **J** (our initial guess or initial trial for the parameters). It also means that $\mathbf{(J^T J)^{-1} J^T Y}$ will only give us a *better* estimate of $\boldsymbol{\beta}$, not the *best*. That's no problem: we can keep applying the process until no more improvement is observed. This iteration process is called ***refinement***. The Levenberg-Marquardt algorithm adds to this a procedure for making rational step sizes when the parameters are changed. The side of the change, δ, is determined by the parameter λ.

1. make guess of parameters
2. calculate the **J** matrix based on that guess
3. calculate $\mathbf{(J^T J)^{-1} J^T Y}$ to get better parameters $\boldsymbol{\beta}$,
4. make a step δ damped by λ (prevents stepping too far)
5. check for convergence; if not converged go to step 1.

The refinement looks for the minimum in the sum of squares (SS) function. Since this function is like a landscape with hills and valleys, you want to make sure that the steps you take do not go too far. The derivative tells you which way is down, but if your step is too large you could step to the other side of the hill or even over the ridge to the next valley. Therefore, you need a good initial guess and a procedure that ensures that the steps are not too large. Otherwise the procedure gets lost in the hills (so to speak).

5.2 Simplex fitting procedure

TBA

5.3 Statistical analysis of the data: Chi-squared and error analysis

When using the least squares criterion, it is possible to calculate errors (as variances) and even covariances from the least squares function, known as chi-squared, χ^2. The assumption is that the functional form is close to quadratic near the minimum. The least squares function can be normalized to the noise in the experiment by finding a region of the data that is essentially flat and determining the standard deviation in that region.

$$\chi^2 = \frac{\sum_{i=1}^{m}(y_i - f(x_i, \beta))^2}{N\sigma^2}$$

(5.7)

Where σ^2 is the variance due to the noise in the data. Clearly one wants to select a large enough region to obtain a good estimate of the noise that is valid over the entire data set. If one can assume that the noise estimate is accurate then a good fit is obtained when $\chi^2 = 1$. Since the

goal of the fitting procedure is to find the minimum of the parameter space, it is possible to then use a method to determine how large a step from that minimum gives a change in the least squares function by 1, i.e. to up to the point where $\chi^2 = 2$.

5.4 Practical implementation of non-linear fitting

Excel

IgorPro

Physical Chemistry Laboratory Experiments

1. Enzyme Kinetics of Dehaloperoxidase, CH454 Physical Chemistry Lab #1

Introduction

Enzymes are widely used in the chemical, biochemical and biotechnological applications. The range of chemical synthesis that is possible using enzymes is quite broad and new methods are under development that will greatly expand the field of enzyme use. Enzymatic catalysis is also one of the best understood types of catalysis. Many catalysts are difficult to characterize because they function at low concentration in complex mixtures and the intermediates are nearly impossible to isolate. In many chemical applications the addition of catalysts is understood as kind of "pixie dust" that just works, but no one knows why. Biological catalysis or enzymatic catalysis consists of many very well characterized reactions. Often we know the structure of the enzyme, the details of the active site, and even how the substrate binds and precisely what aspects of protein structure are responsible for lowering the transition state energy. For these reasons enzymatic catalysis can be considered a model for how we would like to understand all of chemical catalysis.

The importance of enzymatic catalysis has been appreciated for more than 100 years. An early approach to characterization of the kinetics of enzymes is attributable to Menten and Michaelis. While there are many variations of Michaelis-Menten catalysis the simplest version treats and enzyme, E, and substrate, S, that combine to form a complex known as ES, the enzyme-substrate complex and then to form product, P, and reform the original enzyme. We can write this mechanism as follows:

$$E + S \underset{k_{off}}{\overset{k_{on}}{\leftrightarrow}} ES \xrightarrow{k_{cat}} P + E$$

Often the Michaelis-Menten equation is plotted as the initial rate, V_0, which is equal to d[P]/dt. In this form we have,

$$V_0 = \frac{V_{max}[S]}{K_M + [S]}$$

Where the Michaelis constant is:

$$K_M = \frac{k_{off} + k_{cat}}{k_{on}}$$

There are several special regimes that can be useful to understand the Michaelis-Menten equation:

Maximal rate: If there is excess substrate present the rate is limited by the rate at which the ES complex falls apart. The rate of formation of products is a maximum and $V_{max} = k_{cat}[E]_0$ is called the maximum velocity.

Half-maximal rate: If $V = V_{max}/2$, then $[S] = K_M$.

Second order regime: If $[S] << K_M$ then the rate of formation of products is $d[P]/dt = k_{cat}/K_M [E]_0[S]$. The rate depends on [S] as well as $[E]_0$.

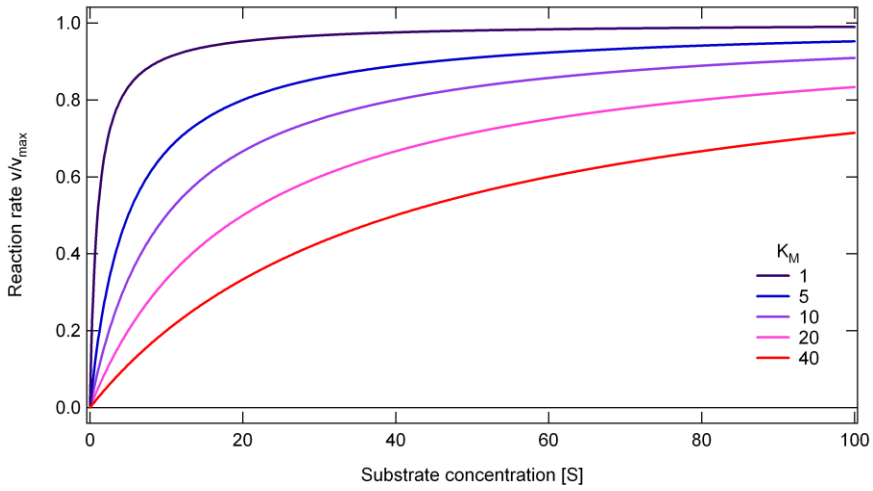

Figure 1.1. Michaelis-Menten curves showing the saturation of the kinetics at high [S]

Our experiment will determine the Michaelis-Menten parameters for a heme peroxidase enzyme. That may be horseradish peroxidase (HRP) or dehaloperoxidase (DHP). HRP is the standard peroxidase enzyme that has been studied for many years. It is sold as a lyophilized powder. Published work suggests that we should be able to use approximately a 0.1-0.3 microMolar solution of HRP as the enzyme in the turnover experiment described in this laboratory.

DHP is a highly versatile and interesting enzyme in its own right. DHP was first discovered as the hemoglobin of a marine organism known as *Amphitrite ornata*. Nearly 20 years later it rediscovered as a peroxidase capable of degrading 2,4,6-tribromophenol, which is a known naturally occurring pollutant in shallow coastal waters. In the subsequent 20 years several unique properties of DHP have been revealed by enzymatic studies. DHP is also a peroxygenase and an oxidase. It has four functions and appears to have activity to oxidize a range of substrates including bromophenols, brominated pyrroles and indoles. In this study we will investigate the kinetics of HRP as a model for DHP. It is of interest to consider studies of DHP or one of its mutants for the project phase. Studies can be conducted as a function of pH from 5.0 to 7.5 or temperature. In project phase we would choose one set of conditions and one mutant in the interest of time. However, our goal will be to compare the values to published values and understand some new feature or prediction about the reactivity. While we can be quite certain that the experiment will work the interesting aspect is that the exact outcome may be a new result.

The mechanism of the peroxidase reaction involves activation of HRP by H_2O_2. We can think of the reaction with H_2O_2 as a preliminary step that creates active form of the enzyme that we call compound ES. It is compound ES that binds to the substrate oxidizes substrate in two steps. Since these aspects are discussed in detail in the references [1-5], we will not discuss the mechanism further in this protocol. Rather we will ask the student to read the publications and to make the discussion of mechanism part of the laboratory report.

Experimental

You can measure the time-resolved kinetics of enzymes using a photo-diode array spectrophotometer. This type of spectrophotometer reads all of the wavelengths from 200-1000 nm simultaneous in less than 1 second. The advantage of this technology is that the instrument can be set up to run in kinetics mode, in which successive spectra are obtained each 3 seconds. If the kinetic change during catalysis by an enzyme has an optical signal in the range of the instrument and a time course that is longer than a few seconds, but shorter than a few hours it is appropriate for measurement using a photodiode array. One of the nice features of enzyme kinetic experiments is that the overall rate can be tuned by changing the enzyme concentration. Since we measure rates relative to the maximal rate, V_{max}, and

$$V_{max} = k_{cat}[E]_0$$

we see that we can get V_{max} to have a range of values by changing the enzyme concentration. Of course, there are limitations since the enzyme concentration cannot be higher than the solubility of the enzyme and there are practical limitations to how dilute the enzyme can be to function in a reliable way.

In order to obtain data appropriate for a Michaelis-Menten analysis, you will need to make 6 dilutions of the substrate with constant concentrations of enzyme and co-substrate hydrogen peroxide. The hydrogen peroxidase concentration should be high enough that complete conversion to product can be achieved at the higher substrate concentration. The volume of solution will need to be sufficient that the optical path of the light in the photodiode array passes only through solution and there is no air space on the top that could give rise to spurious absorption. In a small volume cuvette (with a 0.4 cm pathlength) this volume is 1.2 mL. The reason for the short pathlength is that the absorbance of substrate (and also the product) is too great to measure accurately at the highest concentrations used.

We can summarize the requirements for this experiment as follows:

$[E]_0$ is constant (usually $[E]_0 = 6.0 * 10^{-8}$ M)

$[H_2O_2]$ is constant ($[H_2O_2] > [S]$ for all measurements)

[S] ranges from zero to a maximal value of approximately 1.5 mM.

The buffer used should be KPi buffer at pH 7 with 5% methanol added.

Note finally that [S] will need to have a higher coverage at low concentrations since the Michaelis-Menten curve has a greater rate of change at lower concentrations. For an enzyme

that has an unknown catalytic rate, we will need to make a run to estimate the kinetics. Then once we have an idea what the value of kcat and Km are we can determine the values. Typically, we will want 3 values below Km and at least one values above Km. An approximate distribution of substrate concentrations is:

[S] = 0.1, 0.2, 0.5, 0.8, 1.0 and 1.5 mM

Preparing the stock solutions

The catalyst: Horseradish enzyme (HRP)

The molar absorptivity of HRP is 102,000 M-1 cm-1. You can dissolve a small amount of the lyophilized HRP powder into a solution. The color should be light brown. Take an aliquot of 100 μL and dissolve that into 900 μL of buffer to create 10-fold dilution. Measure the absorbance at 400 nm and determine the concentration. A target concentration for the stock solution is 0.6. You can achieve the target final concentration either by adding 12 μL of this stock to the solution that will total 1 mL. Perhaps it is more accurate to make a 10-fold dilution of the HRP solution and then add 120 μL to the mixture.

The substrate: tri-chlorophenol (TCP)

You will need to make a stock solution of substrate, TCP. The solution should be made fresh for each experiment since phenols degrade by slow light and oxygen-dependent reactions. An appropriate concentration for the TCP stock solution is 5 mM. You can add aliquots ranging from 24 μL to 360 μL to achieve the appropriate concentrations in the final volume of 1.2 mL.

10^{-2} M x 10^{-3} L = 10^{-5} mol is the number of moles of HRP in 1 mL.

10^{-5} mol x 200 grams/mol = 2 x 10^{-3} grams is the mass of HRP in 1 mL.

Weigh out approximately 10 mg of TCP and dissolve it 500 μL of methanol. Add this to 9.5 mL of KPi buffer. This should be a stock solution of TCP at 5 mM. You can measure this by diluting the solution by a factor of 50 into buffer (with 5% methanol added) The resulting concentration of 0.1 mM should have an absorbance of

10^{-4} M x 3750 M^{-1} cm^{-1} x 1 cm = 0.375 in a 1 cm pathlength cuvette.

The co-substrate: Hydrogen peroxide (H_2O_2)

The hydrogen peroxide stock solution is prepared freshly before the kinetic experiments since H_2O_2 tends to react with impurities at room temperature. For a typical HRP peroxidase kinetic reaction with the final hydrogen peroxide concentration at 1200 μM. You can prepare the hydrogen peroxide stock solution by having 10 mL KPi buffer mixing with 7.4 μL of 30% concentrated hydrogen peroxide solution (from Sigma-Aldrich) assuming you will add 200 μL to a total volume of 1200 μL (1.2 mL). [NOTE: a 30 wt% H_2O_2 solution corresponds to 9.7 Molar], using the formula

$$M = \frac{\frac{wt\%1}{M_{m,1}}}{\frac{wt\%1}{\rho_1} + \frac{wt\%2}{\rho_2}}\ x\ 1000$$

to calculate the molarity from weight percent. The density of H_2O_2 (component 1) is 1.45 g/mL and its molar mass is $M_{m,1} = 34\ g/mol$.

Molar absorptivity data and application

The concentration of HRP protein stock solution is determined by using UV-Vis in the Standard mode. The absorbance at 406 or 407 nm which is the λ_{max} of the Soret band is recorded and used to calculate the concentration of HRP stock solution according to Beer's law: $c=A/(\varepsilon_{406}*b)$. The path length b of the quartz cuvette can be either 0.4 cm or 1 cm depending on which face of the cuvette you use.

Extinction coefficients (Molar absorptivities)

For HRP ε_{406} = 102,000 $cm^{-1}\,M^{-1}$ at 400 nm.
For DHP ε_{406} = 116,400 $cm^{-1}\,M^{-1}$ at 406 nm.
For 2,4,6-TCP ε_{312} = 3,750 $cm^{-1}\,M^{-1}$ at 312 nm.
For 2,6-DCQ ε_{272} = 11,400 $cm^{-1}\,M^{-1}$ at 272 nm.
For H_2O_2 ε_{242} = 43.6 $cm^{-1}\,M^{-1}$ at 242 nm

The following procedure is needed only for DHP (Extra credit or research project). DHP is interesting to compare to HRP since it is a globin-peroxidase. DHP has a high reduction potential, which is nearly 0.5 V more positive than that of HRP. Thus, HRP is always in the oxidized (ferric) form, but DHP must be oxidized each time prior to use. The DHP stock solution is prepared by adding about 100 μg or $K_3Fe(CN)_6$ (Potassium ferricyanide) powder directly to the protein solution in an Eppindorf tube. The purpose of this step is to oxidize the DHP to the ferric form. Then pass that solution through a 10 kD gel filtration column using 100 mM KPi buffer to elute the material. You should see a clear separation of the protein, which passes first and has a brown color, from the ferricyanide, which has a yellow color. Collect the protein solution in a fresh Eppindorf and determine the concentration by measuring a dilution in the UV-vis. Typically you will measure this using the 1.0 cm path length using 100-fold dilution (i.e. 10 μL into 1 mL)

Mixing protocol

Calculate the volume of each component (protein, substrate, buffer) for a total volume of 1.2 mL used for each kinetic assay. Add the buffer, substrate solution and protein solution to the cuvette for a total volume of 1 mL. Note that the protein (HRP) concentration is always the same and the volume of that solution is determined from the calculation above for the stock solution. A typical value for the stock solution would be 100 μM protein. In this case you would add 29 μL of that HRP stock solution for a final concentration of 240 nM DHP. The volume for the H_2O_2 solution is fixed at 200 μL and will be added in the end to initiate the reaction. Make a new file for each kinetic assay and set the experimental parameters. When you are ready to start the reaction, press

F7 (or the start tab at the top left of the menu) to start the experiment while at the same time add the H_2O_2 solution, mixing the solution once or twice quickly with the syringe or pipette tip.

Setting up the data acquisition

The data are acquired on a PC using HP 8453 UV-Visible System software. You set the HP 8453 UV-Visible System software to Kinetic mode. You will want to monitor at 272 and 314 nm. The 272 nm wavelength is used to monitor the appearance of the quinone product. The 314 nm wavelength is to monitor the disappearance (consumption) of substrate 2,4,6-trichlorophenol (TCP). We will use 2,4,6-TCP instead of the brominated analog found in nature. The reason is that 2,4,6-TCP is significantly more soluble that 2,4,6-tribromophenol. We will also dissolve the 2,4,6-TCP in a solution that contains 20% methanol. In the final solution for measurement of enzymatic catalysis the concentration of methanol will be 5%. To effectively vary the concentration of 2,4,6-TCP we will need to have a second solution of buffer and 20% methanol. The 2,4,6-TCP solution in the of the 20% methanol solution will need to be 4 times higher than the target in the final solution. The UV-vis instrument will record all wavelengths from 200-1000 nm on each acquisition (i.e. every 1 second in our experiment). Thus, for a 3-minute data acquisition 60 spectra will be acquired. We will extract all of these spectra for analysis using Singular Value Decomposition (SVD). SVD is not required for data analysis, but it is the most sophisticated way to extract the kinetic component that corresponds to enzymatic turnover. But, we can also use the data at 272 nm for fitting the initial slope to obtain V_0 as needed for the Michaelis-Menten protocol discussed in the introduction.

Analysis

Data transfer

The data can be extracted from the software by copying and pasting into an Excel spreadsheet. The spreadsheet can be transferred to your UNITY account using Secure Shell software. Secure Shell is a windows based program that is based on the LINUX sftp (secure file transfer protocol) command. You will find the Secure Shell 3.2.9 Icon on the desktop. You can set up the path for transfer using the software. The procedure is shown on the website using the screen shots of the SSH software.

Uploading the data into IgorPro

To upload data from an Excel spreadsheet into IgorPro the easiest method is the cut and paste method. You may open the Excel spreadsheet and select the rows and columns you would like to analyze. Then these values can be copied (<ctrl c>) and pasted (<ctrl v) into the table in IgorPro. When IgorPro is opened there is always a table presented as a default. When you paste the data into this table the data columns will have the labels wave0, wave1, wave2 etc. As long as you keep careful records there is no need to rename all of these columns. For example, if you have a typical spectroscopic data set with wavelengths from 400 – 600 nm, there will be 200 columns. It would be a bit painful to change the names of 200 data waves. If you do need to change a name of a wave you can do it on the command line of IgorPro.

- Rename wave0 time

- Rename wave1 lamda400

Note that IgorPro waves must have names that begin with a letter and not a number.

Plot all the time courses of the absorbance at the given wavelength. Select all the corresponding absorbance waves as the y axis and the only wave "time" as the x axis at Windows -> New Graph and go ahead to plot them.

Fitting the kinetic data using the method of initial rates

Igor has a number of standard fitting functions. The fit to a straight line is a standard fitting function. As you have learned, fits to a straight line are known as linear least squares fitting and there is a unique solution for the slope and intercept. In this problem the intercept is not important for the kinetic analysis, but the slope tells you how ΔA changes with time. Once you know this you will need to convert ΔA to $\Delta[P]$, the change in concentration. For this step you will use Beer's law.

To fit to a straight line you will need to plot the kinetic data and then use the cursors to select the first few points (6 to 10 points). The data are only linear over a very small range of time. Make sure that you have selected a short enough range that it is linear. However, you will need a minimum number of points to make the fitting meaningful. Experience suggests that 6 points is the minimum.

The procedure for plotting, selecting data with the cursors and defining the fitting function are given on the website. Use the website to guide you in this step. Record the values of your fit for each of your kinetic runs at each of your concentrations. Make a table with the following entries

	$\Delta A_1/\Delta t$	$\Delta A_2/\Delta t$	$\Delta A_3/\Delta t$	$<\Delta A/\Delta t>$	$\sigma(\Delta A/\Delta t)$
$[S]_1$	0.00478	0.00512	0.00499		
$[S]_2$	0.00839	0.00812	0.00806		
…					

Constructing and fitting the Michaelis-Menten plot

Once you have obtained the average values of the initial rate, $V_0 = <\Delta A/\Delta t>$, for each substrate concentration you will need to construct a plot of the initial rates vs. substrate concentration, V_0 vs. [S]. This is the Michaelis-Menten plot. The data in this plot will be fit using non-linear least squares fitting. In IgorPro this can be done by adding a macro to the software. IgorPro has a number of standard fitting functions for non-linear least squares fitting, but the Michaelis-Menten model is not one of them. You may use the macro below, which is available for download on the website. You will need to add these lines of text to the Procedure Window of IgorPro. When you close the Procedure Window it will automatically compile the macro and make it available in the Analysis menu. You may select this fitting function in that menu.

Non-linear least squares fitting differs from least squares in that an initial guess for the parameters is required. In the case of M-M fitting you will need to input the V_{max} and K_m values. How can you "guess" these values? It seems a bit tautological since the whole point of fitting is

to obtain the values. In the case of M-M you can estimate V_{max} since that is the limiting value of the initial rate at large [S] concentration. You can inspect the plot and either simply use the largest value or perhaps a somewhat larger value based on your intuition of how much the curve is increasing over the observable range. Km can be estimating finding the value of [S] the corresponds to $V_{max}/2$, since K_m = [S] gives $V_{max}/2$ in the M-M formula. You will still need to do the fitting in order to obtain accurate values of these parameters. The fitting menu allows you to input an estimated value of the standard deviation (also called the weight). When this is entered the fitting function will return a value of chi-squared, χ^2. In non-linear least squares fitting this is the figure of merit that is most frequently used to indicate the goodness of it. If the errors are properly estimated a good fit should have $\chi^2 = 1$.

SVD analysis of the spectral components of the data

Singular value decomposition (SVD) is a powerful method for global analysis of spectral data sets. The SVD method is a mathematical approach to decomposition of a data set in two dimensions (e.g. wavelength and time or wavelength and pH etc.) into orthogonal basis spectra.

Lab Report

The laboratory report for this protocol should include the usual sections, Abstract, Introduction, Materials and Methods, Results, Discussion, and Conclusion. The references should include some general considerations of Michaelis-Menten enzyme kinetics and other fundamental aspects. Since DHP is quite specialized there is not a great deal of literature outside the groups at NC State that study the protein. However, the field of peroxidase chemistry is quite large and it is important to see the context of the study. There is a large literature on HRP and so the study here will be readily compared to some published work. References on kinetics studies of peroxidases as a comparison to the study here are appropriate in the lab report. It would be appropriate to discuss how the peroxidase mechanism fits within the Michaelis-Menten kinetic scheme (and the assumptions needed for that adaptation). A well-known peroxidase enzymologist, Dr. Dunford has written that it is an egregious error to treat peroxidases using the Michaelis-Menten (M-M) scheme and yet he shows readers how to do it. What is meant by this error? Why is it that we still use the M-M scheme? Try to write a thoughtful report based on the literature that you can. Keep in mind that one recent piece of information comes from the book on “Heme Peroxidases” edited by Drs. Dunford and Raven. There is a chapter on DHP in that book that contains some reflections on how DHP fits in the peroxidase world.

Be sure to use the three replicates of the M-M curve to discuss the error analysis associated with fits of the linear date (method of initial rates) and the non-linear least squares fit of the M-M curve. Use IgorPro to create nice figures with error bars.

Discuss the method of initial rate and its use. Some kinetics applications use the integrated rate law. The M-M rate expression is not an integrated rate law. Why not use the integrated rate law? The answer is not necessarily a simple reason, but rather is based on both experimental expediency (i.e. what the data look like) and mathematical limitations (i.e. the mathematical form of the integrated rate law). Give some thought to these aspects and also see if you can find any information on this question in the literature.

Using SVD analysis, one can obtain basis spectra with corresponding time courses. If a system is a simple two state kinetic process, then there should be two SVD components. One is the grand mean of the data and the other is the change in the spectrum (ΔA) between the reactant and product. In the case of HRP there are three components. Based on the literature why is this? One hint is that the kinetics of both DHP and HRP are highly pH dependent and the dependence on pH is related to a third species. HRP is optimized at pH 5.5, which may sound unexpected until you realize that HRP is secreted by horseradish to help decompose materials in the ambient that may provide nutrients for horseradish growth. DHP has a different function and it is found in the coelom of a marine worm (terrebellid polychaete). Thus, DHP was observed to have optimal turnover at pH 7.5. That is closest to the physiological pH of cells.

In this experiment it is possible to extract kinetics at a single wavelength (e.g. the product lmax). If you choose a single wavelength then you may use the method of initial rates to extract a rate constant. However, you can also extract time-resolved spectra from the UV-vis photodiode instrument. These are amenable to analysis by SVD. Please try to discuss this aspect on the significance of the SVD to the best of your ability. This is a subtle and difficult aspect of this problem and this aspect of the lab is extra credit. Certain aspects are known and discussed in the literature and an appropriate search of references from the Ghiladi and Franzen groups should reveal the answers to questions regarding the significance of kinetic components.

References

1. **Ma, H.; Thompson, M.K.; Gaff, J.; Franzen, S.** "Kinetic analysis of a naturally occurring bioremediation enzyme: Dehaloperoxidase-hemoglobin from *Amphitrite ornata*" J. Phys. Chem. B, **2010**, 114, 11283-11289
2. **Zhao, J.; Franzen, S.** "Kinetic study of the inhibition mechanism of dehaloperoxidase-hemoglobin A by 4-bromophenol" *J. Phys. Chem. B* **2013**, 117, 8301-8309
3. **Zhao, J.; Zhao, J.; Franzen, S.** "The Regulatory Implications of Hydroquinone for the Bifunctional Enzyme Dehaloperoxidase- Hemoglobin from *Amphitrite ornata*" *J. Phys. Chem. B.* **2014**, 117, 14615-14624
4. **Thompson, M.K.; Davis, M.F.; de Serrano, V.; Nicoletti, F.P.; Howes, B.D.; Smulevich, G.; Franzen, S.** "Two-site competitive inhibition in dehaloperoxidase-hemoglobin" Biophys. J. **2010**, 99, 1586-1599
5. **Thompson, M. K.; Ghiladi, R.; Franzen, S.;** "The Dehaloperoxidase Paradox" Biochim. Biophys. Acta – Proteins and Proteomics, **2012**, 1842, 578-588

ATR-FTIR spectroscopy study of hydrogen bonding trends, Physical Chemistry Lab #2

Hydrogen bonding is a central aspect of molecular interactions in chemistry ranging from biochemistry to materials science. In this laboratory experiment we will use vibrational spectroscopy measured in by attenuated total reflection (ATR) Fourier transform infrared (FTIR) spectroscopy.

2.1 Introduction

Hydrogen bonding between phenols and amides to form 1:1 and 2:1 hydrogen bonding complexes has been previously described in the literature.[2] In order to determine the strength of interaction between two molecules one would prefer to have pure 1:1 bonding complexes. In this lab we will assume that the 1:2 hydrogen bonding complexes are a minor component and do not interfere with the observations. IR spectra of the phenol-amide hydrogen bonding complexes reveal a shift in the stretching frequency of the amide carbonyl group (Figure 2.1).[2] The magnitude of the shift is dependent on the identity of the phenol.

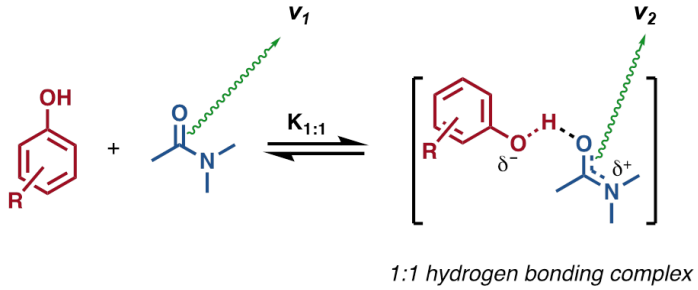

Figure 2.1. Diagram of the formation of a 1:1 hydrogen bonding complex between a phenol and an amide. The stretching frequencies of the uncomplexed and complexed amide are designated v1 and v2.

Figure 2.1 shows the target molecules studied in this laboratory experiment, N,N-dimethylacetamide (DMA) and a series of substituted phenols. We will explore the relationships between phenol pK_a, the Hammett values for the phenol substitutions (σ), amide carbonyl stretching frequencies, and hydrogen bonding complexation energies.

2.2 Experimental

The experiments will be carried out on a Bruker single reflectance ATR FTIR instrument. Each sample should be measured by a minimum of 16 scans from 400 cm^{-1} to 4,000 cm^{-1} with 4 cm^{-1} resolution. We will use the following phenols were used in the experiments: 4-chlorophenol, 4-bromophenol, 4-methoxyphenol, 4-cyanophenol, 4-nitrophenol, and para-cresol (4-methylphenol). These molecules will be dissolved in toluene with DMA added to create solutions that can be deposited on the ATR-FTIR element for measurement. Measurements should be made quickly to avoid losses of solvent due to evaporation. Evaporation is unavoidable in the experimental configuration used and is one of the sources of systematic error in this experiment.

2.2.1 Sample preparation

1. Make solutions with the following phenols; 4-nitrophenol, 4-cyanophenol, 4-methoxyphenol, 4-chlorophenol, 4-bromophenol and phenol. Make solutions by weighing out *ca.* 100 millimoles of each phenol and then dissolving the phenol in 5 mL of toluene. For example, for phenol this would be 94 mg of sample added to a 5 mL volumetric flask followed by addition of toluene solvent up to the mark. The para-phenol solutions are then added to 10 mL volumetric flasks. Add 0.25 mL of N,N-dimethylacetamide (DMA) to each 10 mL volumetric flask containing the phenol solution, and dilute to 10 mL with toluene. Note that DMA is a liquid and you may dispense the neat liquid using a syringe. Five drops of a sample

solution, delivered with a glass Pasteur pipette, is then added to the ATR crystal and the measurement is immediately started. These samples were not used for equilibrium studies. You should also measure the frequency of DMA by itself without any phenol. However, in each of the above mixtures, there will likely be an equilibrium such that there is some free DMA and some bound DMA, which has a frequency shift due to hydrogen bonding with the respective phenol.

2. For binding/equilibrium studies of 4-chlorophenol, the general procedure described above was employed with the exception that *ca.* 0.200 moles of 4-chlorophenol should be weighed and diluted in a volumetric flask to make a 10 mL stock solution. Various volumes of this solution ranging from 0.1 mL to 5 mL will be added to 10 mL volumetric flask, 0.25 mL DMA is added the solution is diluted to the mark. Thus, the concentration of DMA is held constant and the concentration of 4-chlorophenol binding is changed over a factor of 10 to cover an important range of binding. For example, the 10 mL stock solution can be added in the following volumes, 0.1 mL, 0.2 mL 0.3mL 0.5 mL 1.0 mL, 3.0 mL, 5.0 mL.

2.2.2 Comparison of frequency shifts due to hydrogen bonding

The shift in the DMA carbonyl stretching frequency (Δv) is defined as:

$$\Delta v = v_{uncomplexed\ DMA} - v_{complexed\ DMA} \quad (1)$$

The value obtained for the carbonyl stretched of uncomplexed DMA is 1660 cm^{-1}, and is in accordance with literature reports (although in different solvents).[2] Typical values for the carbonyl stretches of DMA complexed with various phenols ranged from 1625 cm^{-1} to 1633 cm^{-1}, giving Δv values of 27-35 cm^{-1}. Δv measurements are taken from the wavenumber that gives the maximum peak height for the desired peak (figure 2).

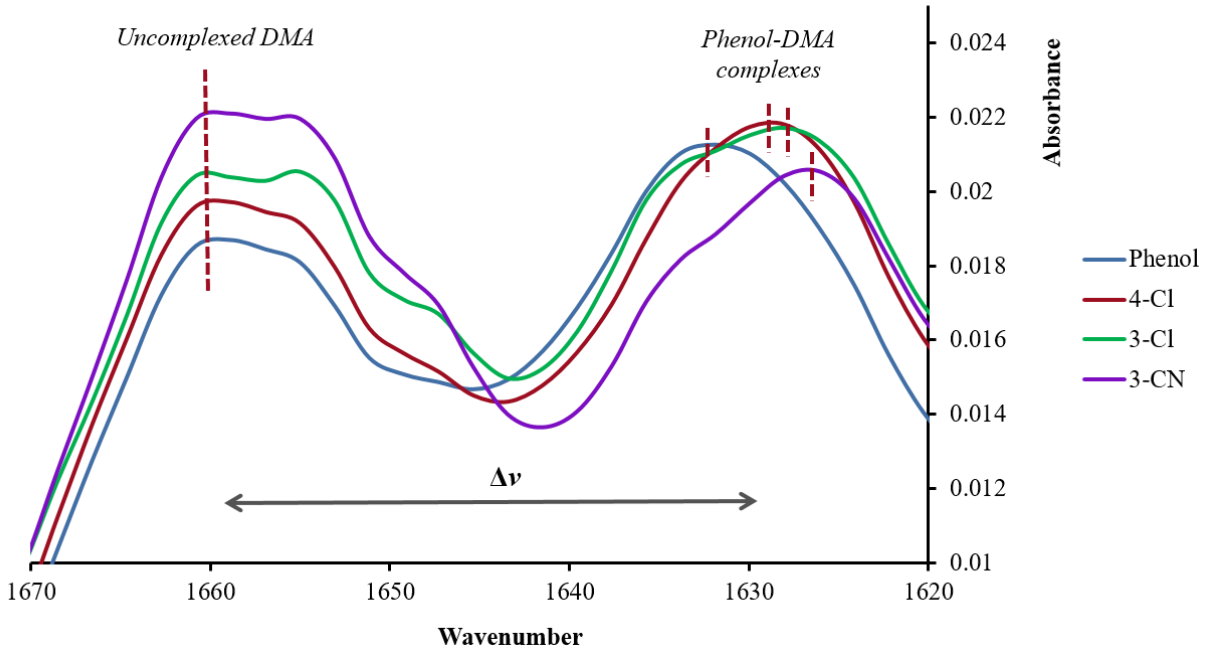

Figure 2. Typical FTIR spectra of DMA/phenol mixtures observing the shift in the carbonyl stretching frequency between DMA and select DMA-phenol complexes.

2.2.3 Equilibrium binding study

Given the following equilibrium:

$$DMA + Phenol \rightleftharpoons 1{:}1\ Complex \tag{2}$$

We have the following:

$$K_{1:1} = \frac{[AP]}{[A][P]} \tag{3}$$

where $K_{1:1}$ is the association equilibrium constant for the formation of the 1:1 phenol-amide complex, [AP], [A] and [P] are the concentrations of the complex, amide (DMA), and phenol, respectively.[2] Assuming the ratio of concentration of the complex to the sum of the concentration of the complex plus the concentration of amide is proportional to the ratio of their absorbances, we may write:

$$\frac{[AP]}{[AP] + [A]} \approx \frac{\mathrm{A}_{AP}}{\mathrm{A}_{AP} + \mathrm{A}_{A}} \equiv \frac{\mathrm{A}_{AP}}{\mathrm{A}_{T}} \tag{4}$$

Re-writing in terms of equilibrium constant and phenol concentration, we have:

$$\frac{\mathrm{A}_{AP}}{\mathrm{A}_{T}} = S\frac{K_{1:1}[P]}{1 + K_{1:1}[P]} \tag{5}$$

where S represents a scaling coefficient. Ideally, S would have the value of one; however, this arises from when the ratio of concentrations is equal to the ratio of the absorbances. The value of S may deviate from one because of experimental factors such as baseline corrections or absorbance from interfering species.

The absorbance for a given peak may be obtained from maximum absorbance for that peak. However, the peaks are overlapping in this case and that way of estimating the intensity has a potential error. Fitting the peaks of A_{AP} and A_A is a more accurate way to obtain the relative populations of molecules in each configuration (hydrogen-bonded and non-hydrogen-bonded). You may use a model with two Gaussian functions to fit the data and thereby to obtain an estimate for the relative concentration in each configuration. Irrespective of the method used to obtain the absorbance, A_{AP}/A_T is plotted as a function of phenol concentration to obtain the experimental function given by Eqn. 5 . The absorbance data may then be fit to the equation using non-linear least squares fitting with $K_{1:1}$ and S as parameters. Non-linear least-squares fitting can be implemented in Excel using the Solver function.

2.3 Analysis

2.3.1 Application of the Hammett equation

The Hammett equation provides a linear free-energy relationship that relates reaction rates and equilibrium constants for reactions involving benzoic acid derivatives. Specifically, meta- and para-derivatives are classified in terms of their electron donating or withdrawing capability and these inductive effects are quantified with two parameters: a substituent constant and a reaction constant. The equation published by Louis Plack Hammett in 1937.

The basic idea is that for any two reactions with two aromatic reactants only differing in the type of substituent, the change in free energy of activation is proportional to the change in the Gibbs free energy. The Hammett equation is

$$\log\frac{K}{K_0} = \sigma\rho$$

The equilibrium constant K in a benzoic acid with a substituent (e.g. chloro-, fluoro-, nitro-, methyl- etc.) is related to the reference equilibrium constant, K_0, when hydrogen is the bonded atom. The σ depends on the substituent and has a tabulated value. The ρ constant depends on the type of reaction. Although these relationships were derived for benzoic acid, subsequently they have been used for a wide range of aromatic compounds, including phenols. The reaction can be loss of H^+ and therefore the σ constant relates to K_a of the acid. This relationship can also apply to reactions such as hydrogen bond formation as described above in this laboratory.

2.3.2 Gaussian fitting using the non-linear least squares method

2.4 Laboratory Report

The report should present an analysis of the two types of data obtained. The series of frequency shifts can be plotted vs. the Hammett σ parameter or even the pKa of the phenols. The pKa also should be correlated with the Hammett σ parameter, which is one reason why the latter correlation should provide a linear relationship. It should be born in mind that the pKa is determined in water, while the solvent used in this experiment was toluene. Nonetheless, the electron-withdrawing or donating character of the para substituent in the phenol plays an analogous role in each of these observations.

The equilibrium data can be plotted as a function of the fraction bound vs. the phenol concentration. The fraction bound is determined from the area under the curves of the A and AP FTIR bands. The fit to two parameters described above gives an estimate of the equilibrium constant. An equilibrium constant in turn gives the free energy of the reaction, which in this case is the formation of a hydrogen bond.

All plots should be presented with an appropriate error analysis. Two types of fitting are involved, linear least squares for the first part and non-linear least squares for the second part.

References

1. **Roy, K.; Popelier, P. L. A.** *J. Phys. Org. Chem.* **2009**, *22*, 186 – 196. (diff solvents)

2. **Malathi, M.; Sabesan, R.; Krishnan, S.** *Current Science* **2004**, *86(6)*, 838 – 842.

3. **Gordy, W.** *J. Chem. Phys.* **1946**, *14(5)*, 305 – 320.

4. **Badger, R. M. *J.*** *Chem. Phys.* **1934**, *2*, 128 – 131.

5. **Gross, K. C.; Seybold,** *Int. J. Quantum Chem.* **2001**, *85*, 569 – 579.

6. **Myshakina, N. S.; Ahmed, Z.; Asher, S. A.** *J. Phys. Chem. B.* **2008**, *112(38)*, 11873 – 11877.

7. **Cunningham, I. D.; Bhaila, K.; Povey, D. C.** *Computational and Theoretical Chemistry* **2013**, *1019*, 55 – 60.

8. **Liptak, M. D.; Gross, K. C.; Seybold, P. G.; Feldgus, S.; Shields, G. C.** *J. Am. Chem. Soc.* **2002**, *124*, 6421 – 6427.

9. **Frohlich, N. S.; Ahmed, Z.; Asher S. A.** *J. Phys. Chem. B.* **2008**, *112(38)*, 11873 – 11877.

Luminescence Quenching Experiment

CH454 Physical Chemistry Lab #3

Introduction

This laboratory experiment will provide you with an introduction to the study the quantum yield and kinetics of luminescence quenching. Luminscence encompasses emission by both the singlet and triplet states, fluorescence and phosphorescence, respectively. Your study will use either fluorescein (uranine) or the $Ru(bpy)_3^{2+}$ complex as the sample. Fluorescein is moderately soluble in water while uranine is a water soluble variant. Fluorescein and its derivatives has been widely used in protein labeling studies and microscopy. $Ru(bpy)_3^{2+}$ has been used as a photosensitizer in photoelectrochemistry (solar energy) applications. $Ru(bpy)_3^{2+}$ is a convenient laboratory example, because it has a long-lived excited state of several hundred nanoseconds. It should be understood that $Ru(bpy)_3^{2+}$ undergoes rapid intersystem crossing to the triplet state so it is technically not a fluorophore, but rather a phosphor. Fluorescein is a fluorophore and has an observed lifetime of less than 10 nanoseconds.

3.1 Photophysical processes and quenching

Fluorescence vs. Phosphorescence. Excited states can be deactivated either by be **radiative** or **nonradiative** processes. Spin allowed radiative transitions are usually short-lived ($< 10^{-8}$ s) and give rise to luminescence, which is known as ***fluorescence***. Spin forbidden radiative transitions can also be observed as a long-lived luminescence, which is called ***phosphorescence***. Since singlet-triplet transitions are spin-forbidden, triplet excited states can be form only by means of a process known as **intersystem crossing**. The intersystem designation refers to the fact that the molecular system crosses from the singlet to the triplet state manifold. Although phosphorescence is often difficult to observe in many organic molecules, it is readily observed in $Ru(bipy)_3^{2+}$. Fluorescein, on the other hand normally radiates from the singlet state, but can undergo quenching via formation of a triplet state in the presence of a heavy atom, such as iodine in triiodide.

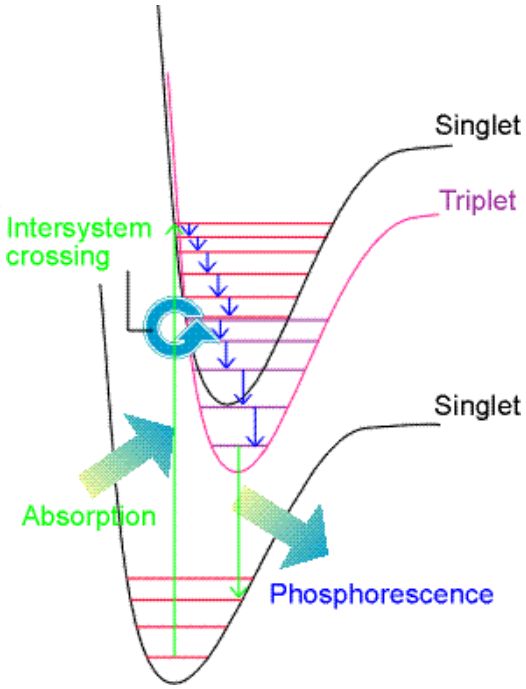

In order to understand the observations in this experiment you will want to review first order and second order kinetics, fluorescence and phosphorescence, and various quenching mechanisms. These include energy transfer, charge transfer and intersystem crossing mechanisms among others. Experiments involving $Ru(bpy)_3^{2+}$ are based on energy transfer quenching. Since $Ru(bpy)_3^{2+}$ rapidly forms a triplet state, quenching can be combined with a

second process of triplet-triplet annihilation in the acceptor to make a higher energy singlet state. Fluorescein, on the other hand, radiates from a singlet state and is quenched by intersystem crossing to form a triplet state.

3.1.1 Quenching of ruthenium (tris)-bipyridine

The donor for triplet energy transfer used in this experiment is $Ru(bpy)_3^{2+}$, which is shown in Figure 3.1.

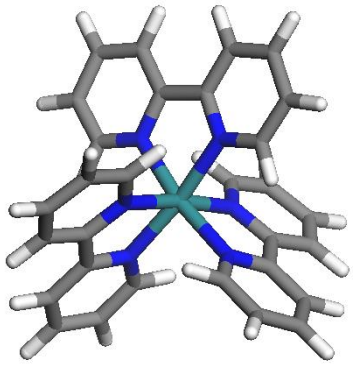

Figure 3.1. The structure of the $Ru(bpy)_3^{2+}$ ion

These bidentate ligands form *tris* complexes with Ru(II) that have approximately D_3 point group symmetry. The electronic absorption spectrum of $Ru(bpy)_3^{2+}$ at room temperature consists of a broad band from 400-460 nm. This transition consists of a (spin allowed) metal-to-ligand charge transfer (MLCT) from a molecular orbital that has mostly Ru(II) *d* orbital character to a molecular orbital that has mostly ligand π orbital character. Since the band is a MLCT band it has a large excited state dipole moment.

Ru(II) complexes are excited by metal-to-ligand charge transfer (MLCT) transitions. For example, in the bipy complex the process initially forms a singlet MLCT state. However, this singlet state forms a triplet state by intersystem crossing.

$$^1Ru(bpy)_3^{2+} \rightarrow {}^3Ru(bpy)_3^{2+}$$

One reason for this is the heavy atom effect of Ru, which increases the spin-orbit coupling process leading to a spin flip. Once the triplet state is formed the excited state of $^3Ru(bpy)_3^{2+}$ can be quenched by anthracene. Since $Ru(bpy)_3^{2+}$ has evolved to the triplet state the luminescence is phosphorescence rather than fluorescence. However, many people mistakenly refer to the luminescence as fluorescence. In this experiment we will use 9,10-diphenylanthracene (DPA) since that molecule cannot undergo photochemical crosslinking reactions.

$$^3Ru(bpy)_3^{2+} + DPA \rightarrow Ru(bpy)_3^{2+} + {}^3DPA$$

This aspect of the experiment is fairly routine since phosphorescence quenching of $Ru(bpy)_3^{2+}$ obeys standard quenching kinetics, so-called Stern-Volmer kinetics. The Stern-Volmer model is the same for fluorescence and phosphorescence quenching. The experiment we will study has an added process, which is the combination of two 3DPA molecules by triplet-triplet annihilation to make a higher energy singlet DPA.

$$2\ {}^3DPA \rightarrow\ DPA + {}^1DPA$$

When these reactions are combined they are given the name "upconversion" to refer to the fact that the output photon from the fluorescence of 1DPA has a higher energy than the input photon used to excite $Ru(bipy)_3^{2+}$. The issues surrounding the quenching of phosphorescence are the core of the lab. The observation of upconversion is mainly to show you one of the numerous applications of quenching processes.

Ru(II) diimine complexes are relatively highly luminescent, even though observed emission is from a triplet ^{3}MLCT excited state. The reason for that is in a high spin-orbit coupling (Ru is a *heavy* metal) which couples singlet and triplet manifold of states in so called 'configurational interaction' and results in relatively short radiative lifetime. At room temperature and in aqueous solution, $^3Ru(bpy)_3^{2+}$ shows strong luminescence at about 600 nm with lifetime around $\tau_o \sim 600$ ns. There are two processes that compete with the phosphorescent deactivation. These are internal non-radiative process intrinsic to $^3Ru(bpy)_3^{2+}$ and quenching processes. In this case we will focus on energy transfer quenching, which means that the triplet state of $^3Ru(bpy)_3^{2+}$ is transferred to the energy transfer acceptor, which is 1,9-diphenylanthracene (DPA).

Luminescence:	$^3Ru(bpy)_3^{2+} \rightarrow Ru(bpy)_3^{2+} + h\nu$	(1)
Nonradiative deactivation:	$^3Ru(bpy)_3^{2+} \rightarrow Ru(bpy)_3^{2+} + heat$	(2)
Quenching:	$^3Ru(bpy)_3^{2+} + Q \rightarrow Ru(bpy)_3^{2+} + {}^3Q$	(3)

As discussed below it is necessary to measure both the relative quantum yield and lifetime of luminescence to obtain fundamental properties of the molecule.

3.1.2 Quenching of fluorescein

Fluorescein is an aromatic molecule that has a very high fluorescence quantum yield. It can be synthesized in a functionalized form with an isocyanate group that is reactive towards primary amines, appropriate for labeling proteins. Fluorescein has some disadvantages such as pH-sensitivity and tendency to photobleach. Fluorescein undergoes a protonation with a pKa of 6.8. Below pH ~ 7 it has low absorption consequently it is a poor fluorophore. However, above pH 8 it has a high absorption cross section and it is an excellent fluorophore. The photobleaching has been addressed by replacement of the hydrogen atoms with fluorine atoms in the derivative

Oregon Green. Fluorescein's relatively low solubility in water has been overcome by synthesizing soluble analogs, such as uranine.

3.2 **Kinetics of luminescence and quenching.**

In the following discussion, we will refer to the luminescence as fluorescence. The discussion applied equally well to phosphorescence. Without a quencher, a fluorophore decays radiatively with an observed rate constant of $k_{obs} = k_r + k_{nr}$, where the radiative rate constant is k_r and the non-radiative rate constant is k_{nr}. If we assume that the laser pulse produces a population N_o of excited molecules, ^1F at time $t = 0$, the population can be shown to decay exponentially (first order kinetics), resulting in the following time dependence of the emission intensity I (photons/sec):

$$I = k_r[\,^1F] = k_r N_0 \exp\{-t/\tau_0\} \tag{4}$$

where

$$\tau_0 = (k_r + k_{nr})^{-1} \tag{5}$$

The quenched emission decay will proceed with an accelerated speed. In other words, its lifetime will be shorter:

$$I = k_r N_0 \exp\{-t/\tau\} \tag{6}$$

Where

$$\tau = (k_r + k_{nr} + k_q[Q])^{-1} \tag{7}$$

Thus, the rate constant for the quenching reaction, k_q, can be obtained by analyzing the luminescence data. The quenching rate constant, k_q, is determined from the so-called **Stern-Volmer** relation:

$$\frac{\tau_0}{\tau} = 1 + \tau_0 k_q[Q] \tag{8}$$

which can be obtained from the rearrangement of Equations 5 and 7. The quantum yield of luminescence is proportional to the luminescence intensity, so that the Stern-Volmer relation may also be written as:

$$\frac{I_0}{I} = 1 + \tau_0 k_q[Q] \tag{9}$$

where I_o and τ_o are the luminescence intensity and the luminescence lifetime of $^3Ru(bpy)_3^{2+}$ in the absence of quencher.

The equations above suggests that k_q may be obtained from an experiment where the luminescence lifetime or the luminescence intensity of $Ru(bpy)_3^{2+}$ is measured at different quencher concentrations. A plot of τ_o/τ (or I_o/I) versus [Q] is expected to be linear, with a slope:

$$K_{sv} = \tau_0 k_q \tag{10}$$

where K_{sv} is the Stern-Volmer rate constant.

Stern-Volmer quenching is derived with the assumption of dynamic quenching, which means that the quenching is free to diffuse in solution and that it interacts with the luminescent molecule by a second-order process. However, one must always be aware of the possibility that two molecules have formed a complex and therefore that the quenching is static, rather than dynamic. In order to be sure that a process is due to dynamic quenching it is necessary to determine both the yield and the lifetime.

Diffusion limited reactions. In a dynamic process the quenching rate constant k_q is a bimolecular rate constant (has units $M^{-1}s^{-1}$) and describes a process, in which the reactants first have to encounter and then react. Such reactions are often referred to as diffusion-assisted reactions. It is convenient to separate a reaction into two steps. First, there is a diffusion controlled formation of intermediate complex (A*...Q) or transition state, with k_{diff}, and second the transition state can either react with the (first order) rate constant k_p or dissociate without reacting with the rate constant k_{-diff} (also first order) :

$$A^*+Q \underset{k_{-diff}}{\overset{k_{diff}}{<=>}} (A^*...Q) \xrightarrow{k_p} \text{Products} \tag{11}$$

Then the overall rate constant k' can be written as:

$$k' = \frac{k_{diff} k_p}{k_{diff} + k_p} \tag{12}$$

which in the limit of fast reaction rate $k_p >> k_{-diff}$ simplifies to:

$$k' = k_{diff} \tag{13}$$

when the diffusion becomes a limiting step. This case would correspond to the diffusion controlled (or diffusion limited) regime, when no matter how fast k_p is, the observed k' would be defined by how fast molecules encounter due to diffusion. The value of k_{diff} obviously depends on the diffusion coefficients of both reactants:

$$D = D_A + D_Q \tag{14}$$

According to the rate equation:

$$k_{diff} = 4\pi N_a D R_q \quad (15)$$

where N_a is the Avogadro's number 6.022 x 10^{23} mol^{-1}, and R_q is the separation at which the quenching takes place, also called the quenching radius. For neutral molecules, the quenching radius equals the sum of molecular radii:

$$R_q = R_A + R_Q \quad (16)$$

but the situation can differ dramatically if both species are charged. The Coulombic interaction leads to the following condition:

$R_q > R_A + R_Q$- for oppositely charged ions (17)
$R_q < R_A + R_Q$- for ions of the same charge (18)

Mechanisms of quenching. A variety of inorganic and organic species may act as quenchers. Determining k_q does not give any insight into the mechanism of quenching. For a given system, k_q may reflect a combination of energy and electron transfer processes. Energy transfer could occur in either the singlet or the triplet manifold. By detailed study of the system and application of control experiments one can determine whether the mechanism involves energy transfer or electron transfer. Triplet energy transfer can be established in part using the sensitivity of the process to O_2. Since O_2 has a triplet ground state it is an effective triplet quencher (see below). When applied to simple systems, these criteria help determine the predominant mechanism of quenching.

***Energy transfer**:*	$^*Ru(bpy)_3^{2+} + Q \rightarrow Ru(bpy)_3^{2+} + Q^*$	(19)
*Reductive **electron transfer**:*	$^*Ru(bpy)_3^{2+} + Q \rightarrow Ru(bpy)_3^{+} + Q^{+}$	(20)
*Oxidative **electron transfer**:*	$^*Ru(bpy)_3^{2+} + Q \rightarrow Ru(bpy)_3^{3+} + Q^{-}$	(21)
Intersystem crossing:	^{1}Fluorescein + Q $\rightarrow$ ^{3}Fluorescein + Q	(22)

3.3 Experimental Protocols

3.3.1 Quenching of $[Ru(bpy)_3]^{2+}$ by DPA

Quenching of $[Ru(bpy)_3]^{2+}$, spectral profile of emission and measurement of lifetime

We will use a nitrogen laser which provides excitation pulses of about 4 nsec half-width. A pulse excites a dilute solution of $[Ru(bpy)_3]^{2+}$ and produces a population of excited states $*[Ru(bpy)_3]^{2+}$.

Protocol

This laboratory experiment consists of two parts, 1. The measurement of the emission spectrum and 2. The measurement of the emission lifetime of $Ru(bipy)_3^{2+}$ in solution with added DPA quencher molecules. You need to make solutions of both $Ru(bipy)_3^{2+}$and DPA in dichloromethane (DCM). The ideal solution for measurement of the phosphorescence quenching will have an absorbance of ~ 0.2 in the MLCT band of $Ru(bipy)_3^{2+}$ at ~ 452 nm. However, for observation of upconversion a higher concentration is desirable such that the A ~ 1.0 at 452 nm. Thus, the experiment should be run at two different concentrations of $Ru(bipy)_3^{2+}$. To determine the appropriate concentrations you may use the extinction coefficient of 14,600 $M^{-1}\,cm^{-1}$ at λ_{max} = 452 nm. Note that we will use the PF_6^- salt with the chemical formula $(PF_6)_2Ru(bipy)_3$ with a formula weight of 859.6 a.m.u. The solutions of DPA will need to be much more concentrated since you will need to inject small volumes of this solution into the solution of $(PF_6)_2Ru(bipy)_3$ in order to study a series of different concentrations of the quencher DPA (formula weight 330.4 a.m.u.). Using this background you may prepare the sample using the following step-by-step procedure:

1. The volume required in the quartz cuvette for phosphorescence and time-resolved measurements is ~3 mL.
2. You will need to add aliquots of DPA of volumes ranging from 10-100 μL to this solution. The stock solution of DPA should be approximately 20 mM. Add aliquots of this solution successively to the cuvette and acquire an emission spectrum and a time-resolved kinetics trace for each concentration. Use at least 5 concentrations of DPA (in addition to the pure $Ru(bipy)_3^{2+}$ sample) ranging from 0 – 500 μM. In general, all transfers in such experiments can be carried out using so-called Hamilton syringes. Hamilton has been the leading company that makes gas tight syringes for many years. Standard Hamilton syringes range in volume from 10 μL to 1000 μL.
3. It is important to obtain the absorption spectrum of each solution since the absorption spectrum can be used to correct for any change in concentration in $Ru(bipy)_3^{2+}$ due to the addition of DPA.
4. Each sample will be studied by two experiments:
   A. Fluorescence emission from 550 to 850 nm. You will use the Edinburgh Instruments fluorescence spectrometer. The instructions are given below.
   B. Time-resolved kinetics using the nanosecond fluorescence spectrometer. The instructions are given below.
5. Save the data in each experiment in ACSII format. For example, on the Edinburgh Instruments spectrometer use the EXPORT selection on the menu to write the data to disk. The data on the time-resolved nanosecond kinetics apparatus are stored on a Tektronix fast oscilloscope. The data need to be saved to a thumb drive of < 2Gb.

CAUTION #1: Xe arc lamps output a high voltage spike when the initially powered on. It is a good idea to power on the Xe arc lamp before other more sensitive circuits. Computers are fortunately not sensitive to these spikes.

CAUTION #2: Photomultiplier tubes (PMT) are sensitive detectors that can be destroyed by high light levels. Please follow the guidelines of each instrument closely and never change settings without consulting with your instructor. DO NOT CHANGE THE PMT VOLTAGE SETTINGS!

Edinburgh Instruments Fluorometer

There are three power supplies that need to be switched on. These are on the rack above the laser table. These consist of the Xe-arc lamp (always turn this on first!), then the photomultiplier tube (PMT) power supply and the temperature controller (in any order after the lamp). There is also a power switch on other side for the internal controls of the fluorometer. This switch is sometimes left on.

The software on the computer is FL900. Open the software and check the signal at the initial wavelength settings. There are two digital meters, one of the reference and one for the sample PMT. Monitor the number of counts per second recorded by the PMT. The bandwidth (Dl) will mostly be set to 4.00 nm for both the excitation and the emission. However, it is a good idea to set it to a smaller value (for example, 1.00 nm) when you first make a measurement. The idea is to limit the number of photons striking the PMT. This number should be less than 8×10^6.

Set the excitation wavelength to 470 nm. Set the emission scan from 550 – 850 nm. The dwell time should be 0.1 seconds and the increment 1 nm. Set the number of scans to 3. The data will be written to a binary data file on the hard drive. In order to be able to use the data for analysis you will need to export it. In scientific software the export function is the usual way to write data in ASCII format as columns of numbers separate by either a comma or tab. This format can be read by programs such as Excel, Origin, Igor, etc. that are used for data fitting and analysis.

Time-Resolved Emission Apparatus (Optional)

There is a black notebook on the table describing the steps to setup a time-resolved scan. You will work with your instructor to turn on the instrument and set up to take data. You may take data on your own by switching out samples and recording data, but do not change settings for the PMT or laser. You may examine the settings on the digital oscilloscope and your instructor will show you how to check for the trigger level, the settings in terms of time scale, voltage scale and so on. These are described in the book as well.

The Upconversion Measurement (Done as Demo)

Upconversion is an idea that has been developed and demonstrated in the Castellano research group. We have chosen a quenching experiment that added functionality. We can attempt to estimate the yield of upconversion by measuring the fluorescence emission of ^{1}DPA

created by triplet-triplet annihilation. You measure that emission between 250 and 400 nm. However, may need a concentrated sample to see the effect.

This laboratory experiment will provide an example of energy transfer quenching. When energy transfer takes place according to a transition dipole-transition dipole mechanism it is known as Förster energy transfer. Efficient energy transfer depends on a number of factors. There is a $1/R^6$ distance dependence for Förster energy transfer. This distance dependence arises from the dipolar nature of the process since the electric field that results from a dipole decays at $1/R^3$. A pair of dipoles that interact mutually has a distance dependence of $(1/R^3)^2 = 1/R^6$. There is also an orientation dependence for Förster energy transfer since the probability of energy transferring from one dipole to another depends on the square of the cosine of the angle between the two transition dipole moments. Clearly, there are many orientations in solution and one must carry out an orientation average. For a given distance, energy transfer depends on the Franck-Condon factors of the two molecules. The luminescence of the donor must have overlap with the absorption of acceptor. This condition does not mean that light is emitted by the donor and then absorbed by the acceptor. Indeed, energy transfer is NOT such a process, but it is a coherent oscillation of the two transition dipole moments subject to the correction conditions of orientation and energetics. One of your tasks in this laboratory will be to compare the emission of the donor ($^3Ru(bipy)_3^{2+}$) with the triplet absorption spectrum of the acceptor (DPA $\rightarrow$ ^{3}DPA).

Degassing of samples. We will not be degassing the solutions in the experiment due to lack of time. Given the role played by O_2 as a triplet quencher it would be ideal to degas the solution of any sample, in which one wishes to measure the triplet energy transfer yield or rate constant. Degassing can be accomplished by two methods. First, one can use freeze-pump-thaw as a method. Second, one can bubble a gas such as N_2 or Ar through the sample for a period of time (usually about 20 minutes). Freeze-pump-thaw is considered the best way to degas a sample. However, it is quite time consuming. One usually freezes the sample in liquid N_2 or some other cryogen, then pumps on the sample by attaching it to a vacuum manifold and finally permits the sample to thaw after it is sealed so it has no contact with the atmosphere. Usually this process is repeated three times to ensure that all of the residual O_2 gas is removed from the sample. Degassing by bubbling a solvent is much faster, but is not as well controlled and has the disadvantage that one will often lose a fair amount of volatile solvent due to evaporation. One can control for evaporation by weighing the sample and either recording the new concentration or adding a small amount of (degassed!) solvent to the sample using a gas tight syringe. All of these steps are prone to leaks or other imperfections, which tend to reduce the reproducibility of the measurements. If different samples are degassed to different extents the measurement becomes very poor. Hence, we will determine the quenching constant with a background of O_2 present in the samples.

Compare the $Ru(bipy)_3^{2+}$ emission spectrum to the DPA absorption spectrum. Keep in mind the criteria for energy transfer and discuss the features and relationship of these two spectra. In this case the transfer is from $^3Ru(bipy)_3^{2+}$ to ^{3}DPA so that the absorption spectrum of interest is the DPA $\rightarrow$ ^{3}DPA transition. What are the consequences of incomplete deoxygenation of the sample? Which observables are the most sensitive to O_2 quenching. Include the production of $^1O_2$ in your discussion.

3.3.2 Quenching of uranine by iodide

Fluorescence quenching of uranine can involve either intersystem crossing using the heavy atom effect or energy transfer, using an acceptor fluorophore such as rhodamine 6G. We will focus on intersystem crossing in the protocol. One of the advantages of studying fluorescence is that there is no competing quenching by O_2 (see above). Hence, we do not need to concern ourselves with degassing. However, given the much shorter lifetimes we will need to use a time-resolved experiment that has nanosecond time resolution. For this we will use time-correlated single photon counting (TCSPC). The Horiba XXX is both a fluorometer and TCSPC instrument. Please use appropriate care when turning on the instrument. The order is very important.

Protocol

To conduct this experiment you will need the following reagents:

A. 1 M sodium borate buffer at pH 8.5.
B. Stock solution of uranine.
C. 0.5 M KI Solution

See Appendix 2 for more information on the borate buffer system used in this experiment.

Weigh out approximately 14 milligrams of uranine and place it in a 10 milliter volumetric flask. Add pH 8.5 0.1 M borate buffer to the mark. This stock solution is approximately 100X The uranine solution can be conveniently diluted first by a factor of 10 by dispensing 200 μL of the stock solution into 2 mL. After the first dilution the absorbance at 494 nm was approximately 1.0. A second dilution by a factor 10 can be used to dilute the sodium borate buffer to 0.01 M and to permit various concentrations of KI to be present in the final solution. After the second dilution the absorbance of uranine at 494 nm was close to 0.1.

Instrumental procedures

1. First use the switch on the side of the main fluorometer to turn on the instrument. NOTE: This switch turns on the Xe arc lamp, which has a damaging voltage pulse. This should always be turned on before any other instrumentation including the computer.
2. Turn on the DataHub and NanoLED last. First turn on the FluoroMax and then the computer. Make sure the lamp is on (on the left-hand side of the Fluoromax). Finally, turn on the DataJHub and NanoLED.
3. Turn on the computer. Use DataStation software.
4. Set the detector bias voltage to 950 V using the software. Open the shutter. The bandwidth should be set to 1 nm. Peak Preset: 10000 counts.
5. For the Prompt collection (i.e. the standard sample used to obtain the instrument response function) you will use a monochromator setting of 509 nm, which is equal to

the laser frequency. The scatterer used to obtain instrument function is a 0.01% solution of LUDOX. (Ludox AS40 colloidal silica(Sigma-Aldrich order code 42, 084-0 is used in purified water). We have used DI water.

6. The Decay function is the sample of interest. Note that you must save the decay together with the "prompt", which contains the instrument function. Once you have saved it you may delete the decay, but keep the same instrument function for repeated use on a series of samples, e.g. with different quencher concentrations.

Before commencing a decay measurement, collect absorbance data and steady-state fluorescence data for the sample to be measured, which will aid in determining the best wavelengths for excitation and emission. Verifying that the absorbance at your chosen excitation wavelength is approximately 0.1 (certainly no greater than 0.2). This is important to ensure that you do not encounter inner filter effects during your measurement.

3.4 Experimental and analytical methods

3.4.1 Obtaining kinetic data using time correlated single photon counting (TCSPC)

TCSPC is used to measure fast kinetics of fluorescence or other emission processes. Direct measurement of processes that have lifetimes less than 10 ns is difficult since most circuits have an RC time constant that is at least several ns. This time constant limits the rise time of the circuit. We would like the rise time of the electronics to be rapid relative to the kinetics. The "trick" of counting single photons permits us to measure rapid kinetics down to 1 ns or even less with high quality equipment.

The method uses a laser that has low power and high repetition rate. In our instrument, the laser is a 1 MHz laser with a pulse that is approximately 1 ns at 509 nm. The laser light may be scattered in which case there is no delay between the incident light and the light on the detector. Actually, to be precise there is a delay equal to the time it takes for the light to reach the detector from the sample. Let's estimate this as 0.1 m. Then given the speed of light of 3.8 x 10^8 m/s that delay is

$$\tau_{delay} = \frac{0.1\ m}{3.0\ x\ 10^8\ m/s} = 3.33\ x\ 10^{-9}\ s$$

But, this 3.33 ns delay is a constant for any sample. If a molecule in the cuvette has a fluorescence emission then there is an additional delay possible as the photon promotes the molecule to the excited state and then an photon at a different wavelength is emitted some nanoseconds later. The idea behind TCSPC is to measure the individual delays of the emitted photons in electronic bins that count how many photons are emitted with a given delay. More photons will be emitted in the 1 ns bin than the 2 ns bin etc. So by collecting thousands of photons we build up a histogram of the delay times. That histogram should have the form of a kinetic trace. In theory it is the same as what we would measure with a photodiode if it were possible to build a circuit with a response time that is fast enough. But, there is one caveat. The laser itself has a pulse shape on the nanosecond time scale. There are lasers that can generate very short pulses, but these are more expensive than our laser. Therefore, we must measure the

shape of the pulse of the 509 nm laser and then "deconvolve" that pulse from our kinetic signal. For this reason we perform an experiment with a sample that scatters light (LUDOX) as a means of measuring the laser pulse. This is called the "prompt". Then we measure the kinetic trace of the fluorescence. Both of these are stored together in one data file.

3.4.2 Fitting data based on the instrument response function convolution integral

You may import your data into the fitting program provided by Horiba for data analysis. The data set consists of the instrument response function (prompt) and the fluorescence data (decay). If we assume that the instrument response function has the form $f(t)$ then the fitting of a single exponential $g(t) = e^{-kt}$ involves non-linear fitting of the convolution integral

$$S(t) = \int_0^\tau f(t)g(\tau - t)dt$$

Where $S(t)$ is the signal in the data (decay) and $f(t)$ is the prompt. The deconvolution integral becomes

$$S(t) = \int_0^\tau f(t)e^{-k(\tau - t)}dt$$

This type of fitting is non-trivial. It has been described in article by Tang and Norris.[10] Fortunately, the software provided by Horiba carries out this fit. It also properly estimates the noise based on the base line. You should understand that the x-axis of the data is not time, but bin number. Normally, your time window is 200 ns. There are 4096 bins in that time. Thus, there are approximately 20 bins per ns. The program takes all of this into account and provides you with the rate constant, baseline and error estimate for the non-linear fit.

3.5 Report

You will acquire three kinds of data in this laboratory experiment, 1. UV-vis absorption spectra (on the HP8453 photodiode array), 2. Fluorescence or Phosphorescence spectra from a fluorometer and 3. Time-resolved emission kinetics. You will use the Stern-Volmer relation to make a linear plot of the relative integrated fluorescence/phosphorescence yield as a function of [Q], the quenching concentration. From a straight-line fit of these data (using linear least squares) you will obtain a slope. However, to further analyze that slope you need an independent measure of the observed fluorescence/phosphorescence decay time from the time-resolved setup. If the quenching is dynamic quenching then you should also see a change in the lifetime as you increase the quencher concentration. Thus, the time-resolved experiment is a check on the assumptions of the Stern-Volmer derivation (dynamic quenching).

In the analysis, you will first need to normalize the data to the initial fluorophore/phosphor concentration using the UV-vis spectra. You can prepare separate samples or add aliquots of quencher to a sample and correct for the change in volume. The latter method should never result in an increase of more than 20% in volume. As you add aliquots of the

quencher, the absorbance will decrease slightly. Thus, you can multiply the fluorescence by the value $A_{initial}/A_{sample}$ for each sample you study ($A_{initial}$ means the absorbance of pure fluorophore and A_{sample} refers to the same measurement on each sample studied. Keep careful notes and a simple consistent nomenclature to avoid confusion in the interpretation of the files.

Integrate each phosphorescence/fluorescence signal in a software package such as Excel, Origin or Igor. Fit each decay to an exponential model in a software package. Examine the residuals to ensure that the fit to a single exponential is adequate. Use the integrated values obtained from the experiment to determine the Stern-Volmer rate constant (Eqn. 9). You will then need to use the measured lifetime, τ_0, to determine the quenching rate constant (Eqn. 10).

Points for discussion

Look in the chemical literature and find diffusion coefficients for the molecules studied here or similar molecules. Using an estimate of the diffusion coefficient calculate the quenching radius. Discuss the assumptions that go into this calculation (as discussed above).

References

1. Wilke B.M. and Castellano, F.N. “Photochemical Upconversion: A Physical or Inorganic Chemistry Experiment for Undergraduates Using a Conventional Fluorimeter” J. Chem. Ed. 2013, 90, 786-789
2. Singh-Rachford, T.N.;Castellano, F. N. "Photon upconversion based on sensitized triplet-triplet annihilation" Coord Chem. Rev. 2010, 254, 2560-2573
3. Stern, O; Volmer, M "The Fading Time of Fluorescence" Phys. Zetischr. 1919, 20, 183-188
4. Wilkinson F.; Helman, W.R.; Ross A.B. "Quantum Yields for the Photosensitized Formation of the Lowest Electronically Excited Singlet State of Molecular Oxygen in Solution" J. Phys. Chem. Ref. Data 1993, 22, 113-150
5. Chmyrov, A., Sanden, T. & Widengren, J. “Iodide as a Fluorescence Quencher and Promoter-Mechanisms and Possible Implications.” Journal of Physical Chemistry B 2010, 114, 11282-11291
6. Liu, M.W., et al. Instrument Response Standard in Time-Resolved Fluorescence Spectroscopy at Visible Wavelength: Quenched Fluorescein Sodium. Applied Spectroscopy 2014, 68, 577-583
7. Pan, H.F., et al. “Quenched Fluorescein: A Reference Dye for Instrument Response Function of TCSPC. Spectroscopy and Spectral Analysis” 2014, 34, 2284-2288
8. Ponce, C.P., Steer, R.P. & Paige, M.F. “Photophysics and halide quenching of a cationic metalloporphyrin in water.” Photochemical & Photobiological Sciences 2013, 12, 1079-1085
9. Tomin, V.I. “Determination of the Stern-Volmer constant in quantum systems with dual fluorescence.” Optics and Spectroscopy 2008, 105, 223-227
10. Tang, J., Norris, J.R. “Deconvolution of kinetic decays and fitting of multiple exponential decay curves by the linear prediction method” Nuclear Instruments and Methods A 1988, 273, 338-342

Appendix. Quenching mechanisms

A discussion of electron transfer quenching of the $Ru(bipy)_3^{2+}$ excited state.

The electron transfer rate constant, k_{ET}, depends:
(i) distance between the donor and acceptor,
(ii) the degree of quantum mechanical coupling between the molecular orbitals of donor and acceptor, and
(iii) the free energy change, $\Delta G°$
(iv) the reorganization energy, λ.
The latter parameter refers to the energy cost incurred by molecular rearrangements that must result from the transfer of charge along a finite distance. Generally, it is expected that rates of electron transfer will increase with decreasing donor-acceptor distances, and that the maximum rate will be observed when the reaction is activationless, i.e., when $\Delta G°$ is **negative**, preferably when $\mathbf{\Delta G° = - \lambda}$. In other words, the rate is optimized when the standard free energy change for the reaction is matched exactly by the energy required for reorganization of the donor, acceptor, and solvent molecules. In the table below you see the redox potentials for the species involved in this experiment. By analysing it you should conclude what quenching mechanisms are plausible for different quenchers. **NB**. The exact expression for

Species	Redox potential
$Ru(bpy)_3^{3+} + e^- \rightarrow Ru(bpy)_3^{2+}$	+ 1.26 V
$Ru(bpy)_3^{2+} + e^- \rightarrow Ru(bpy)_3^{+}$	+1.28 V
$*Ru(bpy)_3^{2+} \rightarrow Ru(bpy)_3^{3+} + e^-$	+ 0.84 V
$Ru(bpy)_3^{2+} \rightarrow *Ru(bpy)_3^{2+}$	(+ 2.1 V)
$Fe(CN)_6^{3-} + e^- \rightarrow Fe(CN)_6^{4-}$	+ 0.36 V
$Fe(H_2O)_6^{3+} + e^- \rightarrow Fe(H_2O)_6^{2+}$	+ 0.77 V
$O_2 + e^- \rightarrow O_2^-$	– 0.365 V

In principle, there is sufficient potential energy in a photo-generated redox pair that one devise a scheme to split water into H_2 and O_2. The goal of light-driven water splitting has been approached by hundreds of different research teams. The processes relevant to the process using $Ru(bipy)_3^{2+}$ are summarized below, where L represents the diimine ligand and Q represents the oxidant:

$$RuL_3^{2+} + h\nu \rightarrow *RuL_3^{2+}$$
$$*RuL_3^{2+} + Q \rightarrow RuL_3^{3+} + Q^-$$
$$2\ RuL_3^{3+} + H_2O \rightarrow 2\ RuL_3^{2+} + 1/2\ O_2 + 2H^+$$
$$Q^- + H^+ \rightarrow Q + 1/2\ H_2$$

In other words, solar energy can be is used to make fuels from water. Although the chemistry of such a solar cell is straightforward, there are some technological barriers to be overcome before ruthenium (II) complexes can form the basis of a commercial photovoltaic device.

Other applications for photooxidation of ruthenium (II) complexes involves development of due-sensitized photovoltaic devices, where $*RuL_3^{2+}$ is oxydized by a network of TiO_2 nanoparticles and consequently RuL_3^{3+} is reduced with a help of I_3^-/I^- redox pair. Resulting charges recombine at the electrodes, thus, producing a phovoltage equal (without a load) to the overall redox potential through all the steps.

Appendix II. Borate buffer system

There are various procedures for making a borate buffer. One method is to prepare a working buffer by using H_3BO_3 and NaOH, or by using sodium tetraborate and HCl. Perhaps the most elegant method is to use sodium tetraborate also known as borax ($Na_2B_4O_7 \cdot 10H_2O$) and H_3BO_3. The boric acid-borate system is quite complex. We use this rather that other high pH buffers such as Tris or ammonium ion buffers because any free amines will act as quenchers of uranine. We cannot very well measure the quenching by iodide if the buffer we choose also acts as a quencher.

One fact that makes borate buffer particularly difficult is that orthoboric acid (H_3BO_3, also written $B(OH)_3$) and borax ($Na_2B_4O_7 \cdot 10H_2O$) do not appear to be stoichiometrically related. However, if we treat a solution of boric acid with NaOH and then evaporate to dryness, we obtain borax ($Na_2B_4O_7 \cdot 10H_2O$).

Boric acid actually ionizes by accepting a hydroxide ion (and thus an electron pair) from water, rather than by donating H^+. This makes it a Lewis Acid:

$$B(OH)_3(aq.) + H_2O \rightarrow B(OH)_4^-(aq.) + H^+(aq.) \quad (1)$$

When protonated, the tetrahydroxyborate ion yields the tetraborate conjugate base

$$4\,B(OH)_4^-(aq.) + 2\,H^+(aq.) \rightarrow B_4O_7^{2-}(aq.) + 9\,H_2O \quad (2)$$

We see that boric acid is a Lewis Acid, not a classic proton donor, so these equations don't give us the typical Arrhenius acid-base equilibrium expressions. Notice here the tetraborate ion, $B_4O_7^{2-}$, which occurs also with the ionization of borax. In a borax-boric acid buffer solution (~ pH 9), tetraborate and monohydrogen tetraborate are actually the primary species, as long as the boron concentration is greater than about 0.025 M.

In theory, it takes four moles of boric acid to yield one mole of $B_4O_7^{2-}$ in solution. If we quadruple the coefficients in Equation 1 to correspond with Equation 2, we get $4B(OH)_3$. When we combine the two equations we obtain:

$$4\,B(OH)_3(aq.) \rightarrow B_4O_7^{2-}(aq.) + 5\,H_2O\ + 2\,H^+(aq.) \quad (3)$$

Notice that the H^+ is now on the right, which is consistent with the fact that boric acid yields an acidic solution. Because $H_2B_4O_7$ is not a strong acid, though, it does not completely ionize.

First ionization:

$$H_2B_4O_7(aq.) \rightarrow HB_4O_7^-(aq.) + H^+(aq.) \quad (4)$$

Second ionization**:**

$$HB_4O_7^-(aq.) \rightarrow B_4O_7^{2-}(aq.) + H^+(aq.) \quad (5)$$

These two equilibria look like what we would expect for a typical acid-base equilibrium, the so-called Arrhenius-Ostwald model. The second ionization (Equation 5) is the more important one for the buffer we will make since the monohydrogen tetraborate ion has a pKa of 9. Although this is an approximation we can use the Hendersen-Hasselbach equation based on the second ionization in Equation 5.

$$pH = pK_a + \log\frac{[base]}{[acid]}$$

This equation can be written as

$$\frac{[base]}{[acid]} = 10^{pH-pK_a}$$

Since our target pH is 8.5 we have $pH - pK_a = -0.5$ and therefore

$$\frac{[base]}{[acid]} = 10^{-0.5}$$

If our target concentration is 0.1 M we can find the needed conjugate [base] and [acid] concentrations

$$\frac{0.1 - x}{x} = 10^{-0.5} = 0.316$$

Therefore, $[base] = 0.024\ M$ and $[acid] = 0.076\ M$. Using this calculation we can make the appropriate ratio using three methods. If you have both the acid and conjugate base then method III is the most elegant. Regardless of which method you choose, you will need to check the pH and add a small amount of HCl or NaOH solution to obtain pH 8.5.

The procedures below can be used to make a 0.1 M sodium borate buffer at pH 8.5

Method I

Table 1. Required components to make a 0.1 L of a 100 mM pH 8.5 sodium borate buffer

Component	**Mass**	**Molarity**
Boric Acid (H_3BO_3) (MW: 61.83 g/mol)	0.62 g	0.1 M
NaOH (MW: 39.997 g/mol)	0.304 g	0.076 M

1. Prepare 80 mL of dH_2O in a suitable container.

2. Add 0.62 g of Boric Acid (H_3BO_3) to the solution.
3. Add 0.304 g of NaOH to the solution.
4. Add distilled water until volume is 0.1 L.

Method II

Table 2. Required components to make a 0.1 L of a 100 mM pH 8.5 sodium borate buffer

Component	**Mass**	**Molarity**
Sodium tetraborate ($Na_2B_4O_7$:10 H_2O) (MW: 381.37 g/mol)	3.81 g	0.1 M
HCl (MW: 36.45 g/mol) concentrated acid	0.655 mL	11.6 M

1. Prepare 80 mL of dH_2O in a suitable container.
2. Add 3.81 g of sodium tetraborate decahydrate ($Na_2B_4O_7$:10 H_2O) to the solution.
3. Add 655 μL of HCl to the solution.
4. Add distilled water until volume is 0.1 L.

Method III

Table 3. Required components to make a 0.1 L of a 100 mM pH 8.5 sodium borate buffer

Component	**Mass**	**Molarity**
Sodium tetraborate ($Na_2B_4O_7$:10 H_2O) (MW: 381.37 g/mol)	0.915 g	0.024 M
Boric Acid (H_3BO_3) (MW: 61.83 g/mol)	0.469 g	0.076 M

1. Prepare 80 mL of dH_2O in a suitable container.
2. Add 0.915 g of sodium tetraborate decahydrate ($Na_2B_4O_7$:10 H_2O) to the solution.
3. Add 0.469 g of H_3BO_3) to the solution.
4. Add distilled water until volume is 0.1 L.

Raman and resonance Raman spectroscopy laboratory, Physical Chemistry Lab #4

4.0 Introduction

Most undergraduate courses have limited treatment of Raman spectroscopy, or possibly no discussion at all. Therefore, you will need to learn some of the basics of the method, which will not be covered in the laboratory manual. Raman spectroscopy can be a turnkey experiment if you simply want a spectrum and you are not concerned about resonance, depolarization and other finer points. In fact, Raman spectroscopy has become very widely used because it can be adapted to fiber technology (fiber tip Raman probe), Raman microscopy and imaging, surface enhanced Raman spectroscopy, gas phase Raman (e.g. LIDAR) for detection of molecules from a great distance. The aspect that unites this disparate experiments is that Raman scattering is excited with a laser and so one can use the properties of laser light (high intensity and directionality) to advantage.

Raman scattering is an inelastic light scattering experiment. Energy is exchange during the scattering event so that the scattered light can give up some of its energy to the molecule. In this type of Raman scattering, known as Stokes Raman scattering, the molecule receives the energy of a vibrational normal mode. In the quantum mechanical picture, the molecule is promoted from the $v = 0$ to $v = 1$ level. We say that the molecule receives one quantum of energy from the exciting radiation. For completeness, we should also add that the molecule can give energy to the scattering radiation if it starts out in an excited vibrational state, $v = 1$. In that case, known as anti-Stokes Raman scattering the molecule gives up energy as is demoted by one quantum from $v = 1$ to $v = 0$ and the scattered radiation increases in energy by an equal amount.

In this laboratory experiment you will learn how to think about the properties of a molecule and then to measure those properties experimentally. The two most important properties are the vibrational normal mode wave numbers (frequencies) and the electronic transition energies. A subset of the vibrational modes is Raman active and we can measure those using Raman spectroscopy. We can determine their symmetry using Raman depolarization. We can determine the nature of intermolecular interactions from shifts in the Raman spectrum as well. We can determine the properties of the excited state from the resonant Raman scattering.

4.1 Experimental principles

4.1.1 Basic principles

Our goal in this laboratory manual is to provide sufficient information for you to study the Raman effect on your own. While this is potentially a vast area of spectroscopy, our emphasis will be on certain basic principles. You should be able to understand the basic idea of inelastic scattering, the importance of polarization, and the meaning of resonance. The Raman effect involves a shift in the wavelength of scattered laser light because of an interaction with a molecule that alters the vibrational energy of the molecule. Most commonly the light gives energy to the molecule promotes it to a higher vibrational level.

4.1.2 The Raman depolarization ratio

Since the Raman effect involves two electric field interactions (the incident and scattered fields) the effect on the molecule can be expressed in terms of a transition polarizability. This is a significant difference when compared to infrared (IR) for example where the absorption of light depends on a transition dipole moment. Because of the tensor effect the depolarization ratio defined as:

$$\rho = \frac{I_{\perp}}{I_{||}}$$

depends on the mode frequency. Totally symmetric modes are polarized meaning that $\rho < 1/3$. For ideal totally symmetric molecule such as CCl_4 or CH_4 $\rho = 0$ for the totally symmetric modes. For a planar absorber such as benzene or a porphyrin $\rho = 1/8$ for the totally symmetric modes. For other molecules ρ can be as large as 1/3, but not larger for totally symmetric modes. For non-totally symmetric modes $\rho = ¾$. These differences make it possible to experimentally distinguish between totally symmetric and non-totally symmetric vibrational modes.

4.1.3 Resonance Raman spectroscopy

The resonance enhancement of the Raman effect is one of the most interesting phenomena in spectroscopy. If the laser wavelength is coincident with a molecular transition (i.e. an absorption wavelength) then the light is scattered "on resonance", which means that the laser light can cause a transition to the excited state, but then instead of being absorbed it is scattered and the molecule returns to the electronic ground state (but to a different vibrational state). We can probe resonance Raman spectroscopy by studying a molecule with an absorbance maximum in the range 400 – 430 nm, which is the easy tuning range of the laser. Even if the absorbance maximum is outside this range we can still see the resonance effect if there is a change in absorbance over this range.

4.1.4 Applications

Molecular vibrations are sensitive to the environment. Hydrogen bonding and other molecular interactions can cause shifts in the wave number of normal modes. A simple example can be found in H_2O. In the gas phase the symmetric and asymmetric stretching vibrations of H_2O are 3,825 and 3,935 cm^{-1}, respectively. In liquid water, where this is strong hydrogen-bonding these frequencies shift down to approximately 3,670 cm^{-1} and 3,760 cm^{-1}, respectively. This large shift in the stretching mode wave number is due to the polar interaction of the bond with the lone pair of a neighboring H_2O molecule. We will consider this in the equilibrium of an acid with its salt. The acid and salt differ because of protonation. We will prepare several different mixtures and then use Singular Value Decomposition (SVD) to study the spectral shifts.

4.2 Equipment

4.2.1 Excitation laser

The Raman apparatus in Room 104 of the Partners III building has a pumped Ti:sapphire laser that can be frequency doubled to create wavelengths from 390-430 nm. The Raman apparatus in Room 175 of Partners III uses several different lasers to provide a number of fixed wavelengths

for Raman excitation. We will use the Ar/Kr Ion Laser, which has wavelengths of 488 nm, 514.5 nm, 568 nm and 647 nm. It is important to understand that there are many other lines, which are less intense. A very weak laser line at a wavelength shifted slightly from the main line will show up as a peak in the spectrum. For this reason it will be necessary to measure a blank (consisting of a cuvette with water in it) at each wavelength where a small signal is measured. Since water has essentially no measurable Raman activity under the conditions we are working we can use the blank to determine what signals arise from additional laser lines. For solvents such as CCl_4 or C_6H_{12} , which have very intense scattering (hundreds or even thousands of counts per second on the CCD detector) we can ignore these very small laser additional lines. For the acetic acid studies it will also not be a large contribution. However, the final part of this study where we are looking at much weaker scattering from non-resonant standard, which may the solvent itself or Na_2SO_4 when H_2O is the solvent. We will use a porphyrin molecule for this part of the lab experiment. Porphyrins all have two absorption bands in the visible region. These are known as the Soret band (allowed) and the Q-band(s) (forbidden).

In the Raman experiment in room 175 the laser light is focused on the sample by a camera objective. This apparatus uses a back scattering geometry. This means that the light is focused in the sample and then the scattered light retraces the same path. The same objective is used to collect the scattered light. There is a beam splitter which directs 50% of the incident laser light into the sample. Because of this beam splitter we also lose 50% of the scattered light. This may sound like a lot of losses, but the efficiency of the optics and the small spectrograph make this a very efficient design. The scattered light is collected and focused onto a fiber, which conducts the light to a single-grating spectrograph.

4.2.2 Software

The Raman acquisition software is opened by clicking on the icon on the desktop. It may already be opened, in which case you may begin using. However, in either case you should make sure that configuration is RamanClass. If you do not see RamanClass at the very top of the GUI then you should look for a folder icon at a highest level on the menu and click on it. This folder should give a list of different configurations. Select RamanClass and you should see those words on the top of the menu. There are three sets of parameters that will need to alter as you conduct the experiments.

1. Acquisition time and number of frames (top menu)
2. File name and path for saving data (near the middle of the menu list)
3. Raman excitation wavelength and center wave number (bottom menu)

In 1. you will need to set to set the acquisition time in seconds that tells the program how long to permit the CCD to be irradiated by scattered light before it is read. Each time the CCD is read we can call this a frame. Then you will need to determine the number of frames. If you are doing real time observation of solvent bands to “tweak up” the signal then you should set both the time and number of frames to 1. In that case if you select Run above the spectral window you will see a new spectrum every second. If you want to acquire a Raman spectrum and save it then we recommend the following:

A. Solvents (e.g. CCl_4, C_6H_{12}) [Typical acquisition: Frames 4, Time 5 seconds]
   The solvents are non-resonant (at least in our case in this lab). They have no absorption at the wavelength of the incident laser light. They are also at high concentration. A pure solvent has a concentration of many molar. Think about H_2O, which has a concentration of 55.5 molar. Look up the density of CCl_4 and then figure out what its concentration is.

B. Raman signals from relative weak scatterers (essentially all other acquisitions) [Acquisition parameters: Frames 4, Time 10-60 seconds]. For weak scatterers the time required may be much longer. Some molecules such as acetic acid are solutes at moderate concentration (less than 1 M) that have no absorption and are therefore non-resonant. Others molecules, such as the porphyrins, have a color since the absorb light in the visible and therefore some of the laser wavelengths may be resonant. For this reason we can obtain a Raman spectrum even at lower concentrations (e.g. millimolar or lower).

With these settings you will obtain data in a few minutes. There is always a trade-off in terms of how long want to wait vs. how good you want the data to be. If you would like better looking data you can always set the number of frames to a greater number. If we were trying to get publication quality data from this experiment, we might use 40 frames and a 20 minute acquisition. The signal-to-noise ratio would be better by approximately $\sqrt{N}$ where N is the number of frames so in this case it would $\sqrt{10}$ better. That is quite a lot!

The file name and path are fairly obvious. We have set up a folder in the Data directory that is called CH454. Please make a subdirectory in that folder to avoid a proliferation of names in the Data directory. It is a good practice to include the excitation wavelength in the name of the file. For example if you are exciting CCl_4 at 514.5 nm you could call the file ccl4_514nm. It will generate a file with a SPE extension. When you are done collecting data you will need to export the data SPE data in the CSV (comma separated values) format. You will use the Data tab (upper left of the GUI window). Then you can selected "Recently acquired" and drag down and select all of the files you just obtained. Be careful when exporting since you must input the excitation wavelength (hence the reason it is a good idea to put that wavelength in the file name). You may export multiple files, but you will want to make sure that they are in groups that all have the same excitation wave length.

Finally, the control over the positioning of the grating in the spectrograph is in the bottom menu. This is not obvious. You need to click on the small cm-1 that is in the center of that menu. Then you will obtain a menu that asks you for the excitation wavelength. The only one that is not a whole number if 514.5 nm. You type in the number of the wavelength. Then you need to type in the center cm^{-1} of the Raman window. This will typically be a number between 700 and 1300 cm^{-1}. The width of the window is approximately 1200 cm^{-1} (using the 1800 groove per mm grating which is set by the RamanClass configuration). Therefore, a center of 700 cm^{-1} will give you approximately 100 cm^{-1} – 1300 cm^{-1}. This is a good window for low frequency modes. It will work for the solvents CCl_4 and C_6H_{12}. However, acetate and acetic have interesting modes that are slightly higher (near 1600 cm^{-1}) so you will need to set the center wave number to 1200 cm^{-1} for those experiments. For the Na_2SO_4 and malachite green resonance Raman experiment a similar wave number is probably best. Note that most of the vibrational modes are between 200 – 1700 cm^{-1}. There is a normal mode desert from about 1700 – 2800 cm^{-1}. Above 2800 cm^{-1} one

can observe the X-H stretching modes (X =C, O, N etc.). These are typically weak in Raman. We focus our efforts on the modes below 1700 cm^{-1}. We leave some discretion for the student to play around a bit and find a good window for taking data. The idea is to capture as many modes as possible. We will not be using the information of modes below 300 cm^{-1} (except for CCl_4).

4.2.3 Collection and dispersion of the scattered light

To measure a Raman spectrum we will use a collection optic, a spectrograph and a CCD detector. The spectrograph is a triple monochromator, which consists of two stages. The filter stage is a double monochromator and the main spectrograph is single 0.6 meter monochromator. There are two slits. The most important slit is the entrance to the spectrograph stage, which is shown in Figure 2.1. This slit can be set between 30-100 microns depending on the requirement for resolution and light level. A typical value is 60 microns. The spectrograph has a grating that disperses the light onto the CCD detector.

A Charge-coupled device (CCD) is a detector that can collect an image of the dispersed light. Actually a CCD is just a more sensitive version of the chip used in a digital camera. The CCD is usually binned in vertical strips so the light dispersed over a narrow range can be resolved as shown in Figure 3.

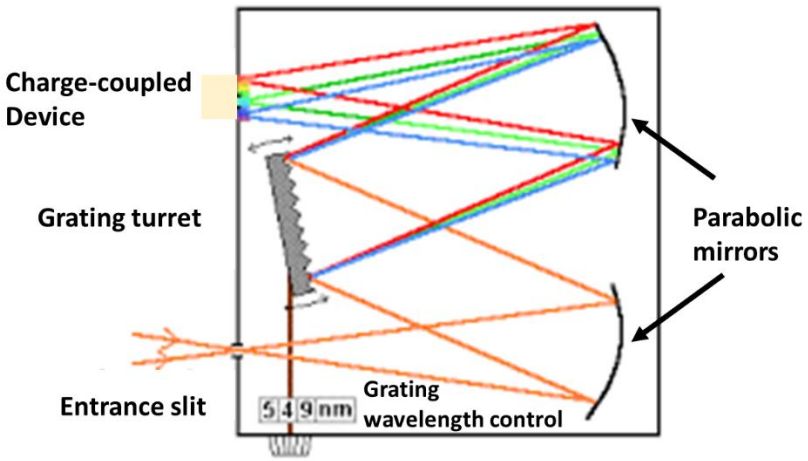

Figure 2.1. Illustration of a spectrograph. The grating disperses the light that enters through the entrance slit. The dispersed light is refocused using a parabolic mirror. However, the focal point of the light is slightly behind the plane of the CCD so that the light is dispersed across the CCD.

The output is digitized using the computer software and stored as a file that contains the number of counts per pixel. We must calibrate the window of the CCD for each setting of the monochromator. The calibration will tell us how the pixels correspond to the Raman shift in cm^{-1}. The simplest way to calibrate the CCD is to use one or more standard molecules (see Section 1.3).

4.2.4 Calibration

A Raman spectrum can be calculated in the same way as the laser line (Rayleigh line). This is quite a bit of work since such a calibration will obtain the Raman spectrum in terms of wavelength. We can then subtract the Rayleigh line and convert to cm-1. In practice a much simpler way to obtain the Raman shift is to record the Raman spectra of several solvents using the same monochromator settings used to obtain the data. For example, we can use toluene as shown in Figure 2.2.

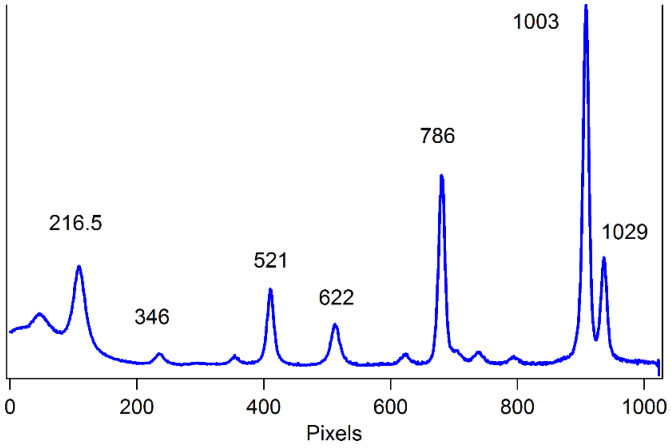

Figure 2.2. Uncalibrated Raman spectrum of toluene as it appears on the CCD. The CCD has 1024 pixels and the data are plotted using these units as the x-axis. Each Raman peak is labeled with its appropriate wave number from the known calibration of toluene.

We can record the peak values of toluene in terms of pixels and then create a table using the known Raman shifts. The table has one column for pixels and one for wave numbers (Raman shift). Table 2.1 reports the actual values from Figure 2.2.

Pixels	Peaks
109	216.5
236	346
354	465.5
410	521
512	622
681	785.8
908	1003
936	1029

A fit of these values to a line gives us the calibration line. The line is shown in Figure 2.2. It should be quite a good line. If not, then there is probably an error in the assumption about the peaks.

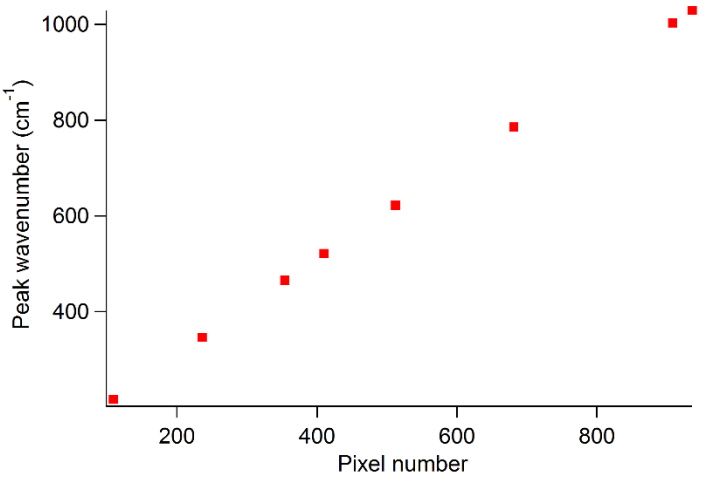

Figure 2.3. Calibration line derived from the data for toluene shown in Figure 2.2.

In this case the fit to the line is given by the equation y = mx + b, where m = 116 $\pm$ 3 and b = 0.98 $\pm$ 0.01. Using these values we can make a calibration for the x-values of the above Raman spectrum for toluene. To show how this is implemented we replot the data above using the calibration line as the x-value in Figure 6. Notice that now the values of the peaks corresponds to their x-values. The spectrum is calibrated.

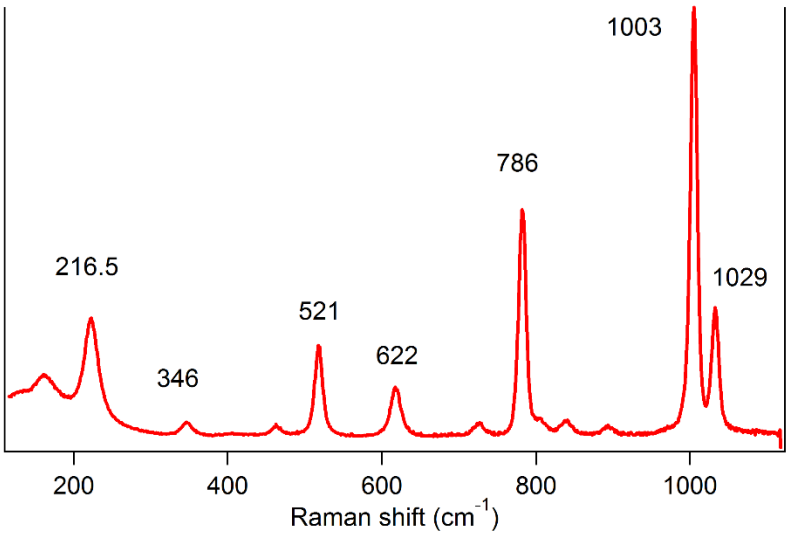

Figure 2.4. Calibrated Raman spectrum of toluene.

4.3 Singular value decomposition

Singular value decomposition (SVD) is a method used to analyze data in a matrix format. This method can be used to obtain a global fit to spectral data that depend on some other

parameter such as time, concentration, pH, temperature, electric field etc. The idea behind SVD is to reduce the data to a set of orthogonal basis spectra in each of the dimensions. For example, if we have a data matrix in the dimensions of wave number, $\tilde{\nu}$, and pH, that has the form $\boldsymbol{I}(\tilde{\nu}, pH)$, we can decompose that matrix into three matrices as follows:

$$\boldsymbol{I}(\tilde{\nu}, pH) = \boldsymbol{U}(\tilde{\nu}, n)\boldsymbol{W}(n, n)\boldsymbol{V^T}(n, pH)$$

In this case the matrix is a function of the intensity of the Raman scattering obtained over a range of wave numbers at various pH values. In this analysis, n is the number of components and the matrices have the following definitions:

$\boldsymbol{U}(\tilde{\nu}, n) \equiv Spectral\ matrix - component\ basis\ spectra$

$\boldsymbol{V^T}(n, pH) \equiv Effect\ matrix - component\ time\ dependence\ on\ pH$

$\boldsymbol{W}(n, n) \equiv Eigenvector\ matrix$

The eigenvector matrix ranks components and assigns them a relative weight. Typically, only the first 2 or 3 components are important in a spectral decomposition. The spectral matrix consists of the following components:

$\boldsymbol{U_1} \equiv grand\ mean\ of\ the\ data\ set$

$\boldsymbol{U_2} \equiv difference\ grand\ mean$

$\boldsymbol{U_3} \equiv second\ difference\ grand\ mean$

And so on. $\mathbf{U_1}$ is the first component and consists of the grand mean, which is simply the average of all of the spectra. The second component $\mathbf{U_2}$ is the average of all of the spectra after subtracting off component $\mathbf{U_1}$. So it is a grand mean of the difference spectrum. Each successive Un spectrum is the grand mean of the (n-1)th difference spectrum. These spectra are orthogonal to one another. A time course corresponds to each spectrum. One can carry out global fitting using the appropriate number of time courses (usually 2 or 3) for the fitting. This fitting procedure is much more robust than the alternative of fitting each wavelength individually.

From a practical point of view we can carry out SVD in IgorPro. The hardest part of this procedure is constructing the matrix. The trick is to create a table with the correct dimensions. Then you can just paste your data into that matrix and type one command (matrixSVD) to get the result. For example, suppose that you have a data matrix of 1000 wavelengths and 200 time points, A(1000,200). You need to create a matrix will 200 columns and 1000 rows. Use the command

$ make /n=(1000,4) **I_Raman**

$ edit **I_Raman**

This syntax automatically makes I_Raman a two-dimensional matrix. You can open the table using the edit command. Then you can paste your data set into the table. Once the entries in the table are filled you return to the command line and type:

$ matrixSVD **I_Raman**

In IgorPro the components are found automatically in the matrices **U_M**, **VT_M** and **W_M**. You can examine the components to determine how many components are useful. The **W** matrix gives you important information as the eigenvalues. The eigenvalue of the second component may be 10% as large as the first (very significant) or smaller. The third component is typically in the range of 1% or smaller. The decision to include two, three or more components is subjective. However, the quality of the components often makes it clear which components are worth including. If you fit the components of the VT matrix to a model then you can use that model to estimate the magnitude of an unknown.

4.4 Materials and Methods

This laboratory experiment consists of three stages. First, you will perform a calculation of the vibrational normal modes of the molecules of interest. You will also estimate its electronic transition energy for the purpose of understanding resonance in the Raman experiment. Second, you will perform a Raman experiment on a solvent molecule (e.g. CCl_4), a molecule with different chemical states (e.g. a perchlorate salt and perchloric acid mixtures at different pH values), and one of two experiments.

4.5 Calculation of the normal modes.

The normal modes of molecules can be calculated from first principles using density functional theory (DFT). In this class we will not ask you to do the calculations, but we will provide you with the output files from DFT calculations so that you may compare these to experiment. This will help you to make assignments and also give a feeling for the accuracy of DFT calculations. It is also a useful exercise in how to interpret somewhat complex data sets. In the case of CCl_4 there are only 4 Raman active modes. Given the high symmetry of the molecule it is quite an easy task to identify each of the modes in the Raman spectrum and to determine the accuracy of the DFT calculation. You can also compare the depolarization to the symmetry of the calculated mode with ease. Cyclohexane (C_6H_{12}) is much more complicated. It has a total of 48 normal modes of vibration. Some of these are C-H stretching modes. These are not very intense in the Raman spectrum and they are clustered at around 2,900-3,200 cm^{-1}. You can use group theory and DFT output to determine how many of these modes exist and then you do not need to consider them further. However, it is worthwhile to compare the Raman spectrum from the lowest possible value (between 200 – 300 cm^{-1}) and 1600 cm^{-1}, which is where the highest wave number skeletal modes are observed.

Make table for both CCl_4 and C_6H_{12}. List the observed Raman active modes in the first column. In the second column report your best estimate for the depolarization ratio. In the third column identify whether the mode is symmetric or non-totally symmetric. In the fourth column report the corresponding mode in the DFT calculation. In the fifth column report the percent difference

between the calculated and experimental mode. Finally, calculate an average percent error in your report based on the data and calculated values in the table.

4.6 Raman experiment

The basic Raman experiment for this laboratory has the following steps.

1. Obtain the Raman spectrum of CCl_4 and cyclohexane for parallel and perpendicular polarization. Determine the depolarization ratio for the Raman bands and compare these to the predicted Raman spectra based on calculation and group theory. You may use the output from DFT calculations provided as supplementary material for your discussion and analysis.
2. Obtain the Raman spectra of an acetic acid/acetate buffer solution at 5 pH values 4-10. Analyze these using SVD to understand the shifts in the bands in a comprehensive manner. Explain the shifts in the Raman bands in terms of the vibrations of acetic acid and sodium acetate. Determine the pH of an unknown based on the correlation.
3. Obtain a basic Raman excitation profile (REP). This means that we will monitor the Raman intensity of vibrational modes as a function of the excitation wave length. In practice, since we only have three wave lengths we will compare the scattering from a dye (resonant molecule) and Na_2SO_4 salt (non-resonant ions) in order to understand the significant of resonant Raman spectroscopy.

4.6.1 Procedure to obtain the Raman spectrum of CCl_4 and cyclohexane. To obtain a Raman spectrum you will need to determine the correct range for the monochromator. The monochromator must be moved far enough from the Rayleigh line that there is no "tail". The Rayleigh line is so strong that you will need to be about 10 nm away from before you can obtain any meaningful Raman signal. However, you want to be close of enough to the Rayleigh line that you can measure low frequency modes. Toluene is a good test case since it has a mode at 220 cm^{-1}. You should be able to see this mode. Once you have set the monochromator and the filter to the right range you will want to ensure that the signal is optimized. You can tweak the beam steering mirrors in order to get the best signal. Once this has been achieved you may obtain a Raman spectrum of CCl_4 and one of cyclohexane. Then put the polarizer in the beam path right before the first slit. Obtain the spectrum for parallel and perpendicular polarization as well for both CCl_4 and cyclohexane. Each of these spectra can be obtained in a short time. Record 6 spectra with an acquisition time of 5 seconds.

Data workup. Read the data into Excel (or other similar program). Using CCl_4 first we will want to establish the calibration factor needed to obtain accurate depolarization ratios using the Raman apparatus. Plot the parallel and perpendicularly polarized data as shown below in Figure 2.5.

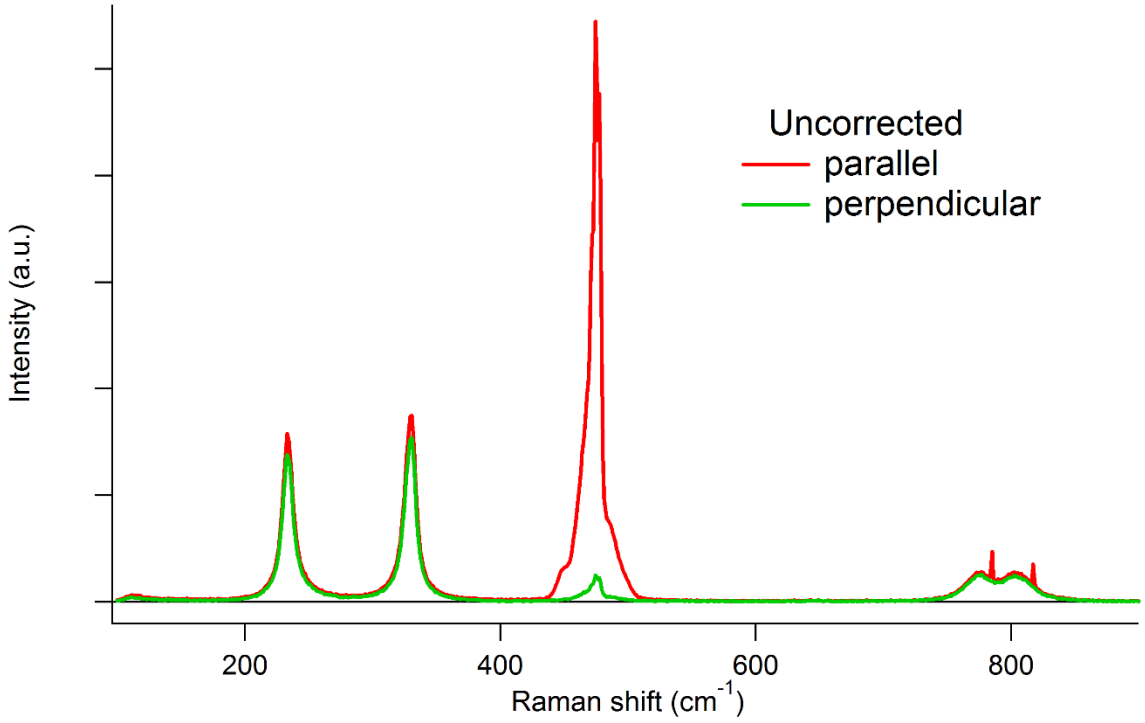

Figure 2.5. Raw Raman data for CCl_4 overlaid.

CCl_4 is a nearly ideal molecule because of its high symmetry. Actually, we should be aware of the fact that there are two isotopes of Cl (^{35}Cl and ^{37}Cl) in CCl_4. For this reason the depolarization ratio of the totally symmetric stretch at 462 cm^{-1} (Figure 2.5) is not exactly zero, as theory would predict for a molecule with spherical symmetry (i.e. tetrahedral, octahedral or icosahedral). However, the remaining non-totally symmetric bands should have $\rho = ¾$. Since they do not have this value and they all deviate by nearly the same amount we will assume that the reason is that the spectrograph is not perfectly balanced in its throughput of parallel and perpendicular light. We will determine that appropriate factor needed to multiply the perpendicularly polarized Raman spectrum in order to obtain the theoretical $\rho = ¾$. Once we have determined this correction fact we will use it for cyclohexane (C_6H_{12}) or any other depolarization ratio measurement. Once we have applied a correction of 0.856 to the perpendicular channel we obtain the Raman spectrum shown in Figure 2.6.

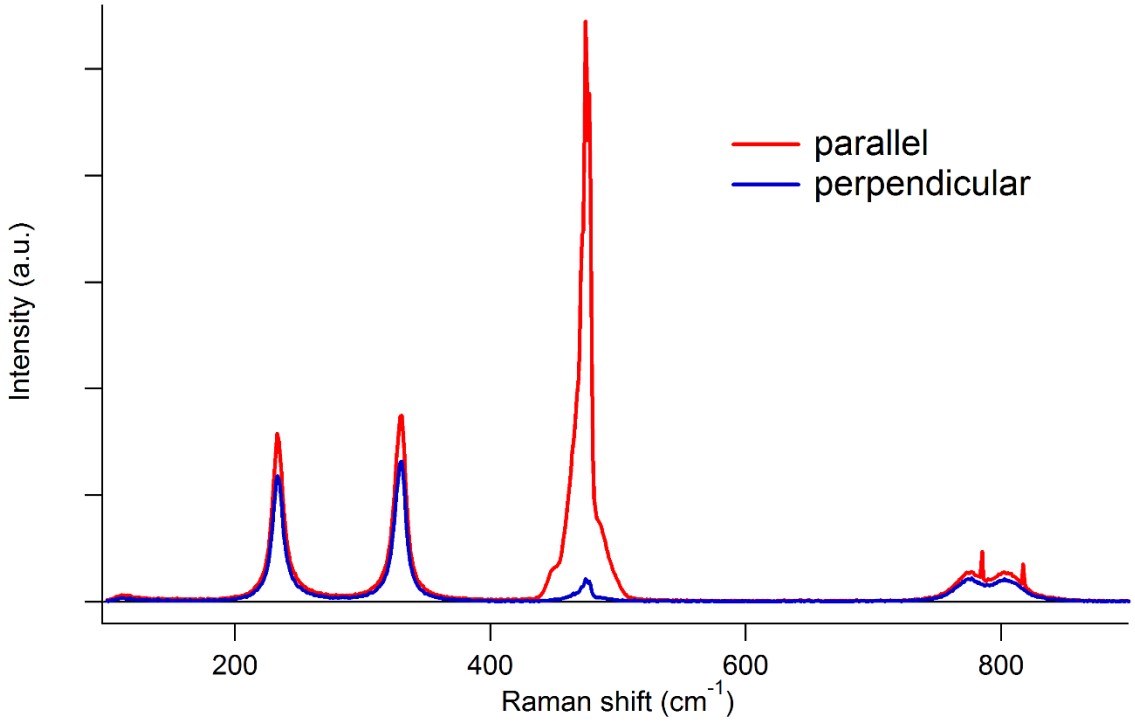

Figure 2.6. Corrected Raman spectra showing parallel and perpendicular polarizations.

Note that after correction the depolarization ratio of the totally symmetric stretch is $\rho = 0.039$, which is in reasonable agreement with the literature value of $\rho = 0.046$.

4.6.2 Procedure to obtain the Raman spectrum of acetic acid and sodium acetate. Make at least 4 solutions in the range from pH 4-10. Place these solutions in NMR tubes so that there is at least 0.5 mL of solution in the tube. Label them according to their pH. The Raman spectrum of each of these will take a few minutes. Record 6 spectra with an acquisition time of 20 seconds. If the signal-to-noise ratio is not ideal record for a longer period of time.

Data workup. Read the data in IgorPro and calibrate the data using the procedure described above. Report the Rayleigh wave number, the spectra and depolarization ratios for CCl4 and cyclohexane. Relate the depolarization ratio to the predicted symmetries of the modes based on quantum chemical calculations and group theory. Finally, create a data matrix of the acetic acid/acetate spectra. Obtain the SVD components of this data matrix. There should be two dominant SVD components in the data set. These should represent the grand mean of the data and the shift of the data over the pH range. This spectral analysis permits you to estimate the pH of an unknown sample. Come up with a method to do this and estimate the pH of the unknown that were given.

4.6.3 Laboratory experiment: Raman excitation spectrum

For this experiment we will use excitation of a metalloporphyrin at a variety of wavelengths in order to observe the concept of resonance enhancement. A second phenomenon

that can be observed is the coupling of totally symmetric modes to the Soret band and non-totally-symmetric modes to the Q-band. This type of observation makes the point that different types of absorption (Franck-Condon active vs. Herzberg-Teller active) are coupled to different types of vibrations. The Raman depolarization ratio can be used to prove what type of mode we have observed. Keep in mind that even in the real world where there are deviations from the theoretical values ($\rho = 0 - 1/3$ for totally symmetric and $\rho = 3/4$ for non-totally-symmetric modes) the values of ρ are sufficiently different that we can almost always tell whether a mode is totally symmetric or not.

In the resonance Raman experiment we will see, for the first time, the effects of changing the laser wavelength. The Ar/Kr laser in room 175 has a number of fixed wavelengths that can be obtained by changing the angle of the prism in the laser cavity. We cannot change these fixed wavelengths, but there are quite a number we could use. If we want to tune a laser, i.e. to change the laser wavelength over a range of excitation energies, we need a different type of laser. The laser in room 102 is a pumped Ti:sapphire laser. It has gain bandwidth from 760-960 nm. When frequency doubled this laser can produce output from 380 – 480 nm. This range is interesting for Soret bands in various porphyrins. Please read the Appendix to this laboratory for an overview of porphyrin spectroscopy that clarifies the significance of the Soret band and Q-band. It also discusses the concept of allowed and forbidden bands using a number of different approaches.

Our goal in this laboratory will be to observe the resonance enhancement phenomenon qualitatively. We do not have time to take a Raman Excitation Profile (REP), which would be a complete set of spectra at different excitation wavelengths. We will compare a few different wavelengths and hopefully obtain some insight into what it means when the laser is in resonance with an absorption spectrum. The laboratory write-up for this section will emphasize a comparison with published Raman experiments on related systems. The point will be to describe the spectra with reference to the Franck-Condon activity or Herzberg-Teller activity, the type of modes that are coupled and significance for the spectroscopic applications.

4.7 Analysis and Laboratory report

Your report should consist of three parts. The first part should focus on the basics including the calibration, depolarization ratio. The second part will describe the application of Raman spectroscopy to a pH determination. The third part will address resonant Raman spectroscopy. The report should contain an Introduction, Materials and Methods, Results, Discussion and Conclusion as usual, but the Results and Discussion will each consists of the three segments described above.

The Raman data provided to you by the software is already calibrated. Your first task is to check that calibration using the CCl_4 data. The CCl_4 Raman lines are:

217 cm^{-1}
314 cm^{-1}
459 cm^{-1}

776 cm^{-1}

Then the discussion of the depolarization ratio should include a table (as described above in the section the depolarization ratio). The table should contain the comparison to quantum chemical calculations and normal coordinate analysis of the molecules. Since you will be provided with the output files, the goal of this section for you to organize the relevant portions of the output and present the modes and their properties (calculated and measured wave number, symmetry and depolarization ratio) in tabular form. You only need to report an analysis of the observed modes. If there are additional modes that are calculated or reported in the literature, but not observed by you, you may discuss this, but it is not necessary to include this information in the table.

Use CCl_4 as the starting point and try to determine whether the spectrograph (CTS-320) has a bias in the throughput of different polarizations. It is unlikely that $I_\perp$ and $I_\parallel$ have the same throughput. What correction factor would you need to apply to correct the spectra of CCl_4? Hint: The modes at 217 cm^{-1} and 314 cm^{-1} are depolarized modes with a theoretical value of $\rho = 3/4$.

The crucial points will be to discuss the totally symmetric and non-totally symmetric modes of both solvents studied. We do not require you to do a normal mode analysis, but you could do it (particularly for CCl_4 in the T_d point group). You may also look up the analysis in the literature. Any paper on these molecules will be really old, but it is rather interesting and educational to go back to the original literature. It is fine to base your discussion and comparisons on the literature. Based on your reading and the in-class discussion it is worthwhile to discuss the significance of the two categories of modes for spectroscopy. You might even examine the literature and see what you can find about the Franck-Condon and (possibly) Herzberg-Teller (or vibronic) electronic transitions. When we say that these Raman spectra are "non-resonant" we can also view them as "off-resonant" or "pre-resonant". How far off resonance are they? What can you say about the idea that non-resonant is best described a excitation far from resonance (as opposed to the conventional language we find in many books that talks about virtual states as the explanation for non-resonant Raman spectroscopy).

For the determination of spectra at various pH values, ideally we would do SVD analysis. Since not everyone has the software, we can provide you with some output and you can discuss the significance. What is changing in the spectrum? Which changes are systematic? Does the analysis depend on the wavenumber region you choose? Can you find any publications that describe the vibrations of the carboxylate dimer?

For part three of the lab report you will consider the spectra of the metalloporphyrin compound at several different wavelengths (488 nm, 514.5 nm and 568 nm). We will compare these wavelengths which are in resonance with the Q-band with the Raman scattering at 402 nm using a different apparatus. In order to analyze resonance Raman data you need an internal standard to compare the various wavelengths. Once again the internal standard may be one or more solvent peaks of if your solvent is water we usually use a salt such as Na_2SO_4 as the internal standard. Water does not have strong Raman bands in the region of interest, but sulfate has a strong totally symmetric stretch at 982 cm^{-1}. The relative intensity of the bands of the internal standard depends only on the ν^4 dependence of non-resonant Raman scattering. Since everything is relative (i.e. we are not going to determine absolute Raman cross section, but rather relative

Raman cross sections), we can pick the longest wave length spectrum (lowest energy of incident photon) to start. We choose one or more peaks from the solvent and we can scale all of the spectra to that peak. Then we want to see the relative intensity of other peaks in the spectrum due to the analyte (which in our case will be a porphyrin molecule that we have selected for the study).

It is interesting to measure the power of the laser at various wavelengths. However, if this was not possible then you simply assume that the intensity of the sulfate peak increases as the fourth power of the frequency (and therefore also the fourth power of the wave number). Of course, you must convert the excitation wavelength to wave number [$\tilde{\nu}(cm^{-1}) = 10^7/\lambda(nm)$] and then you may scale the spectra so that this condition is met.

References

1. Gaynor, J.D.; Wetterer, A.M.; Cochran, R.M.; Valente, E.J.; Mayer, S.G. "Vibrational Spectroscopy of the CCl4 v(1) Mode: Theoretical Prediction of Isotopic Effects" J. Chem. Ed. 2015, 92, 1081-1085
2. Wang, L.; Mizaikoff, B.; Kranz, C. "Quantification of Sugar Mixtures with Near-infrared Raman Spectroscopy and Multivariate Data Analysis A Quantitative Analysis Laboratory Experiment" J. Chem. Ed. 2009, 86, 1322-1325
3. Vickers, T.J.; Pecha, J.; Mann, C.K. "Raman spectroscopy with a fiber-optic probe and multichannel detection" J. Chem. Ed. 2001, 78, 1674-1675
4. Sanford, C.L.; Mantooth, B.A.; Jones, B.T. "Determination of ethanol in alcohol samples using a modular Raman spectrometer" J. Chem. Ed. 2001, 78, 1221-1225

Appendix 1: Overview of the spectroscopy of porphyrins

The field porphyrin spectroscopy is vast. There are porphyrins found in nature in a variety of applications, photosynthesis, oxidative catalysis, signaling and so on. The field of porphyrin chemistry is also a branch of inorganic chemistry since there are many metalloporphyrins. We will study a metalloporphyrin in this laboratory course. For the purposes of comparison among the various molecules we observe that the central molecule of all metalloporphyrins is the 20-carbon ring shown in Figure 1A. The porphyrin has D_{4h} symmetry and even when there are substituents on the outside of the ring, these do not reduce the symmetry in spectroscopic observations. Therefore, in this appendix we will rely on a description based on heme (the cofactor found in dehaloperoxidase and horseradish peroxidase used in the enzyme kinetic studies). This is interesting because it makes a connection to another portion of the course, but the lessons we can learn have general validity for metalloporphyrins.

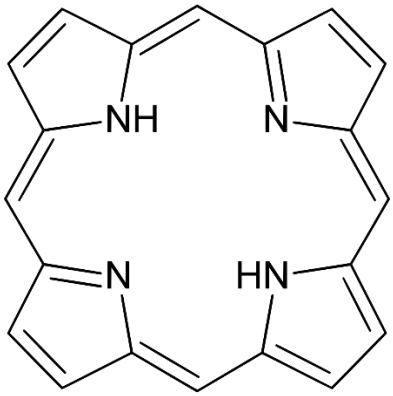

Figure 1A.1 The molecule porphine. The porphine ring has a charge of 2-, which is evident form the two H atoms on two of the central nitrogen atoms.

1A.1 Spectroscopy of the heme group: a model for metalloporphyrins

The heme molecule (Fe protoporphyrin IX) is a useful probe of the state of the protein. Figure 1A.2 shows that the carbonmonoxy (CO) form and has a different spectrum than the deoxy form. The figure shows that there are intense B bands and weak Q bands for both forms. The reason for these two types of electronic transitions can be found in the simple particle-on-a-circle model. In that model, we have shown that the energy levels of the porphyrin can be modeled using an 18-electron π-system shown in Figure 1A.3. Starting with the energy levels of the particle-on-a-circle given by the Schrödinger equation,

$$-\frac{\hbar^2}{2\mu R^2}\frac{\partial^2}{\partial\phi^2}\Phi = E\Phi \tag{1A.1}$$

We have the normalized solutions

$$\Phi = \frac{1}{\sqrt{2\pi}}e^{im\phi} \tag{1A.2}$$

where

$$m = 0, \pm 1, \pm 2, \pm 3, \ldots$$

Figure 1A.3 shows us the meaning of these quantum numbers. They refer to whether the electron is travel clockwise m > 0 or counter-clockwise m < 0 around the circle. Moreover, we

can understand the selection rule based on our study of the interaction of electric fields with matter. The electric fields polarized along x- and y- are

$$E_x = E_0 cos\phi = \frac{E_0}{2}\left(e^{i\phi} + e^{-i\phi}\right)$$

$$E_x = E_0 sin\phi = \frac{E_0}{2i}\left(e^{i\phi} - e^{-i\phi}\right)$$

(1A.3)

Thus, a transition dipole moment operator that connects two states under the influence of the electric field also has the form

$$\mu_x = e\ cos\phi = \frac{e}{2}\left(e^{i\phi} + e^{-i\phi}\right)$$

$$\mu_y = e\ sin\phi = \frac{e}{2i}\left(e^{i\phi} - e^{-i\phi}\right)$$

(1A.4)

where e is the charge on the electron. Only if the transition dipole moment is non-zero will the electric field be able to interact with the molecule. For example, the x-polarized transition dipole moment is

$$e\int_0^{2\pi} e^{-im'\phi} cos\phi e^{im\phi} d\phi$$

(1A.5)

Where m and m' are different quantum numbers. We see from Eqn. 1A.4 that we can write this as

$$\frac{e}{2}\int_0^{2\pi} e^{-im'\phi} e^{i\phi} e^{im\phi} d\phi + \frac{e}{2}\int_0^{2\pi} e^{-im'\phi} e^{-i\phi} e^{im\phi} d\phi$$

(1A.6)

The condition for the integrals to be non-zero are

$$m - m' + 1 = 0$$
$$m - m' - 1 = 0$$

or

$$m' = m \pm 1$$

This condition or selection rule is shown in Figure 1A.3. It is also shown that the number m corresponds to the number of nodes in the wave function when a more advanced molecular orbital picture is applied to understand the spectroscopy. It turns out that any level of quantum theory predicts that the ground state of heme (or any porphyrin) consists of two states that are so close in energy that they act as thought they were degenerate. These are shown a_{1u} and a_{2u} in Figure 1A.3. The excited state is a rigorously degenerate e_g set of levels. Putting these together gives two possibilities for the π–$\pi*$ transition. There are two transition moments (M_1 and M_2 in Figure 1A.3) that can add constructively, $M_1 + M_2$, to give the intense B band or destructively, $M_1 - M_2$, to give the weak Q band. Both the B band and the Q band provide a means to monitor changes in the ligation state of the heme iron. Figure 1A.3 shows that the difference in the CO-bound form MbCO and the deoxy form Mb is significant. We can use these spectral differences to monitor the rebinding of CO heme proteins. This is a spectral probe of ligand dynamics that also teaches us about protein dynamic motions.

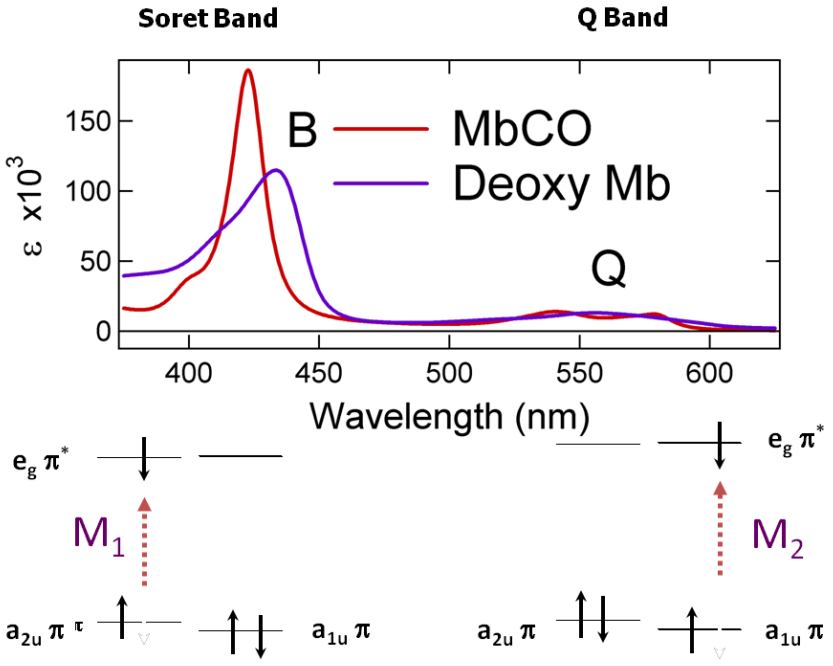

Figure 1A.2. Soret (B) and Q absorption bands for heme. The energy level scheme for heme is shown below. There are two transitions that can add constructively or destructively.

When comparing the free electron model we note that there is a "forbidden transition" with $\Delta m = 9$ that is predicted by the particle-on-a-circle or free electron model. The Q-band is this forbidden transition. Since the Q-band is observed, there must a mechanism that makes the forbidden transition allowed. We can this mechanism vibronic coupling. Distortions along normal modes of vibration can lower the symmetry of the molecule and permit a weak, but still observable band in this region. It is worth noting that when the metal has no spin contribution,

the change in the orbital angular momentum of the Q-band is 9 times larger than that for the Soret band. This means that the simple free electron theory correctly predicts the magnetic behavior of this band.

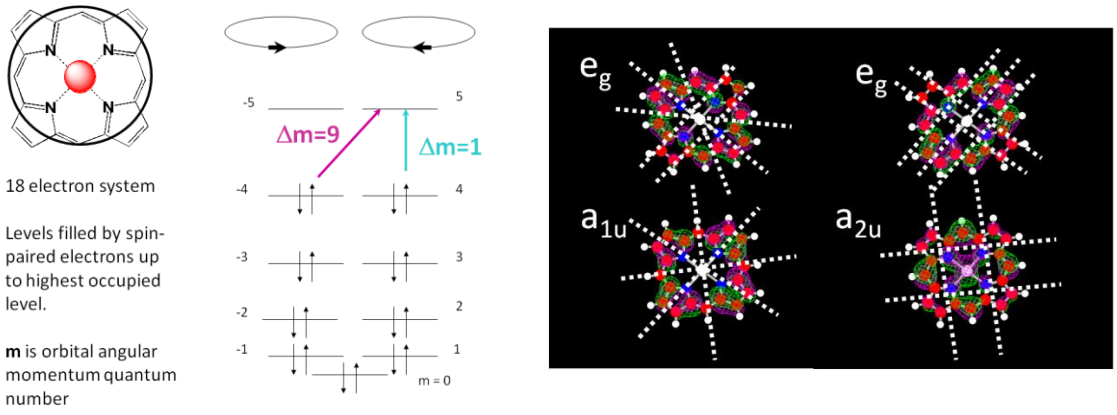

Figure 1A.3. Comparison of the free electron model with a full quantum chemical calculation of the molecular orbitals of the HOMO (π) and LUMO (π^*) orbitals of heme.

The complete description of the electronic transition of heme must include vibronic coupling. We have seen the nuclear coordinate expansion of the transition moment in Albrecht's theory of Raman scattering. The most fundamental expansion in terms of the nuclear coordinate is the expansion of the Hamiltonian,

$$H = H^o + \sum_i \left(\frac{\partial H}{\partial Q_i}\right)_o Q_i + \cdots \tag{1A.7}$$

In this expansion we can include the distortions of the molecule from its symmetry along each relevant mode *i*. These distortions permit the coupling of electronic states that would otherwise be orthogonal. Vibronic coupling theory explains how absorption bands can borrow intensity. Here we treat the vibronic coupling of the Q and B bands of the metalloporphine, which is also valid for heme and other pseudo-D_{4h} symmetry macrocycles.

The molecular orbitals of porphine can be derived in the D_{4h} point group. The use of the projection operator method is described in the Appendix to this chapter. The resulting energy level diagram in terms of the irreducible representations is shown in Figure 1A.4. The ordering of the orbital energies is made qualitatively by inspection of the number of nodes in each molecular orbital. Note that there is a pattern of alternating symmetries. The Eg pairs comprise the odd numbered MOs, with 1, 3, 5 and 7 nodes. Both the 0 and 8 node MOs have A_{2u} symmetry. The B_{1g}, B_{2g} pairs have 2 and 6 nodes, while the A1u,A2u pair in the middle has 4 nodes. The diagram shown in Figure 1A.4 is remarkable because it connects the MO picture

with the free electron picture, and shows a simple interpretation of the ordering of the MOs that can be derived by hand. This is quite a feat for such a large molecule as porphine.

The symmetry of the electronic configuration is the product of the symmetries of all of the occupied levels. This must be distinguished from the state symmetry, which each MO possesses. By definition, the configurational symmetry is totally symmetric for a closed shell ground state molecule. In a closed shell molecule, each occupied orbital has two electrons and the symmetry of each orbital contains the totally symmetric representation since the direct product of an irreducible representation with itself contains the totally symmetric representation.

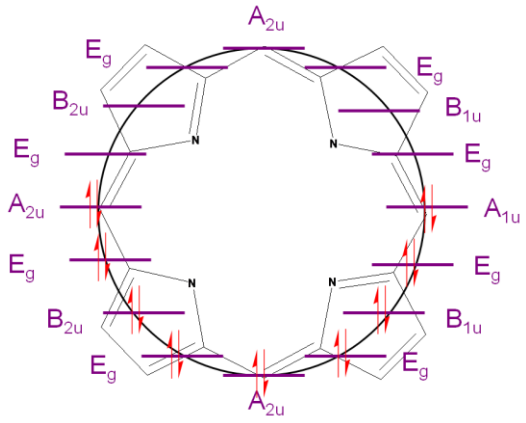

The direct product of A_{1u} E_g

	E	$2C_v$	C_2	$2C'_2$	$2C''_2$	i	$2S_4$	σ_h	$2\sigma_v$	$2\sigma_d$
A_{1u}	1	1	1	1	1	-1	-1	-1	-1	-1
E_g	2	0	-2	0	0	2	0	-2	0	0
E_u	2	0	-2	0	0	-2	0	2	0	0

The direct product of A_{2u} E_g

	E	$2C_v$	C_2	$2C'_2$	$2C''_2$	i	$2S_4$	σ_h	$2\sigma_v$	$2\sigma_d$
A_{2u}	1	1	1	-1	-1	-1	-1	-1	1	1
E_g	2	0	-2	0	0	2	0	-2	0	0
E_u	2	0	-2	0	0	-2	0	2	0	0

Figure 1A.4. Orbital symmetries for the model of the porphine p-system. The model has 16 basis functions and is composed for 4 unit atomic orbitals by the projection operator technique shown in Appendix A.

For example, A_{2u} x A_{2u} = A_{1g}, A_{1u} x A_{1u} = A_{1g} etc. so that all of the occupied orbitals contain A_{1g}. The E_g pair is a little more complicated in that E_g x E_g = A_{1g} + A_{2g} + B_{1g} + B_{2g}, as shown in Appendix 2. Thus, we can still say the E_g pair contains the totally symmetric representation, even though it also contains other representations. Overall, the ground state configuration is A_{1g}. The excited configuration is determined by the direct product of the configuration with one

electron in the HOMO and one in the LUMO. These two configurations are A_{2u} x E_g and A_{1u} x E_g. Figure 1A.4 shows that these two configurations are both E_u. This result means that the two excited state configurations have the same symmetry and can mix. This is an essential aspect of heme protein spectroscopy with two consequences. First, there can be configuration interaction that leads to two different types of transitions, the strong B (Soret) band and the weak Q band. This consequence is the deeper explanation to the allowed and forbidden transitions that are observed in the free electron model in the Dm = 1 and Dm = 9 transitions. The second consequence of the excited state mixing is that the two Eu configurations can be coupled by vibrational modes. The coupling can give rise to electronic transitions in the Herzberg-Teller formalism. These are derived in Appendix B.

$$
\begin{aligned}
|B_y^0\ > &= \frac{1}{\sqrt{2}}\left(a_{2u}e_{gy} + a_{1u}e_{gx}\right) \\
|Q_y^0\ > &= \frac{1}{\sqrt{2}}\left(a_{2u}e_{gy} - a_{1u}e_{gx}\right) \\
|B_x^0\ > &= \frac{1}{\sqrt{2}}\left(a_{2u}e_{gx} + a_{1u}e_{gy}\right) \\
|Q_x^0\ > &= \frac{1}{\sqrt{2}}\left(a_{2u}e_{gx} - a_{1u}e_{gy}\right)
\end{aligned}
\tag{1A.8}
$$

Each of these states can couple in the Herzberg-Teller expansion, which is given by

$$
|nv> = |n^0v> + \frac{\langle r\left|\left(\frac{\partial H}{\partial Q}\right)\right|n\rangle\,\langle u|Q|v\rangle}{E_{nv} - E_{ru}}|ru>
\tag{1A.9}
$$

In this equation there is an electronic coupling between two states

$$
\langle r\left|\left(\frac{\partial H}{\partial Q}\right)\right|n\rangle
$$

coupled by a vibrational mode such that the relationship between the vibrational quanta in the two states is

$$
u = v \pm 1
$$

as required for

$$\langle u|Q|v\rangle \neq 0$$

We can refer to two types of electronic coupling, Herzberg-Teller (interstate),

$$\langle B_y^0 \left|\left(\frac{\partial H}{\partial Q}\right)\right| Q_y^0\rangle = \langle a_{2u} \left|\left(\frac{\partial H}{\partial Q}\right)\right| a_{2u}\rangle - \langle a_{1u} \left|\left(\frac{\partial H}{\partial Q}\right)\right| a_{1u}\rangle + \langle e_{gy} \left|\left(\frac{\partial H}{\partial Q}\right)\right| e_{gy}\rangle - \langle e_{gx} \left|\left(\frac{\partial H}{\partial Q}\right)\right| e_{gx}\rangle$$

(1A.10)

and Jahn-Teller (intrastate)

$$\langle Q_y^0 \left|\left(\frac{\partial H}{\partial Q}\right)\right| Q_y^0\rangle = \langle a_{2u} \left|\left(\frac{\partial H}{\partial Q}\right)\right| a_{2u}\rangle + \langle a_{1u} \left|\left(\frac{\partial H}{\partial Q}\right)\right| a_{1u}\rangle + \langle e_{gy} \left|\left(\frac{\partial H}{\partial Q}\right)\right| e_{gy}\rangle + \langle e_{gx} \left|\left(\frac{\partial H}{\partial Q}\right)\right| e_{gx}\rangle$$

(1A.11)

This leads to an expression for the extinction coefficient in terms of both Franck-Condon and Herzberg-Teller coupling via totally-symmetric and non-totally-symmetric modes, respectively.

$$\epsilon = \sum_v \frac{|\langle i|e\sigma|f\rangle\langle 0|u\rangle|^2}{E_{fv} - E_{i0} - \hbar\omega - i\Gamma} + \sum_v \sum_r \frac{\left|\frac{\langle r \left|\left(\frac{\partial H}{\partial Q}\right)\right| f\rangle \langle u|Q|v\rangle}{E_{fv} - E_{ru}}\right|^2 |\langle i|e\sigma|r\rangle\langle 0|u\rangle|^2}{E_{fv} - E_{i0} - \hbar\omega - i\Gamma}$$

(1A.12)

To arrive at an analytical model, we use the standard model for configuration interaction, i.e. mixing of the excited state configurations in terms of the transition moments,

$$r_\sigma^0 = \langle G|e\sigma|Q_\sigma^0\rangle$$

$$R_\sigma^0 = \langle G|e\sigma|B_\sigma^0\rangle$$

(1A.13)

The mixing of the B and Q states is represented by the "rotation" angle α, such that

$$R_\sigma = \cos(\alpha)R_\sigma^0 + \sin(\alpha)r_\sigma^0$$

$$r_\sigma = \sin(\alpha)R_\sigma^0 + \cos(\alpha)r_\sigma^0$$

(1A.14)

The naught symbol represents the pure (unmixed) states. The mixing results in transitions that are linear combinations of the original ones. These can then be further mixed according the Herzberg-Teller coupling and the "simple" model by Shelnutt, we have two separate cases for vibronic coupling by symmetry. The first case is the B_{1g},B_{2g} case and the second case is the A_{2g} case. For the absorption spectrum these are,

$$\varepsilon = (R_\sigma^0)^2\left(\frac{\cos^2(\alpha)}{(\mathrm{E_{B0}} - \hbar\omega)^2 + {\Gamma_\mathrm{B}}^2} + \frac{\sin^2(\alpha)}{\left(\mathrm{E_{Q0}} - \hbar\omega\right)^2 + {\Gamma_\mathrm{Q}}^2}\right)$$

$$+\left(R_\sigma^0 b_g\right)^2\left(\frac{\frac{\cos(\alpha)sin(\alpha)}{\hbar\omega} + \frac{\cos(\alpha)sin(2\alpha)}{E_Q - E_B - \hbar\omega}}{(\mathrm{E_{B1}} - \hbar\omega)^2 + {\Gamma_\mathrm{B}}^2} + \frac{\frac{\sin(\alpha)sin(\alpha)}{\hbar\omega} + \frac{\cos(\alpha)cos(2\alpha)}{E_Q - E_B + \hbar\omega}}{\left(\mathrm{E_{Q1}} - \hbar\omega\right)^2 + {\Gamma_\mathrm{Q}}^2}\right)$$

(1A.15)

and

$$\varepsilon = (R_\sigma^0)^2\left(\frac{\cos^2(\alpha)}{(\mathrm{E_{B0}} - \hbar\omega)^2 + {\Gamma_\mathrm{B}}^2} + \frac{\sin^2(\alpha)}{\left(\mathrm{E_{Q0}} - \hbar\omega\right)^2 + {\Gamma_\mathrm{Q}}^2}\right)$$

$$+\left(R_\sigma^0 a_{2g}\right)^2\left(\frac{\frac{\sin^2(\alpha)}{E_Q - E_B - \hbar\omega}}{(\mathrm{E_{B1}} - \hbar\omega)^2 + {\Gamma_\mathrm{B}}^2} + \frac{\frac{\cos^2(\alpha)}{E_Q - E_B + \hbar\omega}}{\left(\mathrm{E_{Q1}} - \hbar\omega\right)^2 + {\Gamma_\mathrm{Q}}^2}\right)$$

(1A.16)

The representations in Eqns. 1A.15 and 1A.16 are single mode models, for reasons of simplicity. The experimentally observed absorption spectrum will be a linear combination of the modes observed in these models and the Franck-Condon progression. For metallophyrins, the value of S is small. Thus, the Franck-Condon progression is quite limited in extent. Vibronic coupling turns out to be very important. This was noted from the earliest models by Goutermann.

Goutermann's four orbital model (a_{1u}, a_{2u}, ground state and e_g, excited state) was applied to nearly every known porphyrin and shown to explain a vast number of spectral features. We can understand vibronic coupling by plotting model calculations for each of the frequencies b_g and a_{2g}.

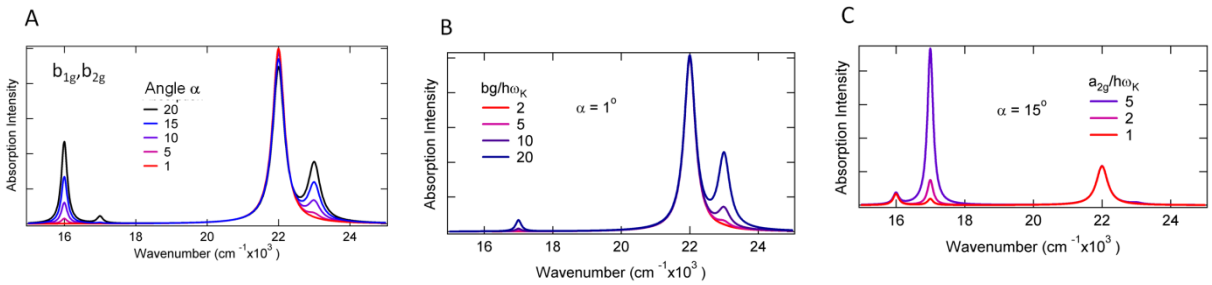

Figure 1A.5. Plots of the vibronic coupling effects of modes of b_{1g}, b_{2g} and a_{2g} symmetry in the D_{4h} point group. These mode symmetries apply to hemes, and other biological chromophores based on the porphine group.

Figure 1A.5 is based on a parameterization of the model equations 1A.15 and 1A.16. The energies are E_B = 22,000 cm^{-1} and E_Q = 16,000 cm^{-1} and Γ = 200 cm^{-1}. The vibronic mode frequency was assumed to be 1000 cm^{-1} for simplicity. The vibronic coupling parameter is given in units of the mode frequency. Figure 1A.5A shows the effect of increasing the configuration interaction parameter, α, when $b_g = \hbar\omega$, where (i.e. b_{1g} and b_{2g} give the same result so that both are unified as a parameter b_g). Figure 1A.5B shows the calculation as a function of the parameter b_g at an angle of $\alpha = 1^o$. Figure 1A.5C shows how different a_{2g} vibronic coupling is from bg-type vibronic coupling. There is little vibronic interaction in the allowed Soret band, but extensive vibronic overtone in the forbidden Q-band. While the use of $\alpha = 15^o$ and $a_{2g} = 5\hbar\omega$ is rather extreme, the case of $\alpha = 15^o$ and $a_{2g} = 2\hbar\omega$ is perhaps the closest to the appearance of six-coordinate heme hemes, which have a double peaked Q-band. As will be shown below, resonance Raman spectroscopy shows that both B_{1g} and A_{2g} modes are strongly coupled to the heme absorption bands.